FINAL TECHNICAL REPORT

MATERIALS FOR INDUSTRIAL HEAT RECOVERY SYSTEMS

Tasks 3 and 4
MATERIALS FOR HEAT RECOVERY IN BLACK LIQUOR RECOVERY BOILERS

DOE Award Number
DE-FC36-04GO14035

Project Period
04/01/2004 to 03/30/2007

Principal Investigator
J. Peter Gorog, Phone – 253-924-6514, E-mail – peter.gorog@weyerhaeuser.com
M.S. WTC 2H22, Weyerhaeuser Company, Federal Way WA 98003

Authors
James R. Keiser, Phone – 865-574-4453, E-mail – keiserjr@ornl.gov
M.S. 6156, Oak Ridge National Laboratory, P.O. Box 2008, Oak Ridge, TN 37831-6156

Joseph R. Kish, Phone – 604-222-3229, E-mail – jkish@paprican.ca
Preet M. Singh, Phone – 404-894-6641, E-mail – preet.singh@mse.gatech.edu
Gorti B. Sarma, Phone – 865-574-5147, E-mail – sarmag@ornl.gov
Jerry Yuan, Phone – 604-822-1245, E-mail – jwyuan@psl.bc.ca
J. Peter Gorog, Phone – 253-924-6514, E-mail – peter.gorog@weyerhaeuser.com
Laurie A. Frederick, Phone – 604-222-3200, E-mail – lfrederick@paprican.ca
François R. Jetté, Phone – 514-848-5555, E-mail – francois.jette@domtar.com
Roberta A. Meisner, Phone – 865-576-9480, E-mail – meisnerra@ornl.gov
Douglas L. Singbeil, Phone – 604-222-3254, E-mail – dsingbeil@ paprican.ca

Recipient Organization
Weyerhaeuser Company

Other project team members
Andritz, Inc.
Babcock & Wilcox – U.S. and Canada
Domtar, Inc.
Georgia-Pacific
Kvaerner Power
MeadWestvaco
Oak Ridge National Laboratory
Sandvik Materials Technology
Welding Services Inc.

December 31, 2007

Acknowledgment: This report is based on work supported by the U.S. Department of Energy under Award No. DE-FC36-04GO14035

TABLE OF CONTENTS

LIST OF ACRONYMS

CFD	Computational fluid dynamics
DOE	Department of Energy
EDS	Energy dispersive spectroscopy
FMT	First melting temperature
FPD	Flame photometric detector
HP	High pressure
HT	High temperature
ID	Inner diameter
LP	Low pressure
LT	Low temperature
NPE	Non-process elements
OD	Outer diameter
ORNL	Oak Ridge National Laboratory
SEM	Scanning electron microscope
TCD	Thermal conductivity detector
TGA	Thermo-gravimetric analyzer
XRD	X-ray diffraction

LIST OF FIGURES

LIST OF TABLES

LIST OF APPENDICES

EXECUTIVE SUMMARY

The DOE-funded project on materials for industrial heat recovery systems included four research tasks: materials for aluminum melting furnace recuperator tubes, materials and operational changes to prevent cracking and corrosion of the co-extruded tubes that form primary air ports in black liquor recovery boilers, the cause of and means to prevent corrosion of carbon steel tubes in the mid-furnace area of recovery boilers, and materials and operational changes to prevent corrosion and cracking of recovery boiler superheater tubes. Results from studies on the latter two topics are given in this report while separate reports on results for the first two tasks have already been published.

Accelerated, localized corrosion has been observed in the mid-furnace area of kraft recovery boilers. This corrosion of the carbon steel waterwall tubes is typically observed in the vicinity of the upper level of air ports where the stainless clad co-extruded wall tubes used in the lower portion of the boiler are welded to the carbon steel tubes that extend from this transition point or "cut line" to the top of the boiler. Corrosion patterns generally vary from one boiler to another depending on boiler design and operating parameters, but the corrosion is almost always found within a few meters of the cut line and often much closer than that. This localized corrosion results in tube wall thinning that can reach the level where the integrity of the tube is at risk.

Collection and analysis of gas samples from various areas near the waterwall surface showed reducing and sulfidizing gases were present in the areas where corrosion was accelerated. However, collection of samples from the same areas at intervals over a two year period showed the gaseous environment in the mid-furnace section can cycle between oxidizing and reducing conditions. These fluctuations are thought to be due to gas flow instabilities and they result in an unstable or a less protective scale on the carbon steel tubes. Also, these fluctuating air flow patterns can result in deposition of black liquor on the wall tubes, and during periods when deposition is high, there is a noticeable increase in the concentrations of sulfur-bearing gases like hydrogen sulfide and methyl mercaptan. Laboratory studies have shown that chromized and aluminized surface treatments on carbon steel improve the resistance to sulfidation attack.

Studies of superheater corrosion and cracking have included laboratory analyses of cracked tubes, laboratory corrosion studies designed to simulate the superheater environment and field tests to study the movement of superheater tubes and to expose a corrosion probe to assess the corrosion behavior of alternate superheater alloys, particularly alloys that would be used for superheaters operating at higher temperatures and higher pressures than most current boilers.

In the laboratory corrosion studies, samples of six alternate materials were immersed in an aggressive, low melting point salt mixture and exposed for times up to 336 h, at temperatures of 510, 530 or 560°C in an inert or reactive cover gas. Using weight change and results of metallographic examination, the samples were graded on their resistance to the various environments. For the superheater corrosion probe studies, samples of the same six materials were exposed on an air-cooled corrosion probe exposed in the superheater section of a recovery boiler for 1000 h. Post exposure examination showed cracking and/or subsurface attack in the samples exposed at the higher temperatures with the attack being more severe for samples

exposed above the first melting temperature of the deposits that collected on the superheater tubes. From these superheater studies, a ranking was developed for the six materials tested.

The task addressing cracking and corrosion of primary air port tubes that was part of this project produced results that have been extensively implemented in recovery boilers in North America, the Nordic countries and many other parts of the world. By utilizing these results, boilers are being operated under more demanding conditions with fewer outages and reduced safety concerns about boiler explosions resulting from failed tubes in the lower boiler. The results of studies on the mid-furnace tube corrosion task and the superheater corrosion and cracking task have become available much more recently, and, consequently, the extent of implementation is far more limited. However, boiler operators are utilizing some of the operational information to minimize corrosion in the mid-furnace area. With construction of new boilers that are designed to operate at higher temperatures and pressures, the guidance on selection of superheater tube materials will almost certainly influence the selection of materials for the more critical areas of the superheaters.

INTRODUCTION AND BACKGROUND

A recently completed, DOE-funded project addressed the issue of "Materials For Industrial Heat Recovery Systems". In addition to a task involving reporting of results and some administrative activities, there were four research related tasks to this project. Two previously published reports addressed two of these tasks: performance of recuperators in aluminum melting furnaces and corrosion and cracking of the co-extruded tubes used for primary air port openings in black liquor recovery boilers [1,2]. The remaining two tasks concerning corrosion of wall tubes in the mid-furnace area of recovery boilers and corrosion and cracking of recovery boiler superheater tubes are addressed in this report.

The black liquor recovery boilers used in pulp and paper mills utilizing the kraft process are critical components of the mills. These boilers generate steam that is utilized for power generation and process applications, and they are the first step in recovering the chemicals used in the pulping process. Boilers that have a lot of corrosion, cracking and plugging issues often operate at less than optimal conditions and generally require more down time in order to address the maintenance issues. Consequently, the recovery of energy from burning of the organic components in such recovery boilers can be considerably less efficient than desired, and significant safety issues can also be introduced.

To address the tasks addressing mid-furnace wall tube corrosion and superheater tube corrosion and cracking, a team of researchers from various organizations was assembled. Most of these team members also participated in the previously reported study of corrosion and cracking of primary air port opening tubes [1]. Project participants and their particular roles included:

- Weyerhaeuser Company – prime recipient of contract
- Oak Ridge National Laboratory – project technical lead
- Georgia Tech's Institute of Paper Science and Technology – lead on mid-furnace studies
- Process Simulations Limited – conducted CFD modeling studies
- FPInnovations-Paprican – major participant in superheater studies

These two tasks have the common feature that they are involved in the recovery of heat from the combustion process that occurs in black liquor recovery boilers. However, there are some important differences. The mid-furnace area constitutes a portion of the boiler walls where carbon steel tubes are used in the region just above the liquor guns and the highest level of air ports. The bottom of the mid-furnace area is the point where the carbon steel wall tubes are welded to the co-extruded 304L stainless steel/carbon steel wall tubes used between the floor and this transition point. These tubes are used to extract heat and raise the temperature of the pressurized water passing through the tubes. The superheater tubes suspended in the upper region of the boiler extract heat from the hot gases exiting the boiler to raise the temperature of the steam passing through the tubes. The boiler sketch in Fig. 1 shows the general location of the mid-furnace and superheater areas of a recovery boiler.

The remainder of this report is divided into two sections: one describing the studies of mid-furnace corrosion and one covering the studies of superheater corrosion and cracking. The mid-furnace study was led by staff of the Institute of Paper Science and Technology at Georgia

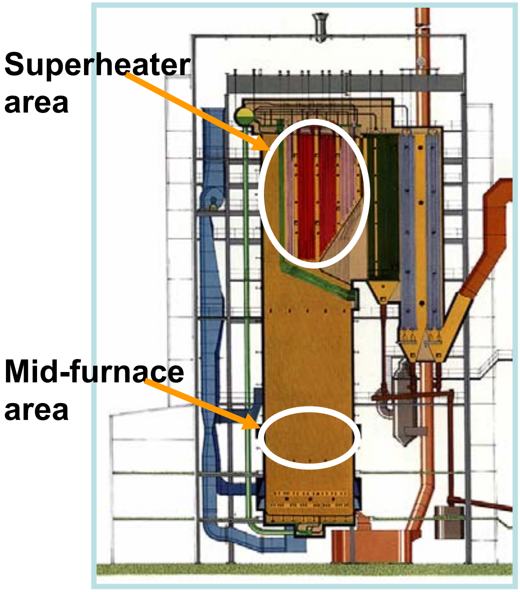

Figure 1. Superheater and mid-furnace areas of a recovery boiler

Institute of Technology with computation fluid dynamics support from Process Simulations Limited. The superheater cracking studies were primarily conducted at Oak Ridge National Laboratory (ORNL) while the corrosion studies were a collaborative effort between FPInnovations-Paprican (originally Pulp and Paper Research Institute of Canada) and ORNL. FPInnovations-Paprican conducted the laboratory corrosion studies while ORNL was responsible for the corrosion probe work.

MID-FURNACE CORROSION STUDIES

Kraft recovery boilers experience localized accelerated corrosion in mid-furnace areas. Corrosion patterns may vary from one boiler to another depending on the operation parameters and general design of the boiler. Local gaseous environments were characterized in areas with corrosion and equivalent areas without accelerated corrosion in a selected boiler over the period of two years. Results from this study indicated that in the areas with accelerated corrosion there was a large variation in the local gas composition at the waterwall surface. Reducing and sulfidizing gases were found in the areas with accelerated corrosion, whereas the gas compositions were more oxidizing in the low corrosion areas. Observations during field tests at Weyerhaeuser's Flint River, Georgia and Columbus, Mississippi mills have indicated that the local waterwall temperature may also vary in the mid-furnace due to localized combustion and air flow patterns. Mid-furnace environments were simulated in the laboratory to evaluate the effect of gas composition and fluctuations on the corrosion kinetics of carbon steel tube material. Laboratory tests with SA-210 carbon steel samples with the gas composition cycling between an oxidizing and a reducing/sulfidizing condition led to an unstable scale formation on the surface. The extent of accelerated corrosion was found to depend upon the extreme partial pressure values of sulfur (S_2) and oxygen (O_2). Carbon steel samples were coated with chromized or aluminized diffusion coatings in the laboratory and were then tested under sulfidizing conditions. Both types of diffusion coatings had superior performance compared to the uncoated carbon steel samples under similar conditions. Mid-furnace corrosion can be controlled by making gaseous environments in the mid-furnace more stable. However, a more practical solution seems to be to use waterwall tubes with a protective outer layer. This may be done by using composite tubes (stainless steel outer layer), thermal spray coatings of resistant alloys or diffusion barrier coatings like a chromizing or an aluminizing treatment.

INTRODUCTION

Water leaks in a kraft recovery boiler can potentially lead to a water-smelt explosion. One of the possible causes for the water leak in recovery boilers is the corrosion of waterwall tubes in the lower- and mid-furnace areas. The lower-furnace area of the kraft recovery boiler has a reducing and sulfidizing environment, which is known to cause accelerated corrosion of carbon steel waterwall tubes due to high temperature sulfidation [3-6]. To protect waterwall tubes in the lower furnace from high corrosion rates, composite tubes, with an outer layer of stainless steel, were introduced. The stainless steel layer of composite tubes has resulted in a generally good performance against the general sulfidation attack in the lower-furnace area [7,8]. However, composite tubes are typically only used in the waterwalls up to the last air-port level. Carbon steel tubes are used in the mid- and upper-furnace areas as the environment in these areas is considered to be oxidizing and far less corrosive than the lower-furnace areas [9].

In recent years, there have been reports of accelerated corrosion of carbon steel tubes in mid-furnace areas [10-12]. This is generally attributed to significant changes in the boiler operation parameters such as a decrease in the air supply to the lower-furnace levels and the practice of firing high-solids black liquor, which may also raise the gas temperatures in the furnace. Mid-furnace corrosion of boiler waterwalls is prominent above the "cut-line" where the stainless steel lower-furnace waterwall section is welded to the carbon steel mid- and upper-furnace waterwall section. Due to the appearance of corrosion of the waterwall tubes near the weld, this type of mid-furnace corrosion phenomenon is also referred to as cut-line corrosion in the pulp and paper industry.

Our previous work on mid-furnace corrosion has shown that changes in the boiler operating parameters seem to have resulted in changes to the local environments in the mid-furnace of boilers [11,12]. These changes vary from one boiler to another or within one boiler from one location to another. Based on field studies and limited laboratory data, it can be postulated that the recent operational changes in boilers to increase boiler efficiency and to control pollution might have led to the changes causing corrosion rates of waterwall tubes in mid-furnace areas to increase significantly. However, the exact nature of these changes was not known. Typically these were short term studies where samples were taken for a few days and our conclusions were made on these observations.

In the present study, the recovery boiler in Weyerhaeuser’s Flint River mill near Oglethorpe, GA was selected and environmental characterization was done over a two year period, without there being any significant operational changes in the boiler or the pulp mill. Mid-furnace corrosion is forcing longer inspection times during annual shutdowns. Loss of production along with panel replacement costs can result in costs of millions of dollars to the boiler owners. The main aim of this task of the project is to understand the mechanisms responsible for this recent problem in kraft recovery boilers so that mitigation strategies could be recommended.

EXPERIMENTAL PROCEDURES

This task on mid-furnace corrosion was divided into two subtasks. In the first subtask, the local gaseous environment in the mid-furnace area within a selected recovery boiler was characterized. In the second subtask controlled experiments were conducted in representative gaseous environments to quantify and confirm the reasons for high corrosion rates of carbon steel boiler tubes in the mid-furnace of a boiler.

Characterization Of The Mid-Furnace Environment In A Kraft Recovery Boiler

This task was related to the characterization of local gaseous environments, in areas with high and low corrosion rates of carbon steel waterwalls, to better understand the reasons behind the difference in corrosion rate. Previous work on gaseous environment characterization had shown that the areas with high corrosion rates in the mid-furnace generally had higher concentrations of sulfur-bearing gases, such as hydrogen sulfide (H_2S) and reducing gases, such as hydrogen (H_2) and carbon monoxide (CO), compared to areas with low corrosion rates at similar elevation in the boiler [9]. In some boilers, the upper part of the mid-furnace (~10 to 30 feet above the tertiary airports) had fluctuating gaseous environments in the areas of high corrosion rates where the environments changed frequently from reducing-sulfidizing to oxidizing (without sulfur-bearing gases).

A long time environment characterization study was planned so that the time-dependent changes could be evaluated. A boiler with mid-furnace corrosion problem was selected for this study. This boiler was a retrofitted boiler with three air levels and it operated with a steam pressure of

10.3 MPa (1500 psig) and a saturated steam temperature of around 320°C. Composite tubes were used to construct the lower-furnace section, ending at the tertiary airport elevation. This boiler experienced significant corrosion of the carbon steel waterwalls in three corners of the boiler. The front-wall and the rear-wall exhibited accelerated corrosion on the carbon steel tubes extending almost 12 feet above the cut-line, as is shown in Fig. 2.

Mid-furnace areas with high and low corrosion rates were identified using waterwall thickness data obtained during annual inspections. Air-tight, stainless steel gas-sampling ports were welded through the web membrane of the waterwall at these selected areas during a planned shutdown, to support the ceramic tubes that were used to extract samples of the gaseous environment. These gas sampling ports were designed to eliminate any air leaks into the gaseous sample and were accessible from the cold-side of the boiler. Gas samples adjacent to the waterwall tube surface were taken with the sampling tube flush with the waterwall surface. These samples were collected in specially designed glass sampling containers with a composite septum seal. During each visit, multiple gas samples were collected from each port to obtain information on the variation in the gas composition. Once collected, gas samples were analyzed in the laboratory using a Perkin-Elmer gas chromatograph. Two thermal conductivity detectors (TCD) were used to analyze the light gases present, whereas a flame photometric detector (FPD) was used to analyze the sulfur-bearing gases present. The chromatographic equipment was calibrated using standard gases.

Laboratory Studies In Simulated Mid-Furnace Gaseous Environments

To confirm the effect of gas compositions and instability on corrosion rates, simulations tests were conducted in the laboratory. These tests involved quantifying the corrosion kinetics for carbon steel (SA-210) and other selected alternate materials in simulated gaseous mid-furnace environments. Various factors included in this study were (i) gas composition (oxidation and sulfidation potential of gas environments), (ii) temperature, and (iii) cyclic gas compositions.

Gaseous environments used in the laboratory tests were based on field measurements and included a typical environment, as well as an extreme environment, which was typically found in areas of high corrosion rates. Coupons of SA-210 carbon steel (30 mm x 20 mm x 5 mm) were cut from unused boiler tubes. Several of the coupons were also used as a substrate for diffusion coatings under study (as described below). The chemical composition of SA-210 carbon steel boiler tube in listed in Table 1. These test coupons were ground using 100-grit paper, fine polished using 5 nm alumina paste, ultrasonically degreased in acetone, and then dried before weighing.

In the first series of tests SA-210 carbon steel samples were exposed to a 1% H_2S - nitrogen (N_2) gas mixture at 300°C within a thermo-gravimetric analyzer (TGA) equipped with a Cahn D101 microbalance (accuracy of 10^{-6} g) to study the corrosion kinetics. Weight change was normalized to exposed surface area to facilitate comparison among the different samples. In another series of tests, SA-210 carbon steel samples were exposed to fluctuating, simulated gaseous environments, which were also based on field measurements. One test involved cycling the gaseous environment between sulfidizing and oxidizing. A second test involved cycling between a sulfur-bearing oxidizing environment and a non sulfur-bearing oxidizing environment. Tests

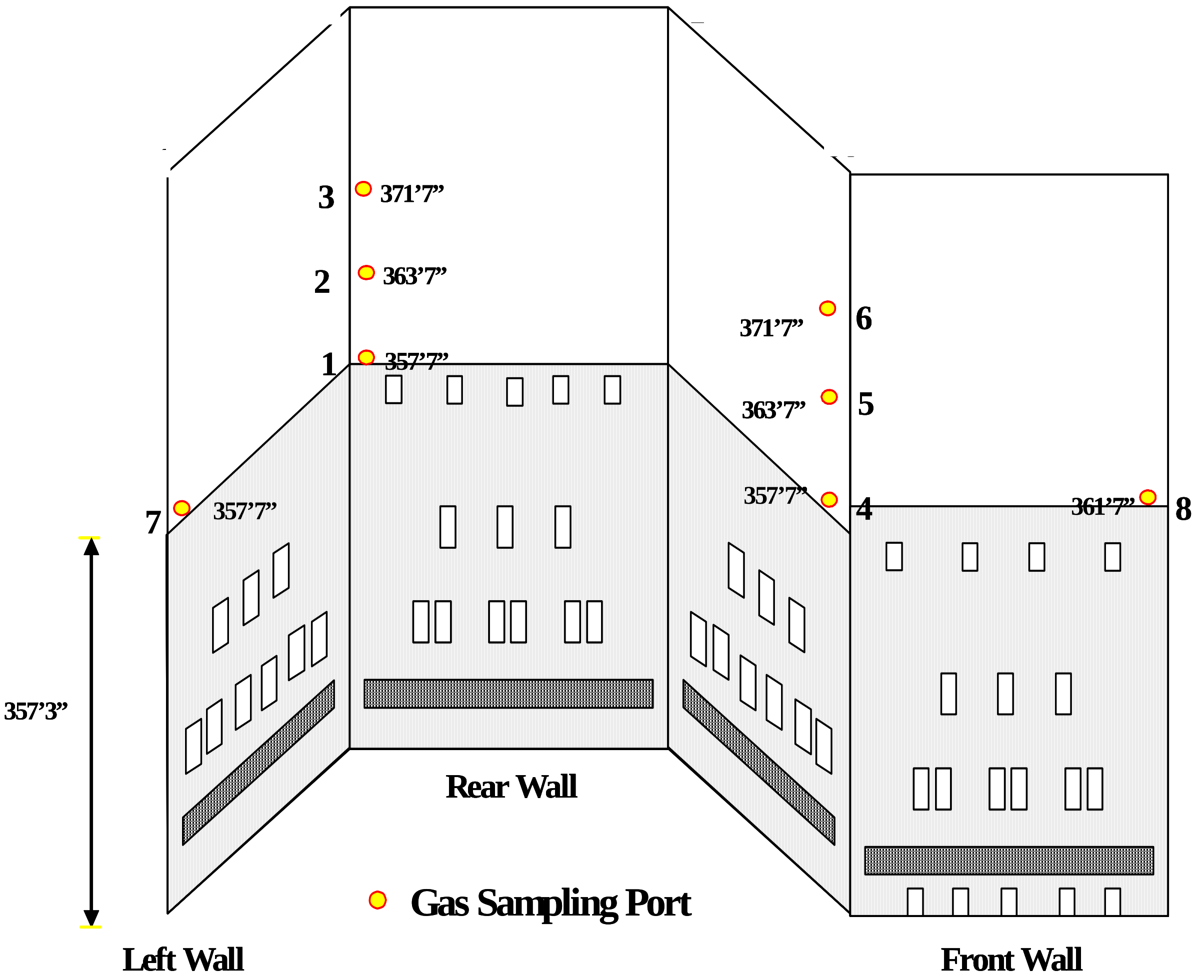

Figure 2. Schematic of the boiler showing the port locations in mid-furnace area (above the cut-line). Heights (above sea level) are given to define relative positions.

Table 1. Chemical composition of carbon steel tube (SA210) used in this study

C	**Mn**	**Si**	**S**	**P**	**Fe**
0.27	0.93	0.1	0.058	0.048	Balance

were carried out at temperatures, representative of the maximum and minimum detected at the waterwall surface. The scale composition and morphology was characterized by X-ray diffraction and by scanning electron microscope (SEM) equipped with an energy dispersive spectrometer (EDS). The thermal balance setup utilized in this study is shown in Fig 3.

Evaluation of Surface Treatments for Mid-Furnace Waterwall Sections

One possible means to address the mid-furnace corrosion problem is to use surface-modified carbon steel boiler tubes to construct the waterwalls in the affected areas. Two commercially available options include a chromizing or aluminizing diffusion coating. To evaluate the suitability of these alternative tube materials, test samples of each were included in the laboratory study. A pack cementation process was used to form a surface layer rich in chromium or aluminum on SA-210 carbon steel boiler tube samples. These coatings were prepared under laboratory conditions to be able to control their properties and thickness. The process involved embedding carbon steel coupons in a pack of composition 75% alumina (Al_2O_3) + 20% (Al or Cr) + 5% ammonium chloride (NH_4Cl) within an Al_2O_3 crucible. The crucible was sealed with an Al_2O_3 cap using high temperature cement and then placed in a horizontal tube furnace purged with argon gas (Ar) for 2 hours. A hole (~1 mm in diameter) was also drilled in the carbon steel coupons before the pack cementation surface treatment to assure a uniform coating was formed on all surfaces exposed to the gaseous environments during testing. Argon was used throughout the coating process to prevent any oxidation. After cooling in the furnace under argon, the surface-treated test samples were cleaned ultrasonically and reweighed. The chemical composition of the surface region of these samples was characterized using both X-ray diffraction (XRD) and EDS.

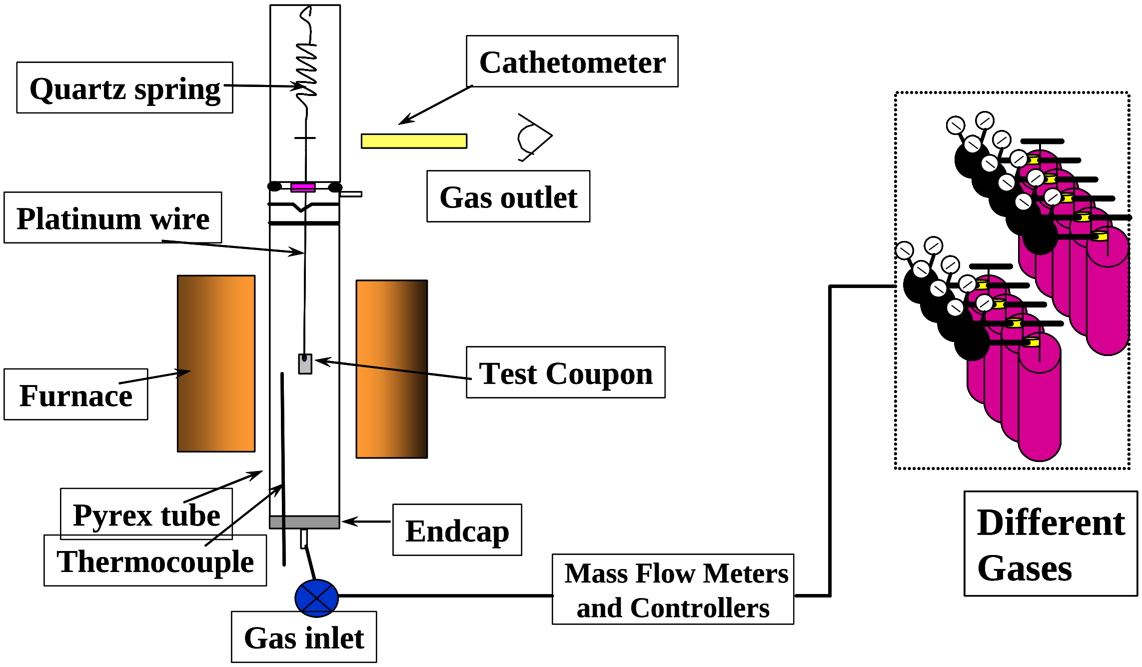

Figure 3. Experimental setup utilized to evaluate the corrosion kinetics of SA-210 carbon steel in simulated mid-furnace gaseous environments.

RESULTS AND DISCUSSION

Mid-Furnace Gas Sampling

Gas samples were collected from the sampling ports seven times, over a two-year period. During this time period, the boiler operation parameters were not significantly changed, so the data presented in this report was viewed as being obtained under a “normal boiler operating” condition, unless otherwise indicated. Typically, samples contained light gases, such as O_2, N_2,

H_2, CO_2, CH_4, and CO, and sulfur-bearing gases, such as H_2S, COS, CH_3SH, $(CH_3)_2S$, and SO_2. Hydrogen sulfide and other sulfur-bearing gases were detected in almost all selected areas near the cut-line, but the concentration of oxidizing gases was higher in the low-corrosion area, as well as at the elevation of about 3 m (10 ft) above the cut-line on both walls (see Fig. 4a). Gases in the samples taken from the high-corrosion areas on both walls were generally sulfidizing and reducing with higher concentrations of H_2 and CO. Results indicated that there was sample-to-sample variation among samples taken on a particular day from the same location. However, this difference was smaller than the difference in the daily average gas compositions of samples taken from the same location. The daily average gas composition for a given location was used to view the day-to-day variation in the boiler.

Some researchers have considered the environment at the waterwall to be similar to the bulk gas environments within a recovery boiler [4,5]. However, for corrosion reactions, the local environment at the tube surface is more important to characterize than the bulk environment [6]. Recent changes in the operating process, limited air supply at the lower level for example, seem to have caused a significant change in the local environment at the tube surface. Thermodynamic calculations indicate that at a pyrolysis temperature of 700°C (> waterwall surface temperature) or lower, the sodium sulfide (Na_2S) and potassium sulfide (K_2S) formation reactions do not occur at appreciable rates, thus CH_3SH and H_2S are more stable and are likely to be higher in concentration in the vicinity of the tubes than in the bulk of the flue gas, particularly away from the air ports [13]. A recent study has shown that the thermal and the chemical environments at the surface of tubes may vary with the local environmental conditions [11]. One such local environment condition would be the combustion of partially burnt black liquor at the waterwall surface [9].

During the heating and combustion of black liquor, O_2 is consumed and pyrolysis gases like H_2, CH_4 and CO are released [14-16]. There are other gases like N_2 that do not participate appreciably in these processes. By analyzing gas compositions at each location, one can determine if pyrolysis and combustion reactions are occurring at the waterwall surface in these areas or not. Hydrogen was detected in collected gas samples at the waterwall surface in different areas of the boiler on different days (see Fig. 4b). It can be seen that, in general, the amount of H_2 is lower at higher elevations. This is likely due to more pyrolysis and combustion reactions occurring at lower levels due to availability of black liquor fuel closer to the point of firing or liquor guns. At each wall the amount of the various reducing gases is different. This shows that the reactions and flow are different near different waterwalls at roughly similar elevations in a boiler.

In cases when black liquor was sprayed on the tube surface and underwent pyrolysis, the reduced sulfur-bearing gases released tended to remain in their reduced form in sampled gases because of the low temperature and the low O_2 partial pressures. This can lead to a change in the ratio of CH_3SH and $(CH_3)_2S$ to H_2S. This can further change the oxygen-to-sulfur (O_2-to-S_2) ratio locally and favor the formation of a sulfide scale rather than an oxide scale on the tube surface. Small variations in the S_2 partial pressure can result in catastrophic corrosion conditions [17].

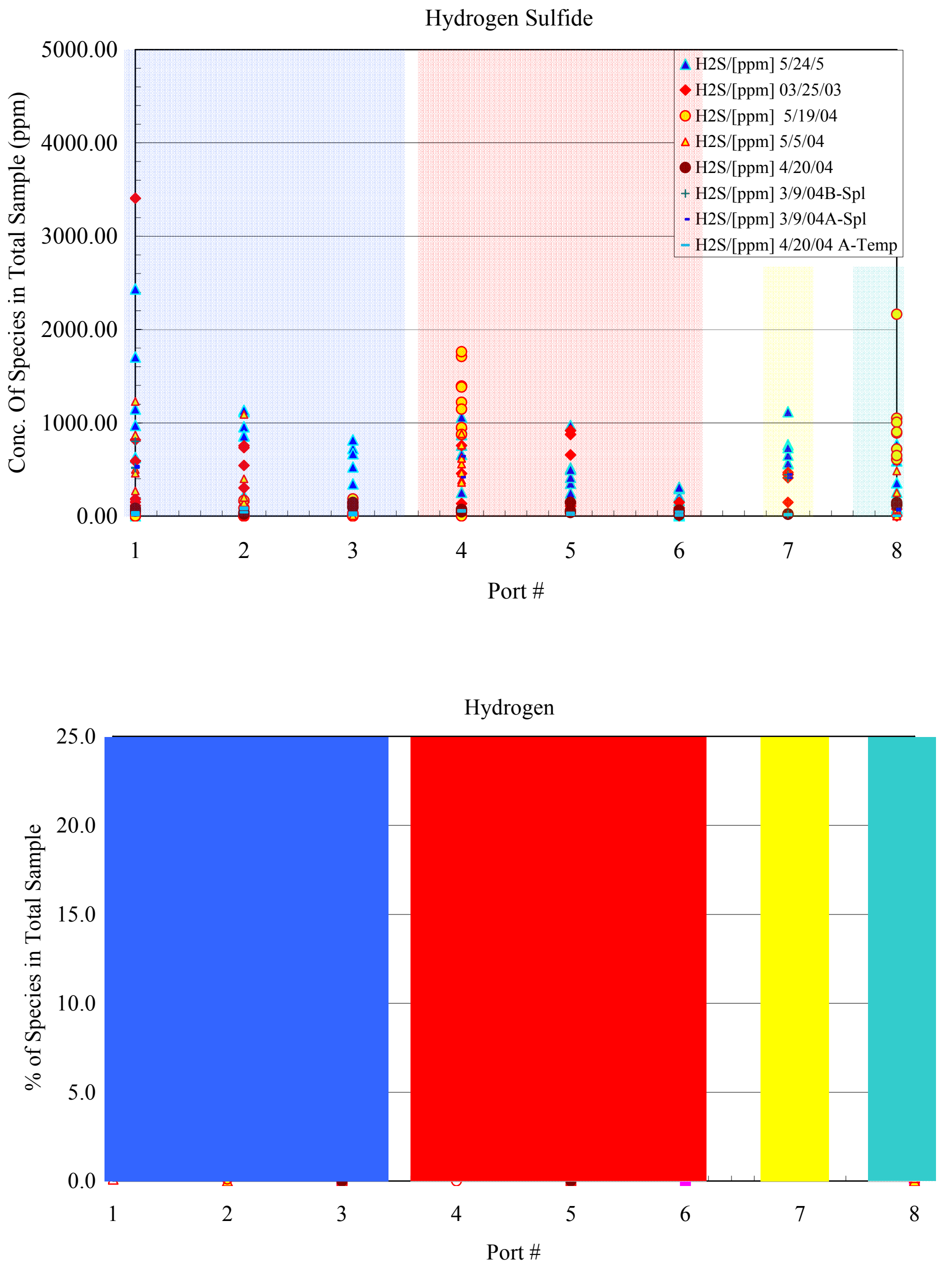

Figure 4. Variation in the concentration of a) hydrogen sulfide (H_2S) and b) hydrogen (H_2) as measured in gas samples taken from the various ports in the mid-furnace shown in Fig. 2 during a 2-year period. The four colored areas represent the four walls, and this pattern identifies which sample points are on the same wall.

Figure 4a shows the H_2S concentration in each sample taken from every port over a 2-year period, whereas Fig. 4b shows the H_2 concentration in each sample from the same locations during the same times. It is clear from this data that the H_2S and H_2 in port #1 varied significantly. Both H_2S and H_2 are produced during pyrolysis of black liquor [14-16], and, therefore their concentrations in the sampled gas tend to follow the same trend. Their presence is indicative of a reducing and sulfidizing environment. For H_2S, the concentration changed from ~3500 ppm to 0 ppm, whereas at a higher elevation, port #2 and #3, the variation was smaller, and the maximum concentrations were significantly lower than measured at port #1. Similarly on the right wall, gas samples from port #4 (at the cut-line) had more variation in the composition and generally higher concentrations of H_2S compared to the gas samples collected from the equivalent locations at higher elevations. Results clearly show that at the lower elevations in the mid-furnace section, near the tertiary air ports, gas compositions were less stable than those measured at the higher elevations. Overall gas compositions in the high-corrosion areas near the cut-line tended to fluctuate between an oxidizing and a reducing and sulfidizing condition.

Figure 5 shows the O_2 concentration in the gas samples taken from the various ports. As the plot shows there is a large sample-to-sample variation in concentration at the waterwall surface. On the right wall, the amount of O_2 in the areas above the tertiary air port level is higher at the lower sampling port levels as the air is supplied from the tertiary air ports and the air/O_2 is consumed at higher sampling port levels. However, on the rear wall (ports #4, #5, #6) this is not apparent. This difference suggests that there may be different O_2 partial pressures on two walls at a similar elevation.

Gas sampling data collected from different mill visits show clear evidence of differences in gas composition. The high-corrosion areas had higher concentrations of sulfur-bearing gases, such as H_2S, and reducing gases, such as H_2, compared to the low-corrosion areas on the same wall at the same elevation. Variation in gas composition on a particular day was not as significant as the visit-to-visit variation observed. Another important conclusion from the field test results is that the gaseous environment in the mid-furnace area is not stable. It is not clear if there is any pattern to this transient behavior. Initial efforts to correlate gas compositions with the boiler operating parameters did not yield any clear patterns. Boiler operation records were compared with the gas composition data to see if there were any changes in the liquor temperature, liquor pressure, air temperature or air distribution to explain the variation in local gas composition. No correlation was found.

An average gas composition assigned to each sampling port location was used to calculate partial pressures of O_2 and S_2 by assuming equilibrium. These partial pressures were then further used to predict the type of scale that may be stable at the tube surface under those gas environments at a given temperature.

Thermodynamic Analysis

The main competing reactions for sulfidation and oxidation of carbon steel at high temperatures are given in the following equations [18-21].

$$2Fe + S_2 = 2FeS \qquad @\ 300^{o}C \qquad \Delta G = -58.6\ \text{kcal}$$

$$2Fe + 1.5O_2 = Fe_2O_3 \qquad @\ 300^{o}C \qquad \Delta G = -159.5\ \text{kcal}$$

The partial pressures of S_2 and O_2 in a given gas mixture at a given temperature was calculated by assuming a thermodynamic equilibrium, which is a reasonable assumption at higher

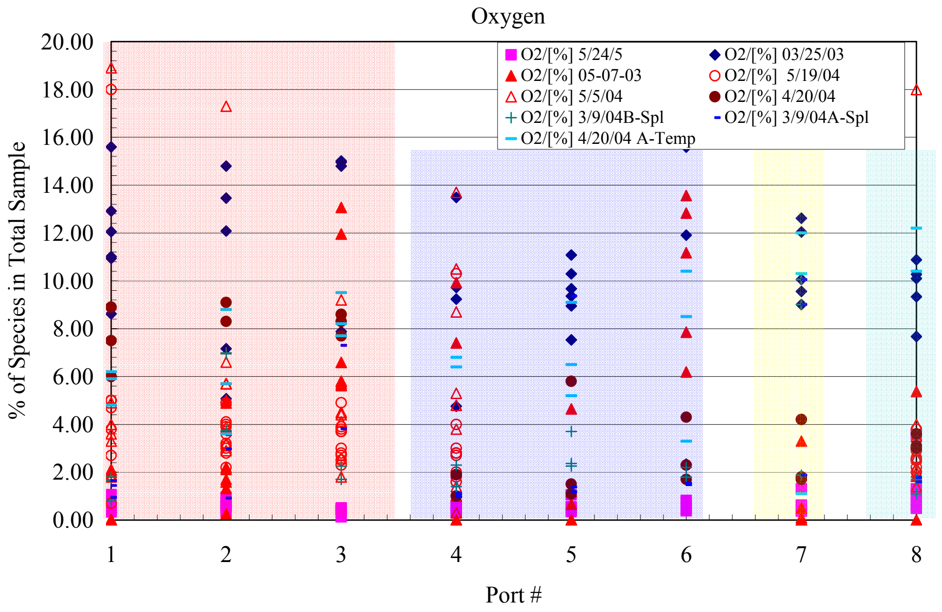

Figure 5. Variation in the concentration of oxygen (O_2) as measured in gas samples taken from the various ports in the mid-furnace shown in Fig. 2 during a 2-year period.

temperatures. Figures 6 and 7 show the calculated partial pressures of O_2 and S_2 in gas samples taken from each port during different days. The amount or partial pressure of S_2 or O_2 for these competing reactions depends upon gas composition of the mixture. For example, the ratio of water vapor (H_2O) and H_2, or CO_2 and CO will contribute to O_2 potential of gas. Similarly ratios of H_2S and H_2, or CH_3SH and CH_4 will contribute to the partial pressure of S_2 at a given temperature.

$$\begin{array}{lll} H_2O = H_2 + \tfrac{1}{2} O_2 & \text{or} & pO_2^{0.5} \propto pH_2O/pH_2 \\ CO_2 = CO + \tfrac{1}{2} O_2 & \text{or} & pO_2^{0.5} \propto pCO_2/pCO \\ H_2S = H_2 + \tfrac{1}{2} S_2 & \text{or} & pS_2^{0.5} \propto pH_2S/pH_2 \end{array}$$

A number of other possible reactions between different gas constituents were considered under the assumption of equilibrium to calculate the overall partial pressure of O_2 or S_2 in a given gas sample.

The thermodynamic stability of the scale formed on the carbon steel surface will depend upon the partial pressure of O_2 and S_2, as is shown in the phase stability or predominance diagram in Figures 8 and 9. Oxide scales are typically more protective due to a lower density of point defects compared to in the sulfide scales [22]. Due to the large amount of lattice defects, sulfide scales allow faster diffusion of reactants and generally result in much higher corrosion rates [23]. This example shows how the gas composition data collected from different ports was analyzed to determine the scale composition and its protective nature. Data from the gas composition at different ports correlate fairly well with the observed corrosion pattern in those locations.

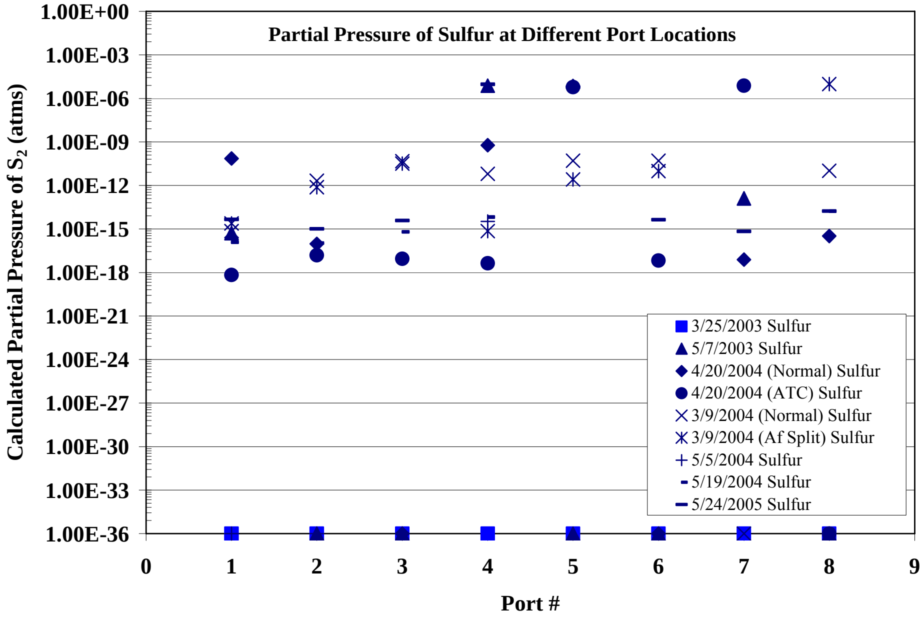

Figure 6. Variation in the calculated partial pressure of sulfur (S_2) for gases collected during a 2-year period from the various sampling ports installed in the mid-furnace section.

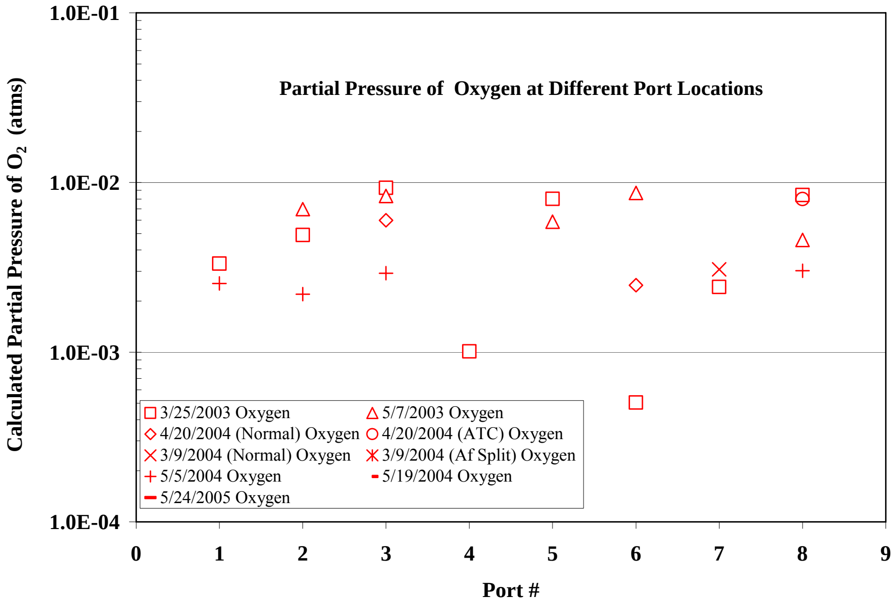

Figure 7. Variation in the calculated partial pressure of oxygen (O_2) for gases collected during a 2-year period from the various sampling ports installed in the mid-furnace section.

Figures 8 and 9 show the regions where phases are thermodynamically stable as a function of O_2 and S_2 partial pressures in the Fe-O-S system at 320°C. The partial pressures calculated from the average gas composition data are superimposed onto these diagrams. Gas samples superimposed onto Fig. 7 were taken from the same port location (port #1) on seven different days over the two-year period. The data indicate that the gaseous environment at this sampling port varies from being very oxidizing to sulfidizing during normal boiler operation conditions. Similarly, when same-day gas composition data collected from the various ports are compared, as shown in Fig. 8, a significant variation in gas composition was found. This clearly indicates that the gaseous environment in the mid-furnace section of this recovery boiler is far from stable. Subtle changes in the gas composition may favor one scale composition over the other, and thus may affect the corrosion kinetics. This instability may explain the difference in the local gas composition at different times under otherwise similar operating conditions.

It is known that the oxide scale formed on the carbon steel surface at typical waterwall boiler tube temperatures is much more protective than the sulfide scale [9,18-21]. If the gas composition cycles between a sulfidizing and an oxidizing composition, the resulting scale may not be very protective, resulting in a high corrosion rate [5]. Previous work on lower-furnace corrosion has shown that the higher corrosion rate of carbon steel may result from the following; presence of gaseous organo-sulfur compounds; alternating oxidizing/reducing conditions; fluctuating temperatures; and elevated temperatures [5,24]. The differences in corrosion rates in the high and the low corrosion areas will largely depend upon the stability of the surface scale. Conditions favoring the sulfide scale or an unstable scale will lead to accelerated waterwall corrosion.

The results in Figs. 4 to 9 show the gaseous environment in local areas can change from being largely oxidizing to largely reducing. Such fluctuation was found to be more prominent in the lower sampling areas, near the cut-line, which coincided with areas of high corrosion rates.

Computational Fluid Dynamics Modeling

A computational fluid dynamics (CFD) model was developed for this particular boiler by Process Simulations Limited. Results from this model have predicted that some liquor could contact the waterwall surface in certain areas of the mid-furnace (see Figures 10 and 11), depending on the air flow pattern, as well as on liquor spray parameters and properties. Due to liquor contacting the waterwall surface, the local environments in these areas can be very different. Release of sulfur-bearing and reducing gases during pyrolysis can lead to higher partial pressures of S_2 in these areas. Figures 10 and 11 show some of the predictions for the model run with a set of normal boiler operating parameters. These figures show there are significant variations in the distribution of black liquor on the walls as well as in the H_2S concentration in the mid-furnace area. Changes in operating parameters and gas flow in the boiler likely cause these variations, and they are one indication of how much conditions change in some parts of the mid-furnace area of the boiler. The model also calculated the local heat flux differences in the mid-furnace section, near the waterwall surface. Local environment near the waterwall will change locally if the boiler operations are altered. The model is capable of calculating these effects, but this model needs to be validated with the actual data obtained from the boiler. Laboratory tests have shown that temperature significantly influences the corrosion rates of carbon steel in the simulated recovery boiler gaseous environments. An increase in test temperature from 320°C to 400°C increased the corrosion rate of SA-210 carbon steel from 0.320 mm/year to 14.66 mm/year in an environment simulating lower-furnace area with low corrosion areas [5,24]. Local heating due to fireside events or due to waterside scaling may increase local tube surface temperatures and lead to local high corrosion rates on waterwall tubes in the mid-furnace areas.

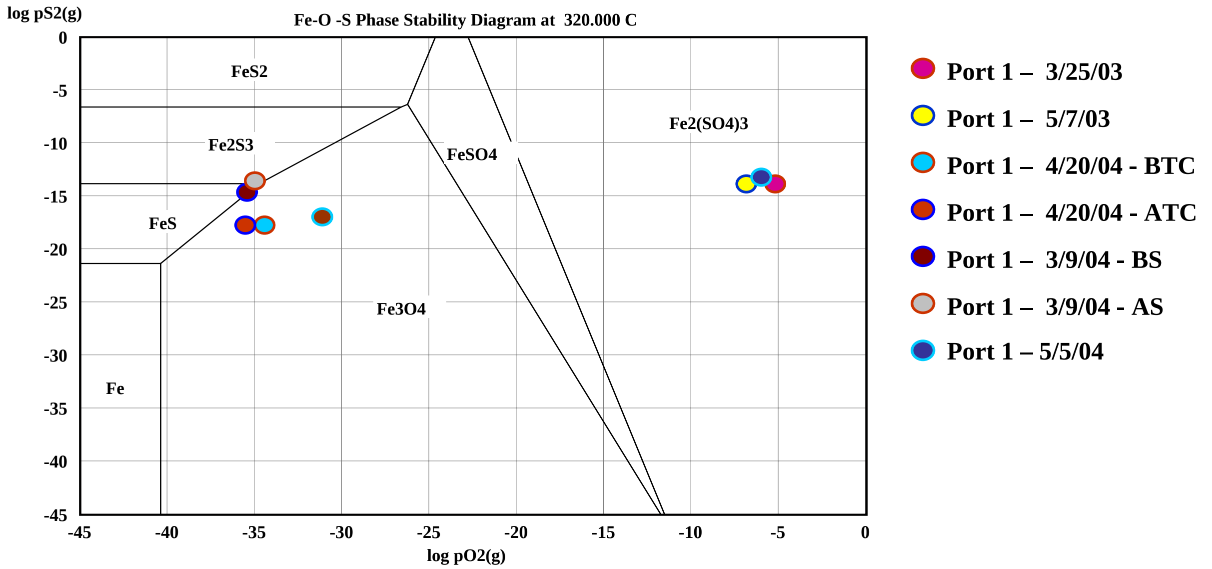

Figure 8. Phase stability diagram for Fe-O-S system at 320^{o}C. Diagram shows partial stability regions for different possible scale compositions as a function of O_2 and S_2 partial pressure in contact with iron. Calculated average partial pressures of O_2 and S_2 from port #1 from different days are superposed, as indicated by different symbols.

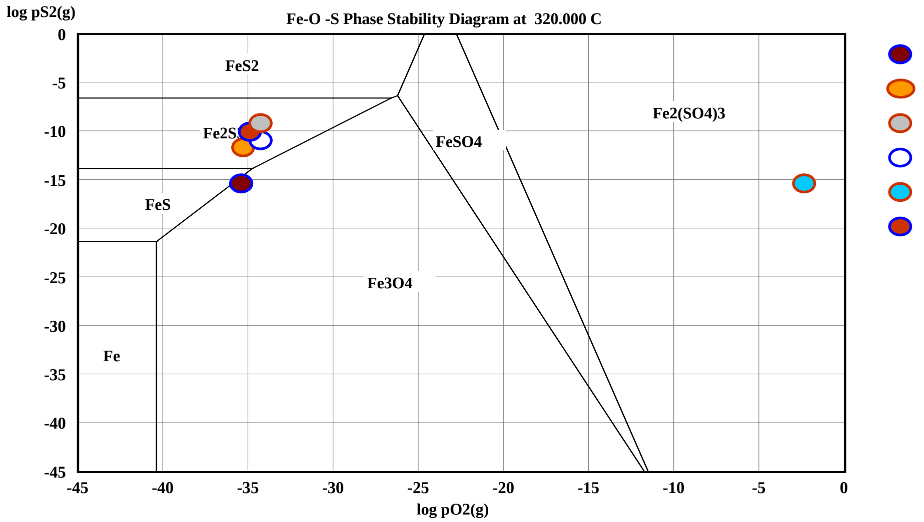

Figure 9. Phase stability diagram for Fe-O-S system at 320^{o}C. Diagram shows partial stability regions for different possible scale compositions as a function of O_2 and S_2 partial pressure in contact with iron. Calculated average partial pressures of O_2 and S_2 for all ports during a visit on 3/9/04 are superposed, as indicated by different symbols.

Carbon Steel: Corrosion Kinetics –Laboratory Simulations

Although the thermodynamic data shown in Figs. 8 and 9 describe the difference in possible scale compositions, it may not accurately predict the real scale compositions or the rate of scale formation, since they are determined by kinetics of competing reactions. The corrosion kinetics need to be determined experimentally, such as in simulated tests. Work in this project involved an evaluation of the corrosion kinetics of SA-210 carbon steel in simulated mid-furnace environments. The test matrix for the simulated gas mixtures covered a range of O_2 and S_2 partial pressures, as calculated from the real gas samples taken from the mid-furnace areas.

Results from the corrosion tests are shown in Fig. 12. The alternating 12-hour zones, marked as A and B, represent different gas compositions during that time. For Test #1 a sharp mass loss was observed after each environmental cycle, which indicates spallation of scale. Figure 13 shows a cross-sectional view of the surface scale after 100 hours of exposure in Test #1 at 300°C. The scale shows a layered structure, which was due to the formation of different oxides/sulfides during each environment change. During the first sulfidizing period, a sulfide scale formed. As the environment changed to an oxidizing one, an oxide scale subsequently formed. This caused the formation of a layered structure as the environments were cycled. The large mismatch between corrosion products can cause the composite scale to crack and spall, thus exposing the metal to corrosive gases [25,26]. The weight change during each period was used to determine if the reaction rate were linear or parabolic during that stage of test. During the first two sulfidation cycles, corrosion showed linear behavior and oxidation showed parabolic behavior. As the scale grows, the sulfidation rate showed a dependence on diffusion of sulfur species through unspalled/adherent scale, as indicated by the transition to parabolic behavior. The qualitative composition of different layers of the surface scale was determined by an EDS line spectra. A sulfur peak indicated a sulfide layer, whereas the absence of a sulfur peak was assumed correspond to an oxide layer. The results are shown in Figs. 13 and 14, and indicate that even a small amount of O_2 introduced during environmental cycling can promote the formation of a stable oxide layer and thus provide protection.

For Test #2, sulfide scales on the SA-210 carbon steel coupons did not show any significant spallation, as evident from TGA plot in Fig. 12. The scale was adherent to the substrate after removal from the TGA apparatus. Results show that the sample tested in Test #2 showed lower mass gain than Test #1, as the scale was adherent and the reaction kinetics were primarily governed by the diffusion of gaseous species through the scale with parabolic rate constant of 0.25 mg^2/cm^4sec. Figure 14 shows the cross-sectional view of the scale after 100 hours of exposure at 300°C in Test #2. The scale morphology suggests the formation of laminated structure of oxides/sulfides. Although the scale looks continuous in cross-section, it exhibited some cracking at the scale/alloy interface. This cracking was likely a result of the large CTE mismatch between the scale and the steel substrate. The scale thickness was roughly 60-80 μm with a dense outer layer (layer #1) of ~50-60 μm thickness, which consists primarily of sulfides, and a highly porous inner layer (layer #2) of ~10-20 μm thickness, which consists primarily of oxide at the scale/alloy interface. Perhaps the presence of a thin oxide layer and its interdiffusion in the sulfide layer provided the good scale adherence observed during Test #2.

Results from Tests #1 and 2 show that the local corrosion behavior in the mid-furnace section depends on the stability of the scale formed. Test #1, in which the environment cycled between a

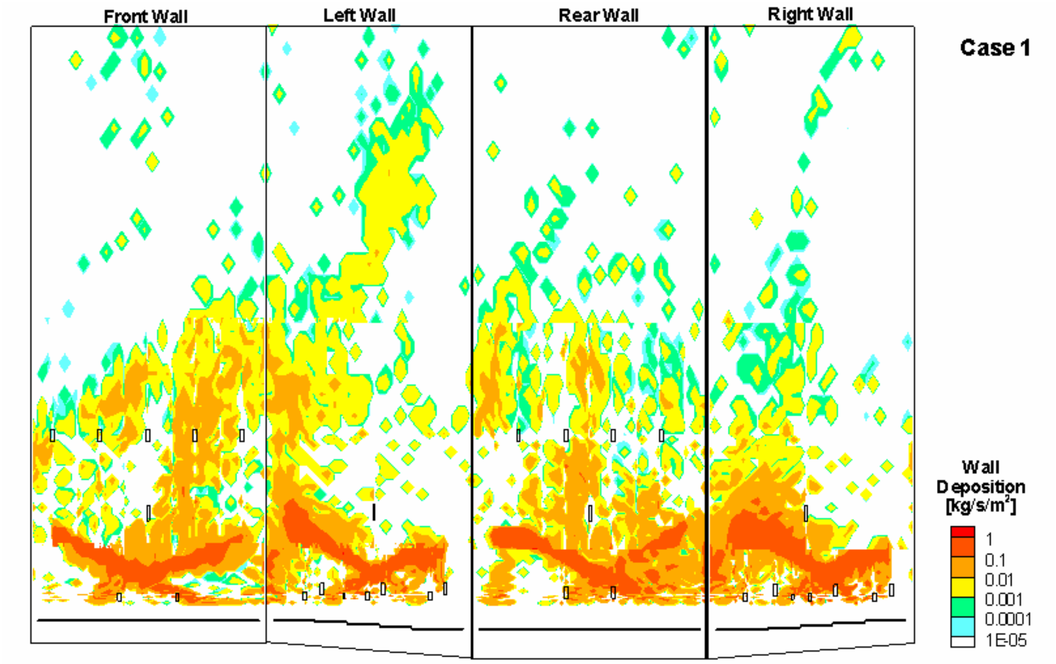

Figure 10. CFD model results showing black liquor spray pattern on waterwall surface in the mid-furnace. Note the differences on the same wall and on different walls.

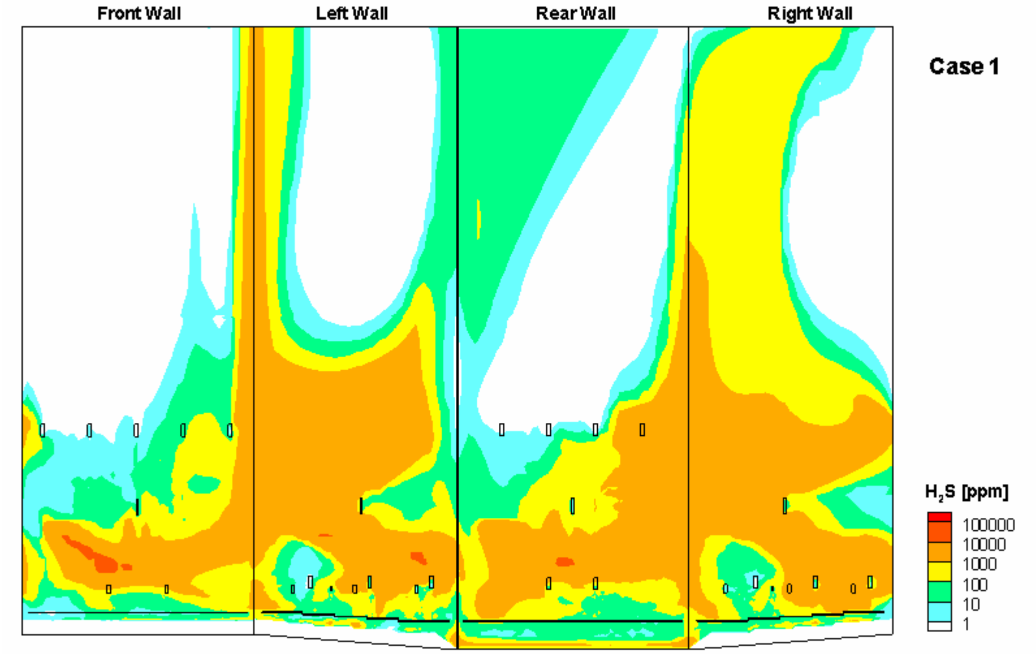

Figure 11. CFD model results showing H_2S concentration on the waterwall surface in the mid-furnace section. Some areas on the waterwalls have a higher concentration of sulfur-bearing and reducing gases compared to other areas at the same elevation. These trends match with the general corrosion patterns found in this boiler.

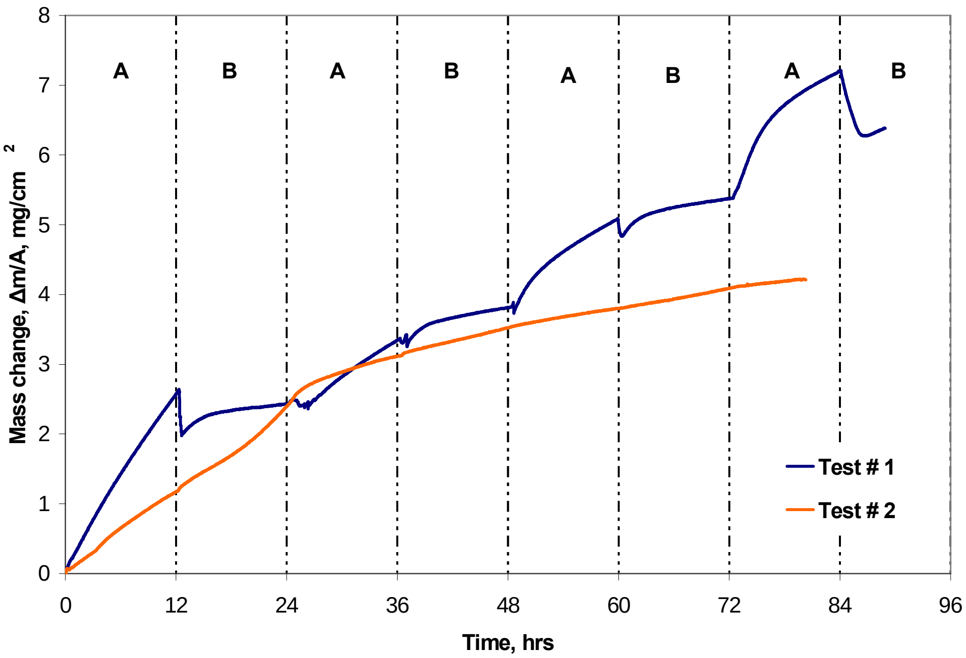

Figure 12. Effect of fluctuating sulfidizing/oxidizing atmosphere on corrosion behavior of SA210; A and B denote gas atmosphere as follows: Test # 1: (A) 1% H_2S in N_2, (B) 1% O_2 in N_2, Test # 2: (A) (1%H_2S +1%O_2) in N_2, (B) 1% H_2S in N_2

sulfidizing and a non S_2-containing oxidizing environment, produced a non-protective scale. In contrast, Test #2, in which the environment cycled between a sulfidizing and a S_2-containing oxidizing environment, produced a more protective scale. Consequently, extreme changes in the local environment are one major reason for the observed accelerated corrosion in the mid-furnace section.

Coated Carbon Steel Corrosion Kinetics - Laboratory Studies

The resulting pack cementation coatings applied to SA-210 carbon steel samples were characterized using XRD and SEM. As Fig. 15A shows, the chromized layer formed on the SA-210 carbon steel substrate was ~60-70 µm thick and it consisted of $(Cr,Fe)_{23}C_6$ and $(Cr,Fe)_7C_3$ as the major components. The aluminized layer formed on the SA-210 carbon steel substrate was found to be ~70-80 µm thick (Fig. 15B), and it consisted of FeAl as the major component. Note that the chromium carbide formed during the chromizing treatment was likely due to the outward diffusion of carbon and strong affinity of chromium towards carbon.

Chromized and aluminized SA-210 carbon steel samples were tested for 100 hours in 1% H_2S in a N_2 mixture to compare their sulfidizing resistance to uncoated SA-210 carbon steel samples. Figure 16 shows the weight change versus time curves at 300°C of the chromized and aluminized SA-210 carbon steel samples compared to that of the uncoated SA-210 carbon steel sample. Both diffusion coatings significantly improved the sulfidation resistance exhibited by the SA-210 carbon steel. The aluminized and chromized SA-210 carbon steel sample exhibited an overall mass gain of ~1 mg/cm^2 and ~0.5mg/cm^2 respectively. In contrast, the uncoated SA-210 carbon steel sample exhibited a much higher mass gain (~8 mg/cm^2) than the two diffusion coated samples. The increased mass gain exhibited by the uncoated sample coincided with the formation of highly porous, non adherent scale. This scale was found by XRD to consist of non-stoichiometric $Fe_{1-x}S$. The scale formed on the aluminized sample was found by XRD to consist

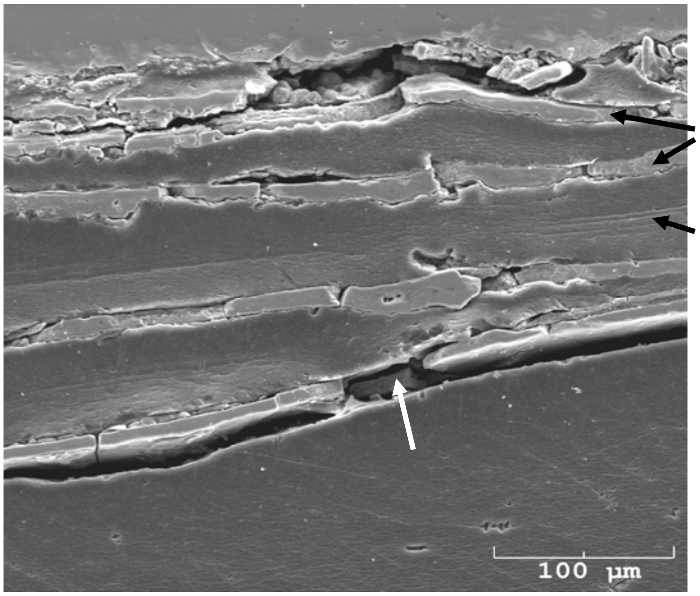

Figure 13. SEM micrograph showing cross-sectional view of laminated scale after Test # 1 exposure. Note alternating oxide/sulfide scale corresponding to each cycle, and the extensive cracking evident in sulfide scale. Oxide scale is relatively continuous and free from cracking.

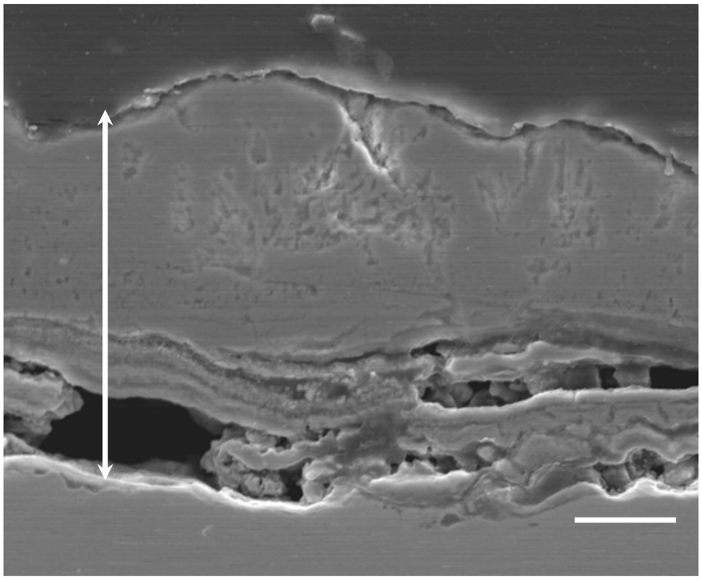

Figure 14. SEM micrographs showing cross-sectional view of laminated scale after Test # 2 exposure. The laminated structure due to cycling of gaseous atmospheres between an oxidizing and sulfidizing environment is evident.

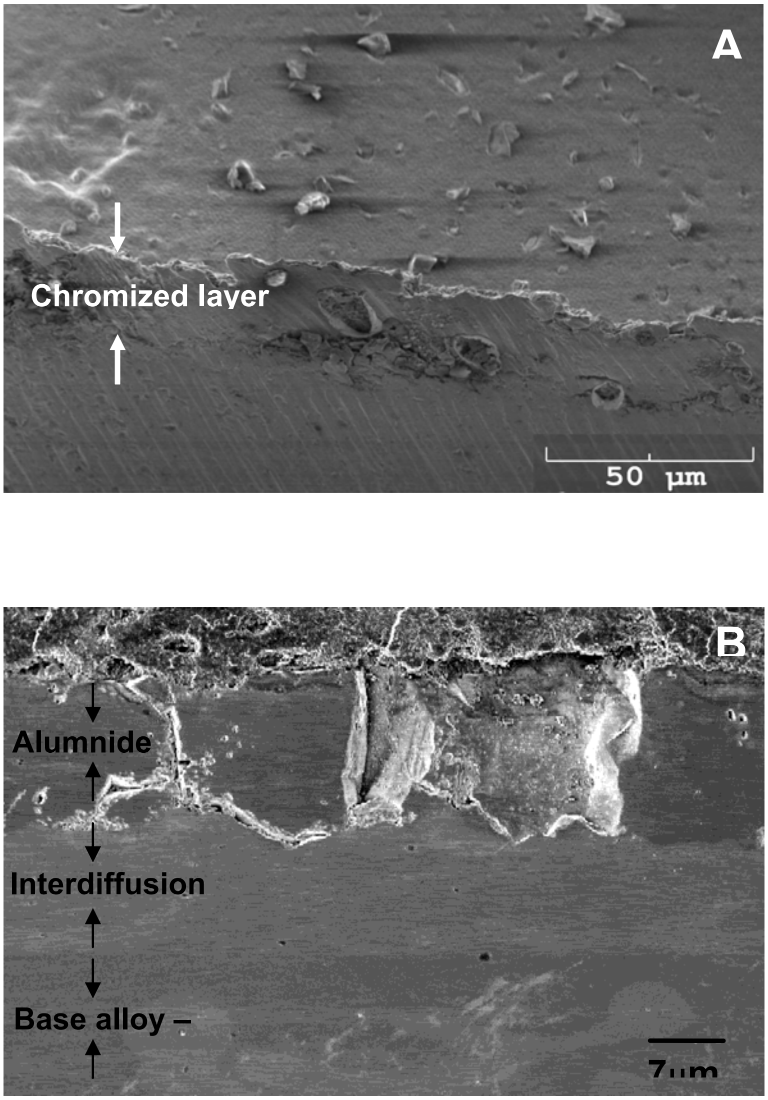

Figure 15. SEM micrographs showing cross-sectional view of pack cemented chromized coating (A) and aluminized coating (B) on carbon steel sample treated for 8 hours at 800^oC.

of an Al_2O_3 scale. On the chromized sample, the scale was found by XRD to consist of chromium sulfide with minor amount of Cr_2O_3 on the surface. These preliminary results indicate that these diffusion coatings could be used to protect the carbon steel boiler tubes against sulfidation attack.

CONCLUSIONS

- High-corrosion areas in the mid-furnace section of the recovery boiler under study had higher concentrations of reducing and sulfur-containing gases at the waterwall surface than did the low-corrosion areas.

- Field data collected over a two year period indicate the gaseous environment in the mid-furnace section can cycle between an oxidizing condition and a reducing condition. This cyclic behavior is believed to be a result of gas-flow instability. This fluctuating situation likely leads to the formation of an unstable or a less protective scale on the carbon steel tube surface, depending upon the extent of the environmental change.

- Fluctuating air flow patterns can result in black liquor contacting the waterwall tube surfaces. In these instances, such contact coincides with an increase in the concentration of sulfur-bearing gases, such as hydrogen sulfide and methyl mercaptan, at the waterwall tube surface in those areas.

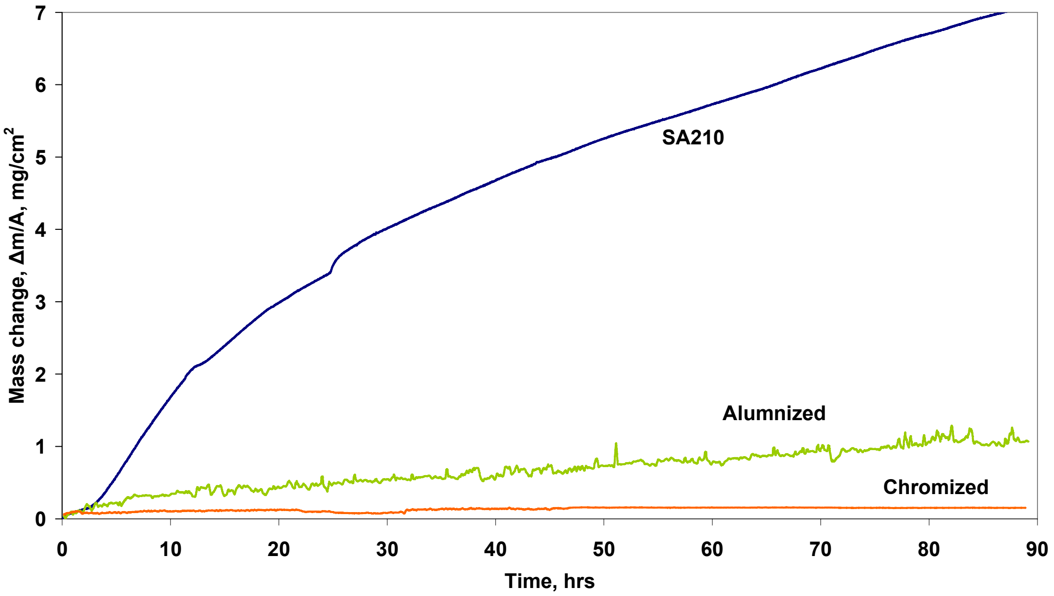

Figure 16. Thermogravimetric analysis (TGA) of aluminized, chromized and uncoated SA-210 carbon steel samples tested in a 1% H_2S in N_2 gas mixture at 300°C. The parabolic reaction rate constants tabulated in Table 2 show the benefits of chromizing and aluminizing for controlling corrosion.

Table 2: Corrosion rates of SA210 as compared to coated samples

Sample	**K_p, parabolic reaction rate (mg^4/cm^2.sec)**
SA210	0.59
Aluminized - SA210	0.01
Chromized - SA210	0.002

- An increase in the local heat flux to the mid-furnace waterwall tube surface may result from high gas temperatures produced by combustion reactions occurring in the presence of excess oxygen. These high temperatures are believed to play a role in accelerating corrosion.

- Corrosion rates of SA-210 carbon steel boiler tubes can be higher in a fluctuating oxidizing/ sulfidizing gaseous environment than in either a predominantly oxidizing or sulfidizing environment due to the formation of a non-protective scale.

- Cracking of protective scales formed on carbon steel waterwall tubes will likely occur in response to any thermal excursions generated at the fireside or waterside surfaces. Such cracking can result in accelerated corrosion. This effect will depend upon the extent or magnitude of thermal excursion.

- Chromizing and aluminizing surface diffusion coatings on SA-210 carbon steel significantly improved the resistance to sulfidation attack relative to uncoated SA-210 carbon steel.

- The effect of frequent environmental changes on corrosion kinetics of diffusion coated and uncoated SA-210 carbon steel needs to be evaluated to confirm the conclusions derived from the field study.

RECOMMENDATIONS

Based on the results from this study, there are several major factors that may influence the observed accelerated mid-furnace corrosion, namely (i) a higher concentrations of reducing and sulfur-containing gases at the waterwall surface, (ii) a variable gas composition due to variations in the gas flow pattern, and (iii) differences in the heat flux due to local combustion of black liquor near the waterwall tube surface. Combustion of black liquor at the waterwall surface is also likely responsible for the higher concentrations of reducing and sulfidizing gases observed.

One way to mitigate localized accelerated mid-furnace corrosion would be to avoid spraying black liquor directly onto the waterwall surface. However, it may not always be possible to predict the gas flow pattern in a particular recovery boiler. Another way to mitigate local accelerated mid-furnace corrosion would be to control the local gaseous environment. However, it is very difficult to control gas flow and instability. The more promising way would be to use corrosion-resistant materials, which form protective oxides on the surface under typical operating conditions. Composite tubes with a 304L stainless steel, or better, exterior layer are expected to perform well in this section [27]. Thermal spray coatings with high chromium should also perform well. However, the performance of thermal spray coatings depends upon the physical integrity, which in turn depends upon the surface preparation and coating procedures used [28]. Most failures of thermal spray coatings in kraft recovery boilers can be attributed to poor adhesion rather that corrosion resistance [8].

In this study, chromized carbon steel boiler tube samples were found to have very good resistance to simulated mid-furnace gaseous environments. Aluminized coatings also showed very good resistance under both static and fluctuating simulated mid-furnace test environments. However, due to less experience with aluminized coatings, chromized carbon steel boiler tubes may be better suited for mid-furnace applications. However, inconsistent chromized coating quality has been reported to be a concern with the use of chromized carbon steel boiler tubes in the lower-furnace areas [5]. Similar concerns are expected unless improved control of the coating process and of the welding process can be achieved.

In conclusion, mechanisms of accelerated corrosion in the mid-furnace section are very similar to the ones operating in the lower-furnace section. Therefore, mitigation strategies applied in the lower-furnace section are applicable in the mid-furnace section. A major difference in the two areas is the fluctuating gaseous compositions due to variations in the gas flow pattern. Any improvement in the boiler design and/or operation that can address the fluctuating gaseous environment should help to improve the corrosion resistance of carbon steel waterwall tubes. Computational fluid dynamics (CFD) modeling can be useful in determining the effect of boiler design or operation change on local gaseous environments.

SUPERHEATER CORROSION AND CRACKING

STUDIES OF SUPERHEATER TUBE CRACKING

Activities addressing cracking of superheater tubes centered on one recovery boiler that had a history of serious cracking problems of superheater tubes. Other boilers have had a history of cracking in the same area, so study of the cracking issue in this boiler was expected to provide useful information for a number of other boilers. Interest in the cracking problem in this boiler began prior to the initiation of this project with the examination of a single, failed superheater tube. Concern about this tube failure as well as previous failures led to the removal of 14 presumably uncracked superheater tubes for determination if cracks were present in these tubes. Two additional cracked tubes were found during a subsequent hydrotest prior to restarting the boiler, and these were also examined. In order to learn more about the motion that might be associated with the cracking, high temperature strain gauges were installed on two superheater tubes to determine the magnitude of oscillations of these tubes. This strain gauge study provided valuable information about the initiation and propagation of cracks in the superheater tubes, and it also demonstrated a new method for characterizing the extent of plugging in the superheater area. These studies have been reported elsewhere [29].

The single failed tube examined previously is shown in Fig. 17, and the location from which it was removed is shown on the right side of that same figure. From the photo on the left it is clear the cut in the high crown box was made very close to the tube. Figure 18 shows the two fracture

Figure 17. The photo on the left shows the two sections of the failed superheater tube that were examined, and the photo on the right shows the position in the high crown seal from which the tube was removed.

surfaces, and it is apparent that portions of the fracture surface of the tube on the left (around 3 and 9 o'clock) were damaged during cutting of the mating section from the high crown seal.

The fracture surface of both sections had accumulated a significant amount of corrosion product (iron oxide) as a result of exposure to moist air. A short section was cut from the failed end of the tube shown on the left in Fig. 18, and this piece was cleaned with inhibited acid to remove the corrosion product without damaging the surface features. This cleaned fracture surface was given a cursory examination using a scanning electron microscope (SEM) to identify the prominent features and to select areas for a second, more thorough, examination. In order to determine whether the high crown seal weld had an influence on the failure, two pieces were cut from the upper section of the superheater tube. If the direction defined by the row of tubes in a crown seal box is viewed as lying in the 6 to 12 o'clock direction (see Fig. 19), the sections were cut at the 3 and 9 o'clock positions. These sections were mounted so that the cross sections could be examined with light microscopy in the as-polished condition and after etching with 2% nital.

Figure 18. Photo showing the fracture surfaces of the superheater tube shown in the previous figure. Note the smooth surface at the 3 and 9 o'clock positions resulting from damage during removal of the tube.

A sketch of the fracture surface examined is shown on the right side of Fig. 19, and distinctive features as well as the original orientation of the tube are indicated. Because of the damage done to the surface during prolonged operation in a partially cracked condition as well as during removal from the boiler, it is not easy to identify the crack initiation sites or the direction of crack propagation. The section of this tube between areas 1 and 4 is shown in the collection of SEM micrographs assembled in Fig. 20. A higher magnification view of the area on the left side of Fig. 20 is shown in Fig. 21, and, based on the "steps" in the center and right side of this micrograph, it appears this is possibly an area where multiple cracks initiated on the outer surface and advanced toward the ID. Figure 22 shows two higher magnification micrographs of areas in the center and upper right of Fig. 20, and the many small cracks on these surfaces suggest the progression of a crack toward the left. Other areas of the fracture surface have microstructural features that suggest a certain direction of crack motion, but the evidence is not sufficient to unequivocally define the crack path.

Examination of the cross sections through the tube at the 3 and 9 o'clock positions provides some additional information. The micrograph on the left in Fig. 23 shows the cross section through the tube and the remnants of the supporting structure. The center and right micrographs show higher magnifications of the lower left corner of the tube in the first micrograph. The

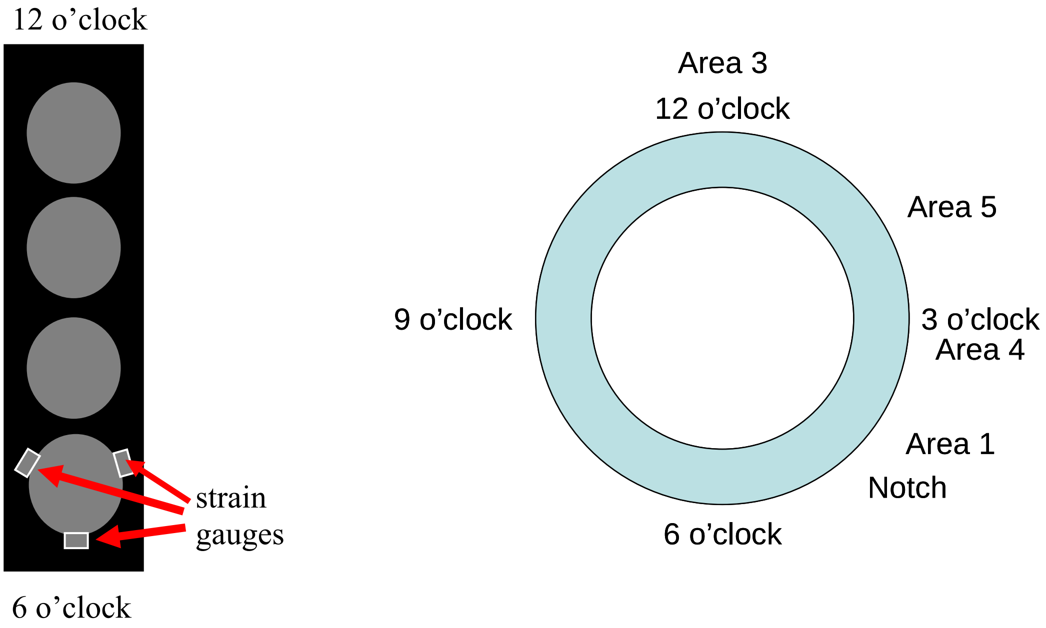

Figure 19. Sketches showing the arrangement of superheater tubes in the platen, the position of strain gauges on the first tubes in platens 5 and 14 and the SEM operator's sketch of the fracture surface of the superheater tube showing the areas examined and their relative position.

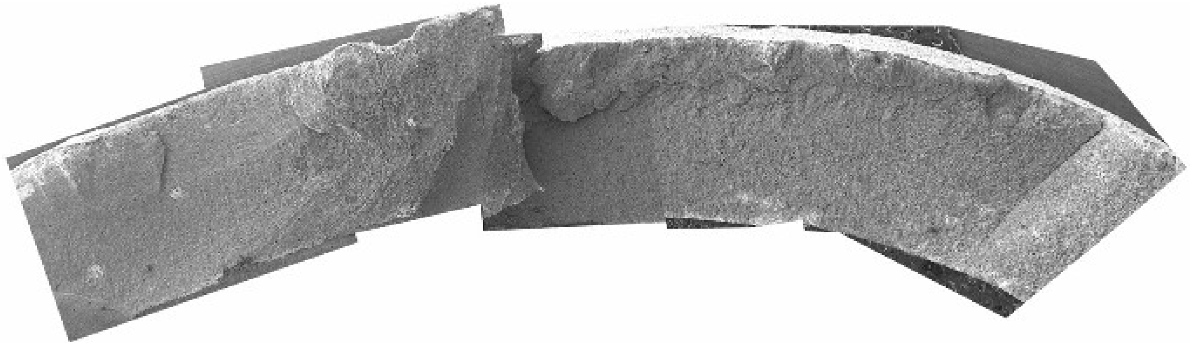

Figure 20. SEM micrographs showing structure of the fracture surface between areas 1 and 4 in the previous figure.

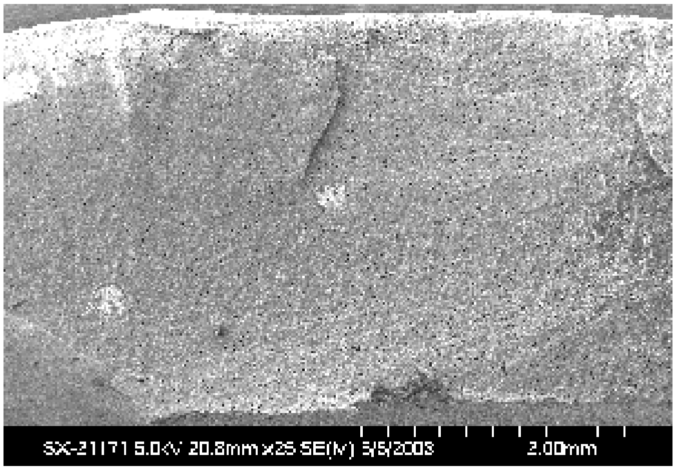

Figure 21. SEM micrograph showing area on the left in the previous figure. Markings on the OD suggest multiple crack initiation sites and a progression of cracks from the OD toward the ID.

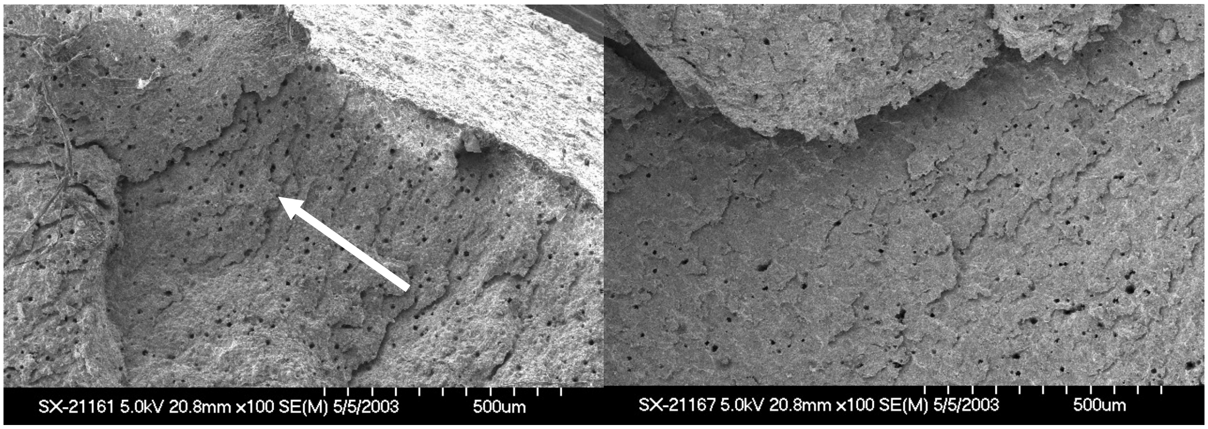

Figure 22. SEM micrographs showing areas to the right and right center in Fig. 20. Both micrographs appear to have secondary cracks advancing into the fracture surface. This type of cracking can be an indicator of fatigue. The arrow indicates the likely direction of crack advance.

micrograph on the right shows that the very edge of the inner diameter (ID) of the tube was deformed in a ductile manner. This deformation could have occurred when the tube failed, or it could have occurred during removal of the tube or during subsequent handling. In any case, failure of this tube was probably the result of slowly progressing crack(s), and the crack(s) likely originated on the outer diameter (OD). A better determination of the crack origin and mechanism in similar tubes was possible with some subsequent studies.

Two other tubes were submitted for examination when leaks were found after a November 2004 shutdown. These tubes are shown in Fig. 24. The remainder of the metal from the high crown seal was ground off these tubes and the tubes were then cleaned in inhibited acid to remove the scale. Dye penetrant examination of both tubes showed strong crack indications (see Fig. 25) along the bottom edge of what had been the weld attaching the tube to the high crown seal. As shown in this figure, three areas were selected for metallographic samples on each tube on the side showing the strongest crack indication, and one sample was cut from the opposite side of each tube. When these tubes were cut open to prepare the metallographic samples, it was obvious, as can be seen in Fig. 26, that both tubes had cracks that penetrated completely through the wall.

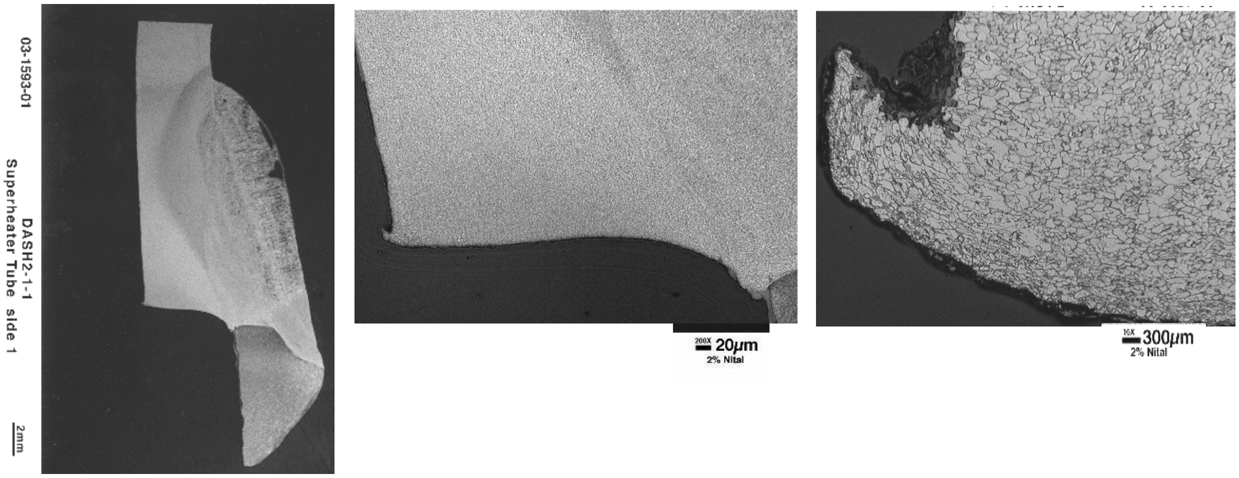

Figure 23. A series of micrographs showing (left) the cross section of the failed tube at the 3 or 9 o'clock position. The center picture shows an enlargement of the lower left corner of the tube, and the right picture shows a further enlargement of the inside edge of the tube. Note the lip indicating a ductile failure on this surface.

Examination of the cross-sections from these two tubes showed through-wall cracks that were wide, filled with corrosion product, and had "fingers" filled with corrosion product that appeared to run roughly parallel to the axis of the tube. The micrographs in Fig. 27 show examples of cracks with a significant amount of the secondary structure that could be cracking or could be corrosion that occurs preferentially along some microstructural defects. This secondary structure suggests the primary cracks were advancing slowly so there was time for a significant amount of corrosion to occur. The other observation of significance gained from examination of these tubes was the fact that the cracks consistently initiated along the heat affected zone of the weld attaching the tubes to the high crown seal. As shown in the micrographs in Fig. 28, the heat affected zone in these two locations extends through the entire tube wall. This indicates significant heating of the tubes when these welds were made.

Destructive Examination Of Unfailed Tubes

Because of the series of superheater tube failures that occurred in the same general area of this recovery boiler, it was decided to remove the first tube from most of the sixteen platens in the intermediate superheater bank on the side of the boiler where the recent failures had occurred. There are 32 platens across the full width of the boiler, but sixteen on the left side had been replaced previously. Of the remaining sixteen, the first tube in three of those platens had already been replaced because of the recent failures. Consequently, the first tube was removed from the remaining thirteen platens plus the second tube from platen #14 as shown in Fig. 29. Approximately 1.2 m (4 ft) of each of the fourteen superheater tubes was removed and sent to the laboratory for examination. Figure 30 shows the fourteen tubes as received with the remnants of the high crown seal box still welded to the tubes. The picture on the left shows a closer view of three tubes and the remnants of the high crown seal.

To prepare the fourteen superheater tube sections for nondestructive inspection, the tubes were cut to approximately 25 cm (10 in.) long sections with the remnants of the crown seal boxes approximately in the center. Much of the crown seal box was sawed off, then grinding was used to remove most of the remaining portion of the seal box. The remaining tube sections were

Figure 24. Sections of two failed intermediate superheater tubes removed during Fall, 2004.

Figure 25. Cracked superheater tubes after dye penetrant examination. Both tubes showed a crack that followed the weld line along the bottom of the tube to high crown seal weld. The vertical lines and the numbers indicate locations from which metallographic samples were cut.

Figure 26. Photos of the inside surfaces of the two tubes shown in the previous figure. Both tubes have cracks that have penetrated through the wall. The crack pattern appears to mimic the directionality of the tube to high crown seal weld.

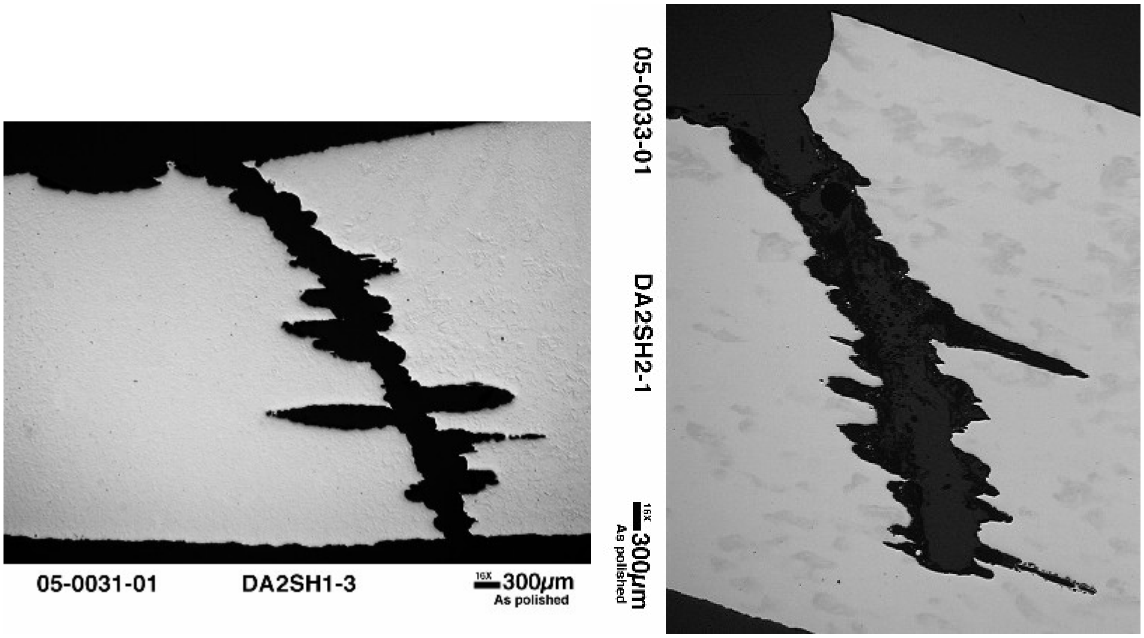

Figure 27. Micrographs of cross sections of the two cracked superheater tubes showing the primary cracks and the areas of secondary attack.

cleaned in an inhibited acid to remove the surface scale without significantly affecting the underlying metal. The cleaned tubes were all inspected with a solvent-based dye penetrant, but no indication of cracks was found on any of the tubes. A second penetrant inspection was conducted on a few of the tubes using the mag particle technique. Again, no crack indications were found.

Following the unsuccessful attempts to find cracks nondestructively, the samples were destructively examined. Rather than try to take a large number of samples from around the circumference of a few tubes it was decided to take four samples from each tube in areas where stresses were presumed to be more highly concentrated. For this examination, the four samples were cut from each tube at 90° intervals at approximately the high and low points on the tube to crown seal weld. Selection of these locations was based on what appeared to be the most likely direction of oscillations, side to side, but it was by no means certain these were the most suitable choices for finding any cracks in the early stages of growth.

The 56 samples were mounted in epoxy, ground, polished then examined microscopically. Photomicrographs were taken of each of the 56 samples in the as-polished condition, then the samples were etched to reveal their microstructures. Micrographs were taken to show the structure in the locations where cracks were thought to be most likely to occur.

None of the samples taken from the high points (6 and 12 o'clock positions in Fig. 19) on the crown seal box to tube welds showed any evidence of cracking. However, shallow cracking was found at the 3 or 9 o'clock positions on four of the fourteen tubes. Micrographs of the as-polished and etched cross-sectioned surfaces are shown in Figs 31 to 35. The micrographs of the crack in the tube from the first row of platen 8 are shown in Fig. 31. This crack is very shallow in the section that was selected for examination, but it is possible that it was somewhat deeper in an adjacent area. In any case, a crack was found, and it originates near the edge of the tube to crown seal weld. On the opposite side of the same tube a second crack was found that goes through about 20% of the tube wall. This crack, shown in Fig. 32, originates at the notch where the tube and high crown seal meet. The crack shows no evidence of branching but contains some corrosion product. The crack also has some wide areas near the surface that are indicative of corrosion that has occurred in a slowly advancing crack.

The first tube in platen 11 also had a crack that originated near the tube to high crown seal intersection, and this crack also advances about 20% of the way through the tube wall. This crack, which is shown in Fig. 33, is straight, narrow and filled with corrosion product and

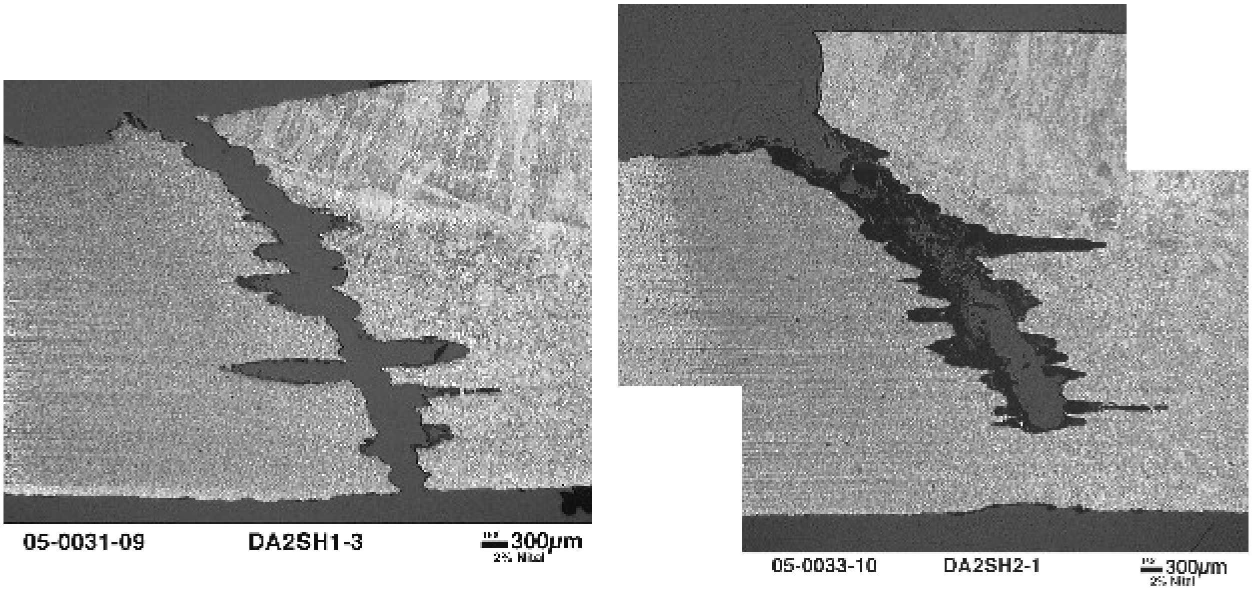

Figure 28. Micrographs of the etched cross sections of the two superheater tubes shown in the previous figure. Cracks are in the heat affected zone next to the weld metal.

appears to run along the edge of the weld heat affected zone. Figure 34 shows a shallow crack in the first tube of platen 12. This crack is very shallow, has no apparent branching and originates at the edge of the weld heat affected zone. The other crack that was detected was found in the second tube of platen 14 even though no cracking was detected in the first tube in this platen. As seen in Fig. 35, this crack is straight, filled with corrosion product and has a region apparently widened by corrosion in the area where the crack originated. From the micrograph of the etched sample, it is evident that the crack originates near the edge of the weld heat affected zone.

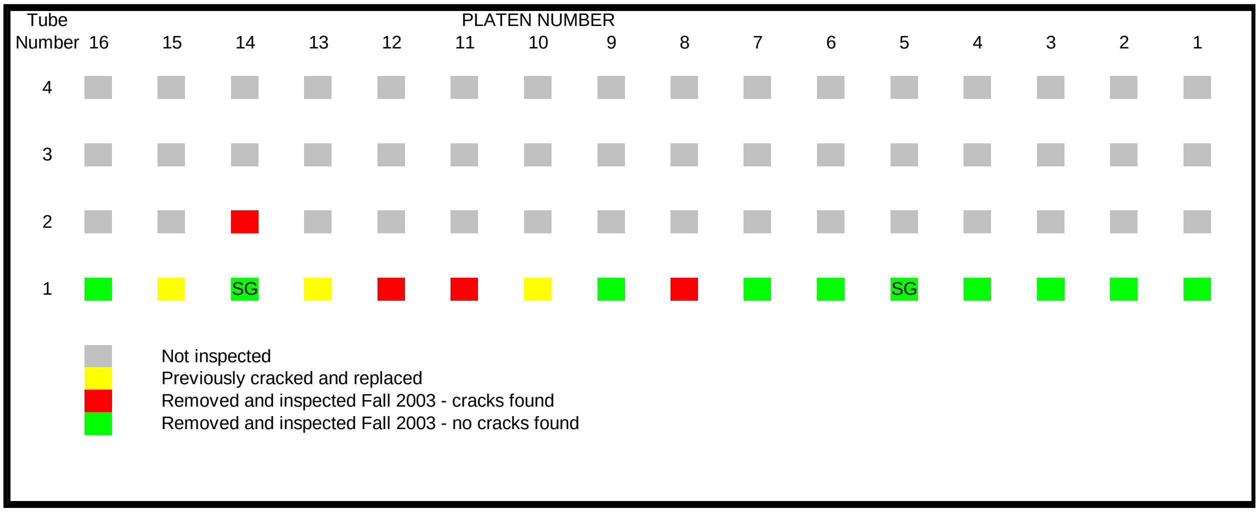

Tube Number	16	15	14	13	12	11	10	9	8	7	6	5	4	3	2	1
	PLATEN NUMBER															
4	⬜	⬜	⬜	⬜	⬜	⬜	⬜	⬜	⬜	⬜	⬜	⬜	⬜	⬜	⬜	⬜
3	⬜	⬜	⬜	⬜	⬜	⬜	⬜	⬜	⬜	⬜	⬜	⬜	⬜	⬜	⬜	⬜
2	⬜	⬜	🟥	⬜	⬜	⬜	⬜	⬜	⬜	⬜	⬜	⬜	⬜	⬜	⬜	⬜
1	🟩	🟨	🟩 SG	🟨	🟥	🟥	🟨	🟩	🟥	🟩	🟩	🟩 SG	🟩	🟩	🟩	🟩

⬜ Not inspected
🟨 Previously cracked and replaced
🟥 Removed and inspected Fall 2003 - cracks found
🟩 Removed and inspected Fall 2003 - no cracks found

Figure 29. Sketch showing arrangement of superheater tubes in the area where the study was being conducted. As shown by the color coding, three tubes were replaced because of cracking around the time this study began, and four of the tubes removed in Fall 2003 were found to have cracks.

Figure 30. Fourteen unfailed superheater tubes removed from the intermediate superheater for inspection to determine if any cracking has occurred.

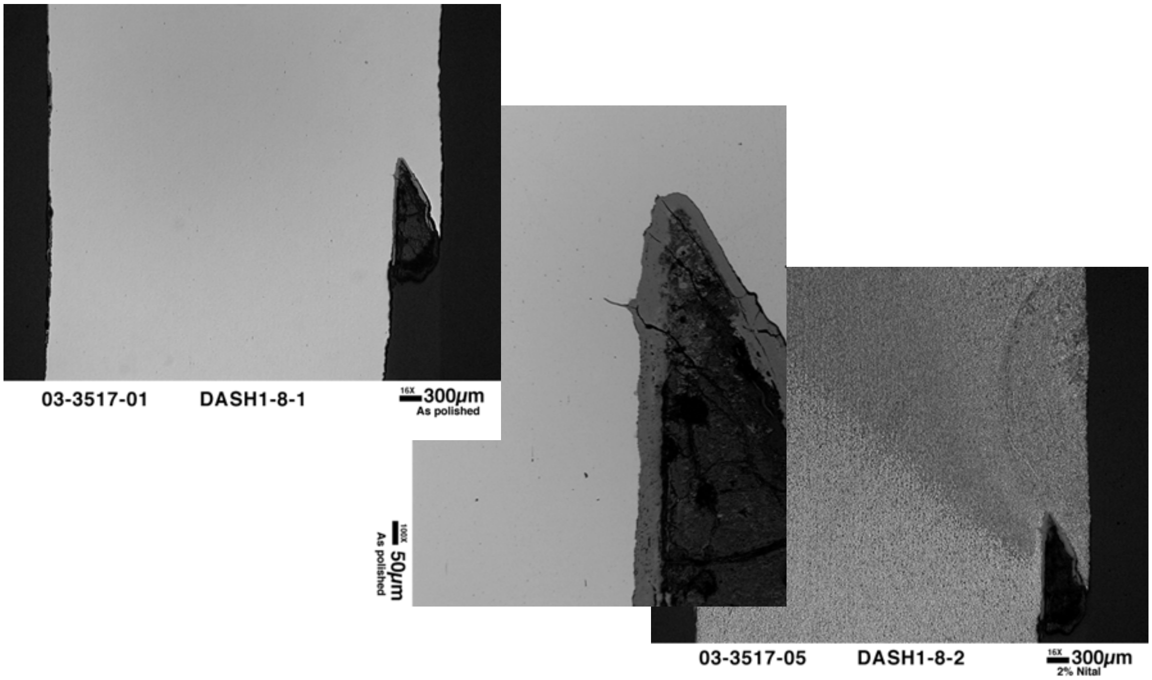

Figure 31. Micrographs showing the cracking on one side of the first tube from platen 8.

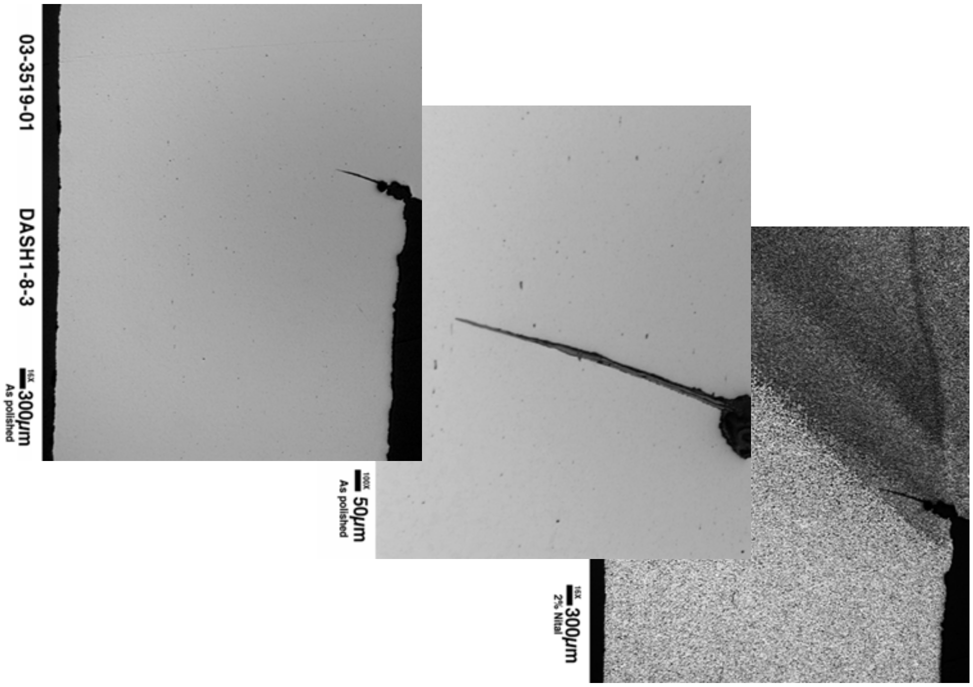

Figure 32. Micrographs showing the cracking on the other side of the first tube from platen 8.

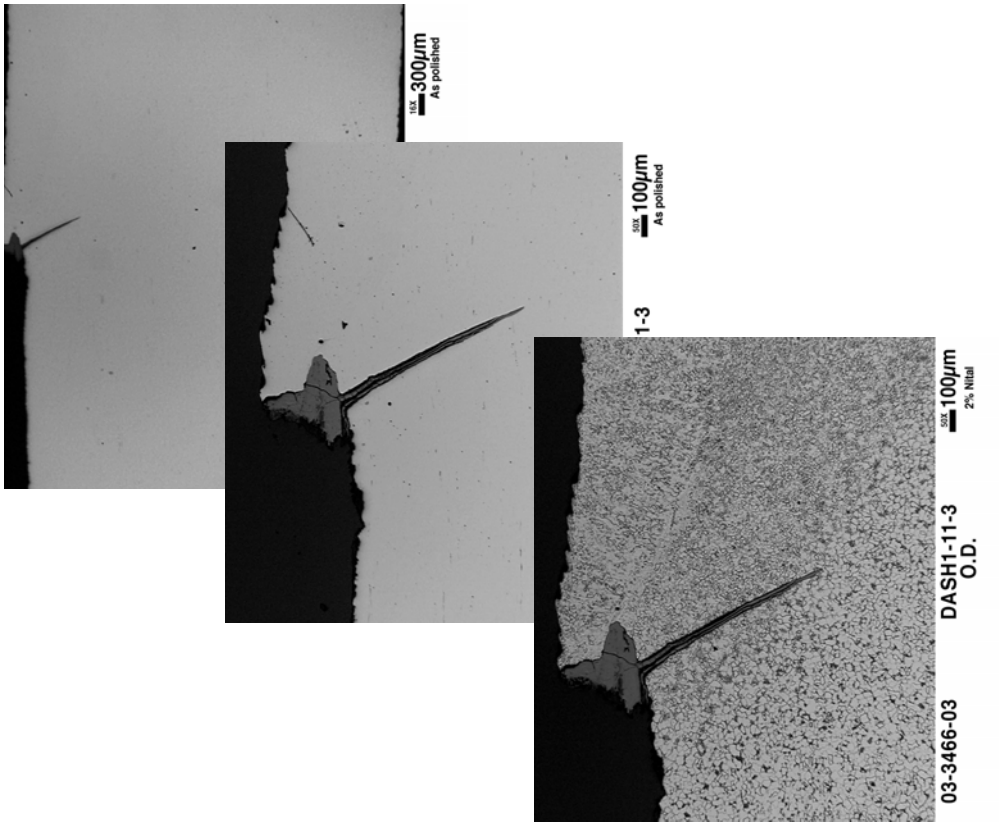

Figure 33. Series of micrographs showing the cracking in the first tube in platen 11.

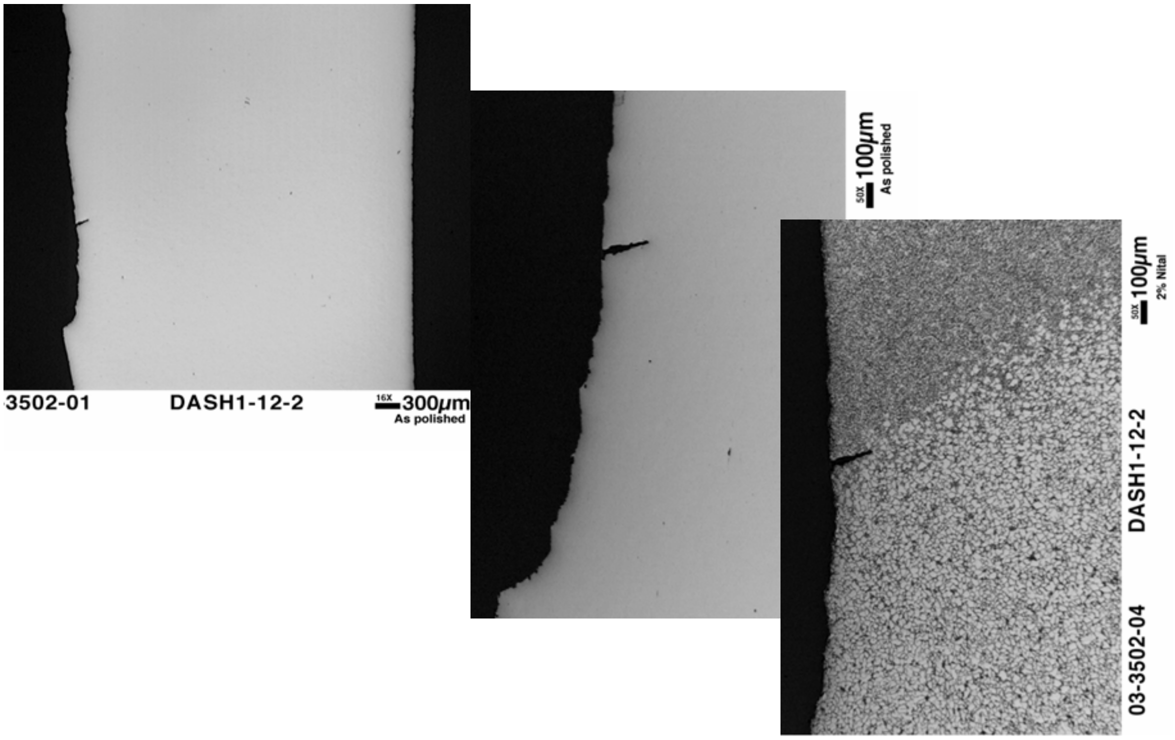

Figure 34. Series of micrographs showing the cracking in the first tube in platen 12.

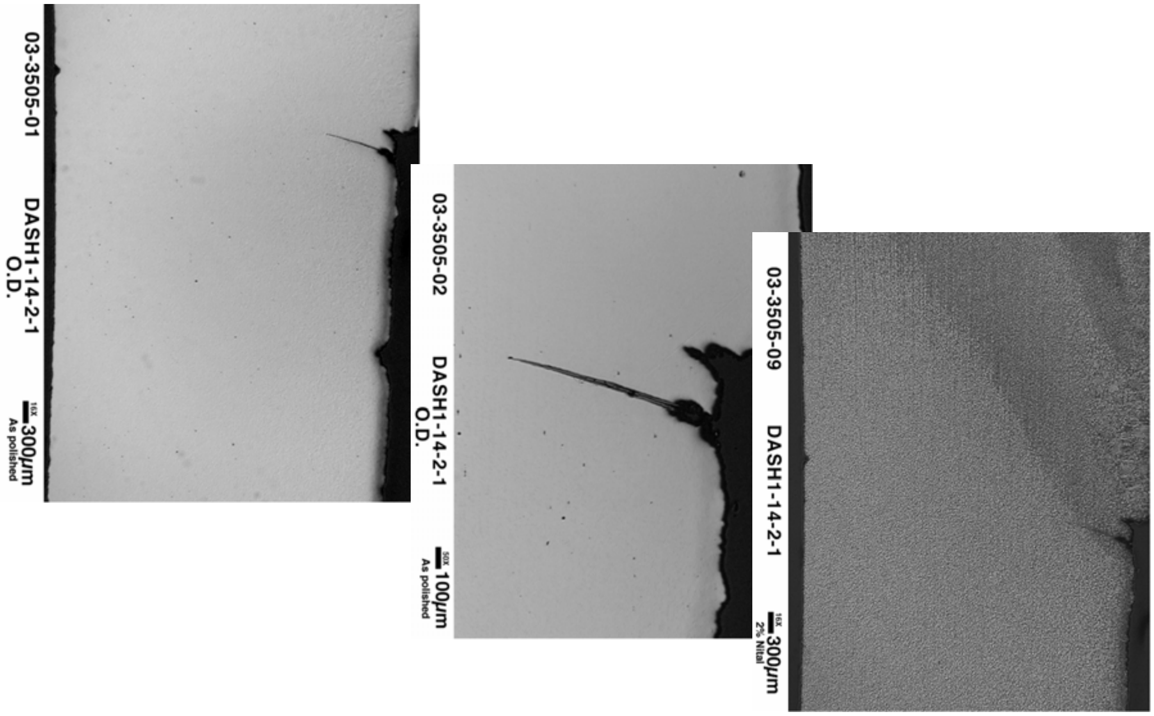

Figure 35. Series of micrographs showing cracking in the second tube from platen 14.

It is worth reiterating that for all the tubes examined, the region selected for examination was not based on information obtained from a dye penetrant inspection; it was chosen to be at or near the “low point” in the tube to crown seal weld. Consequently, the crack depth observed is quite possibly not the deepest penetration of this crack into the tube. It is also possible that some relatively short, shallow cracks might have been missed when areas were selected for examination.

From these examinations it is apparent that a significant portion of the tubes, 4 of 14, had existing cracks, and in three cases, these cracks extended about 20% of the way through the tube wall. Based on the corrosion product in the cracks and the corroded regions at the origin of some of the cracks, these cracks have not been progressing rapidly, but the sharp tips on most of the cracks suggest the cracks could still be advancing through the tube wall. The characteristics of the cracks (transgranular with minimal branching, slowly advancing, etc.) indicate mechanical fatigue is the likely cause of the tube cracking.

Strain Gauge Installation And Data Analysis

The fairly recent failure of three tubes in the same general superheater area, apparently by a mechanical fatigue mechanism, introduced the question of what could be causing oscillations of these superheater tubes. To try and address this question, three high temperature (750 °C) strain gauges were installed on each of two superheater tubes. The tubes on which the strain gauges were to be installed were selected from the locations where tubes had already been removed.

Another consideration in the selection of installation locations was to have one tube near the center of the boiler and one tube near the right side of the boiler.

In advance of the mill shutdown, six high-temperature strain gauges and two sections of superheater tubing were ordered. Because of the very sensitive nature of the strain gauges, the manufacturer installed the gauges on two sections of new superheater tubing. The strain gauges were installed so they were oriented to measure axial strains and were positioned 120° apart around the circumference of the tubes. To provide some protection for the strain gauges, a protective metal cover was positioned over each gauge and then tack welded to the tube. Figure 36 shows one of these tube sections, before installation, lying so that the strain gauge shields and the wires are easily seen. Figure 37 shows a series of pictures that give some indication as to how the tubes and strain gauges were installed. For both tubes, one of the strain gauges was intentionally positioned so that it was in the plane defined by the row of superheater tubes. This gauge was designated as #1 and was defined as being in the 6 o'clock position (see Fig. 19). Consequently, the other two strain gauges were in approximately the 10 and 2 o'clock positions around the circumference of the superheater tubes. A sheathed thermocouple was also mounted on each of the two instrumented tubes in the same area where the strain gauges were mounted.

The strain gauge and thermocouple wires were led out of the boiler "penthouse" area to the closest location outside the boiler where an instrument box could be mounted. This instrument box contained the appropriate signal conditioners for the strain gauges and the modules for translation of the thermocouple measurements. This instrumentation was connected by a cable to a computer housed in a nearby air conditioned room. This computer was equipped with software that collected strain and temperature data every second then stored this data in files created on

Figure 36. Section of superheater tube with thermocouple and strain gauges mounted and a special protective cover installed.

Figure 37. Photos showing the installation of superheater tube with strain gauges. In the picture on the left, the #2 tube has been installed in platen 14, but the hole is still empty where tube #1 with the strain gauges will be installed. In the center photo, the #1 tube with strain gauges is in position, and in the picture on the right, the tube is welded in place and the strain gauge and thermocouple wires extend through a specially made opening.

the hard drive. Other software permitted the computer, when connected to a telephone line, to be accessed by a remote computer and the data downloaded to this second computer. The data were downloaded regularly and then analyzed to provide some information on the temperature and motion of the two instrumented superheater tubes.

An example of the data collected in one day is shown in Fig. 38. More detailed information can be acquired if only about 15 minutes of data are included in a plot as shown in Fig. 39. The periodic spiked regions seen in Fig. 38 are shown in more detail in Fig. 39. Careful examination of the signals from the three strain gauges on a tube show that the signal from strain gauge #1 is almost constant while the other two strain gauges show oscillating patterns. Closer examination of the signals from strain gauges #2 and #3 shows they are 180° out of phase. When one is increasing, the other is decreasing which together with the information from gauge #1 indicates the tube is swinging in a side to side motion approximately perpendicular to the plane defined by the tube platen.

In addition to identification of the swinging motion, the data also provide information on the cause of the oscillations. There is a clear pattern in which oscillations are excited in the first tube of platen 5 followed within about a minute by oscillations in the first tube of platen 14. For example, in Fig. 39 strain gauges #2 and #3 (the 10 and 2 o'clock positions) on platen 5 begin showing oscillations just before 8:21 while the equivalent strain gauges on the tube in platen 14 begin oscillating at 8:22. This is followed about a minute later by another set of oscillations of the tube in platen 5. This sequence is repeated a short while later but with higher magnitude oscillations. Over the period shown in Fig. 39, there are 5 sets of these oscillation sequences. These sequences can be explained by sootblower operation. As a sootblower advances into the boiler, it first blows high pressure steam on the lower number platens, including platen 5. The sootblower advances into the boiler and about a minute later blows steam on platen 14. This sootblower advances as far as platen 16, then it retracts and blows steam on platen 14 and eventually on platen 5. Examination of the sootblower schedule has shown that these sets of oscillations correlate with the sootblower sequence. Several different sootblowers can cause oscillations in these superheater platens, and the difference in the magnitude of the oscillations is determined by the proximity of the sootblower to the superheater tubes.

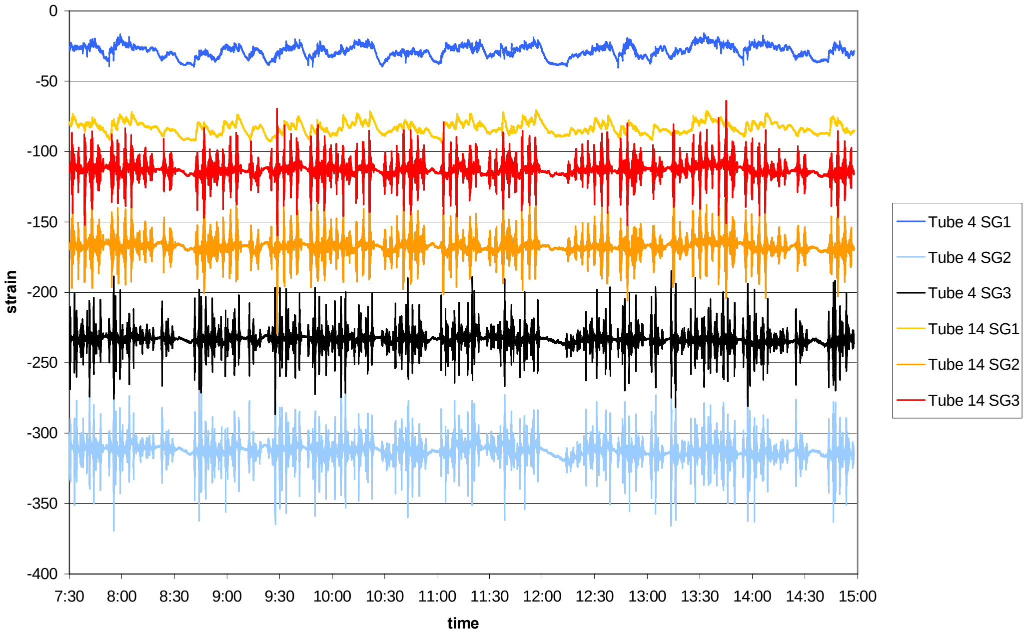

Figure 38. Strain gauge data for a typical day of "clean" boiler operation.

The oscillations set in motion by the sootblowers did not remain at a constant magnitude. Over a period of months, the magnitude of the oscillations changed. Such a pattern is shown in Fig. 40 where the number of cycles varies significantly over the 3 month period of March through May. Fig. 41 shows the strain gauge data for a 10 minute period on the three dates noted in Fig. 40; March 1, April 13 and May 18. Small but discernable oscillations are shown on March 1, but by April 13 the oscillations are almost completely suppressed on both tubes. Near the end of the first week of May, the oscillations resume at a fairly intense level. The suppression of oscillations can be attributed to plugging in the superheater area, and the resumption of oscillations is associated with a cleaning operation in the sootblower area.

Another piece of information that might be available from the strain gauge data is an indication of the total load applied to the tubes by the deposits collecting on the tube. The daily average axial strains shown in Fig. 42 indicate significant changes are seen by some strain gauges. For example, four of the six gauges show a decrease in loading around the first of May, 2004. This happens again in late October, 2004 and mid-April 2005. The significance of these changes is not as well understood as for the short term oscillations, but efforts are continuing to find the association with superheater cleaning operations.

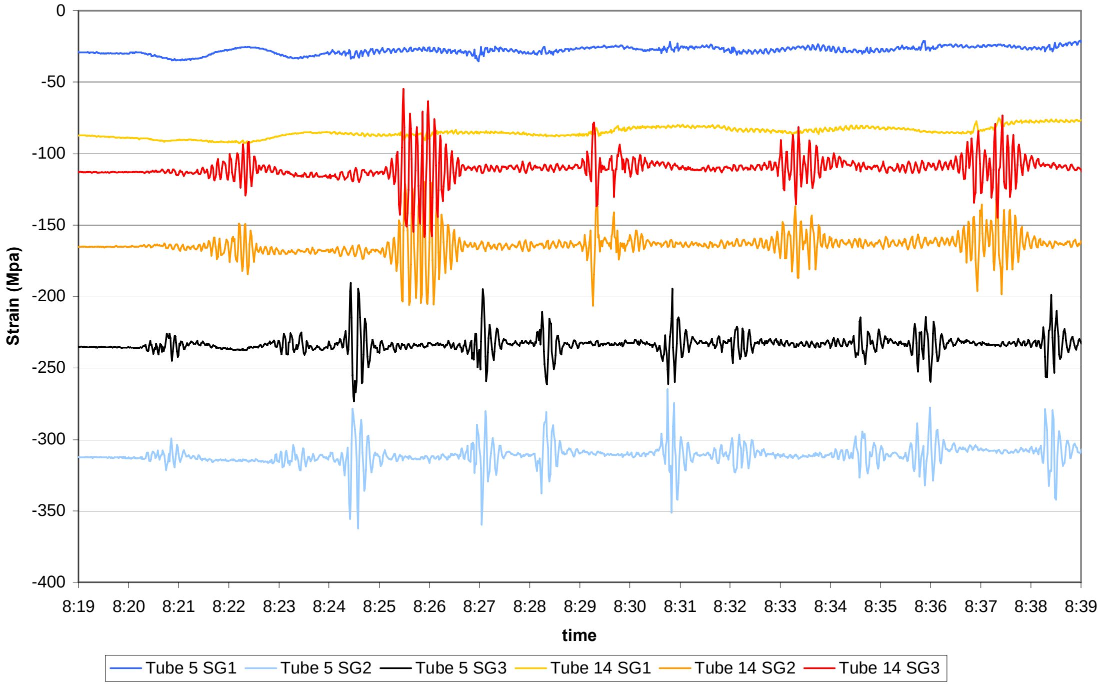

Figure 39. Strain as a function of time for a selected 20 minute period on May 17, 2004. Note the 5 sequences of cycling that corresponds to sootblower operation.

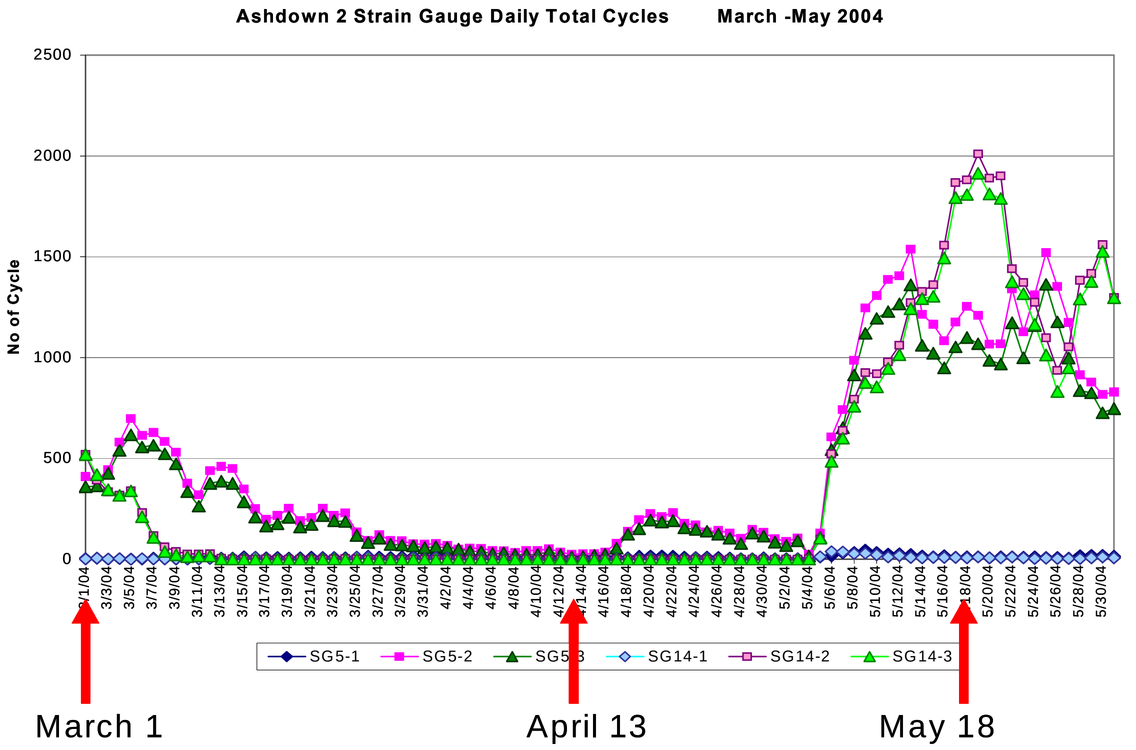

Figure 40. Number of cycles measured during a three month period in 2004. The patterns provide information on the extent of plugging in the superheater area.

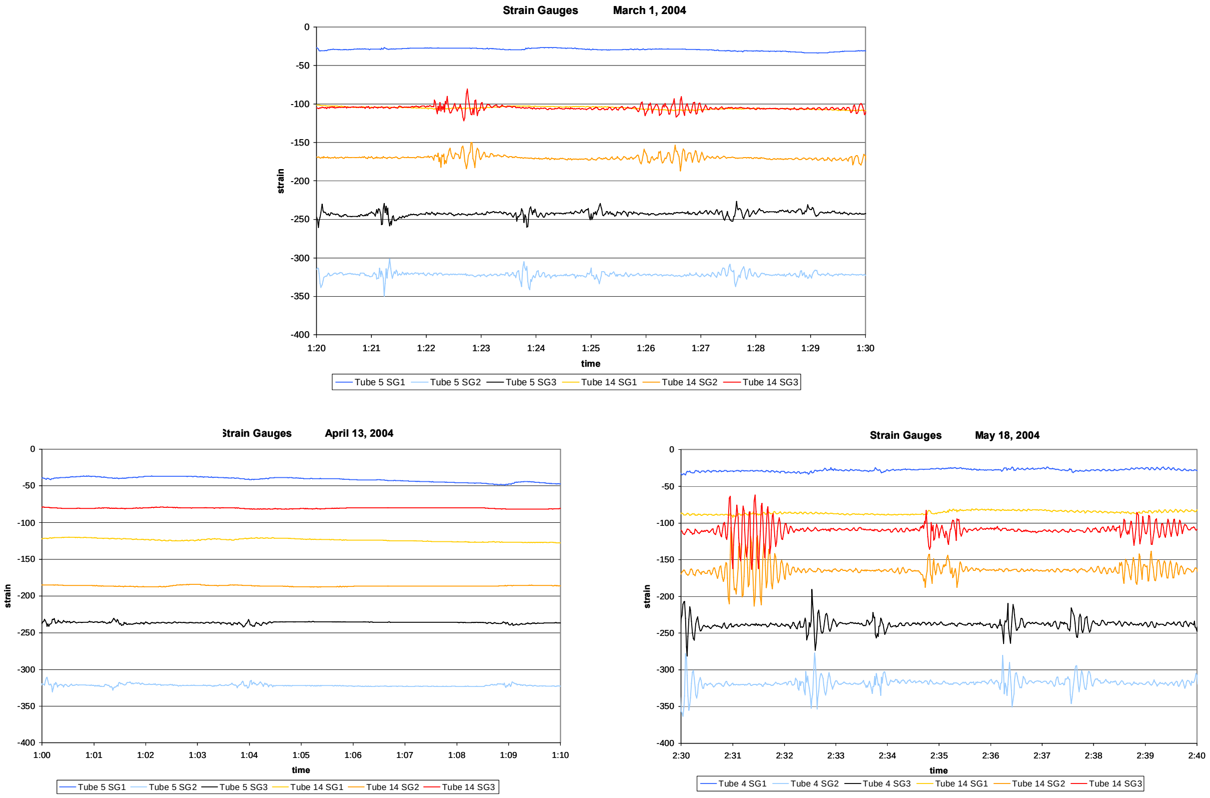

Figure 41. Strain gauge data for the three periods highlighted in Fig. 40. Note that the oscillations are almost completely suppressed during the April period.

Perhaps the most important observation is the translation of the magnitude of the oscillations to stresses on the tubes. As can be seen in Figs. 39 and 41, the largest oscillations have a magnitude of about 100 microstrain units, and most are of significantly lower value. It should be noted these measurements are not at the 3 and 9 o'clock positions where the strains are postulated to be at a maximum. However, geometric considerations suggest there will be less than a 20% difference in the strains between the 2 and 3 o'clock positions. In any case, even with strains of 100 to 120 microstrains, the loading on the tubes calculates to be a few ksi which is not a sufficiently large load to result in crack initiation in carbon steel tubes. According to the Metals Handbook, the stress necessary for development of fatigue cracks is on the order of half the ultimate tensile strength which is about a factor of ten greater than the stress resulting from the oscillations [30,31]. This stress would likely be sufficient to cause propagation of existing cracks, which is consistent with the observation of cracks in several tubes removed and destructively examined and the periodic failure of superheater tubes that continues to occur in this boiler. This suggests that sometime during the early years of operation the tubes had much higher amplitude oscillations, but changes in the platen restraint mechanism reduced the maximum oscillations to the current level. These changes are most likely the steam cooled spacers that were installed many years ago.

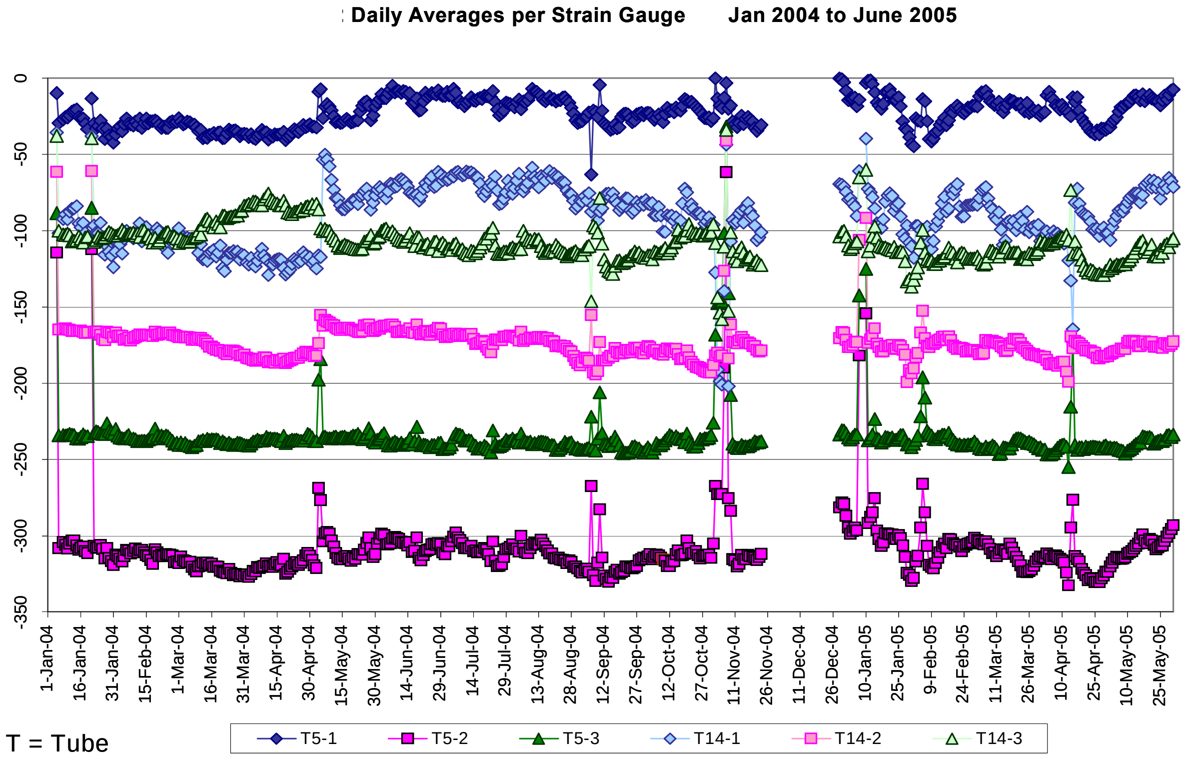

Figure 42. Daily averages of strain value as a function of time for the six strain gauges over a period of 18 months.

SUPERHEATER CORROSION AND ALLOY PERFORMANCE IN CURRENT GENERATION HIGH PRESSURE RECOVERY BOILERS

Another subtask in the superheater activity concerned laboratory and field studies of alternate materials for superheater tubes. As noted previously, the background information was collected and the laboratory corrosion studies were conducted by staff members of FPInnovations-Paprican in their Vancouver, BC laboratories. The field studies were conducted by ORNL staff members.

Corrosion of superheaters is generally not an issue in recovery boilers that are operated at a steam temperature below 450°C [32]. In current generation HP boilers, steam temperatures are somewhat higher, usually ranging from 480°C to 500°C. It is generally accepted that accelerated corrosion of superheaters in a HP recovery boiler is mainly caused by molten salt attack [32-36]. Molten salts are generally a good fluxing agent, effectively removing protective metal oxide scale from an alloy surface. Accelerated corrosion proceeds primarily by oxidation, which is then followed by dissolution of metal oxides in the melt.

Superheater deposits consist mainly of sodium sulfate (Na_2SO_4) and sodium carbonate (Na_2CO_3) with small amounts of sodium sulfide (Na_2S), sodium chloride (NaCl) and similar potassium (K) salts [32,37]. The first melting temperature (FMT) of the deposit depends on the concentration of potassium, carbonate (CO_3^{2-}) and sulfide (S^{2-}) in the deposit, typically ranging from 520°C to 580°C [37]. Another critical factor is the proportion of liquid phase present at the first melting temperature (FMT) which strongly depends on the chloride concentration [38]. Reported field studies and operating experience consistently show that the corrosion rate of superheater tubes increases rapidly when the first melting point of the deposit is exceeded, and more so if the molten deposit contains sulfide or reduced sulfur compounds [33,39-44]. In the past, many superheater corrosion problems were often caused by molten acidic sulfate deposits containing sodium and potassium bisulphate [$(Na,K)HSO_4$] and pyrosulfate [$(Na,K)S_2O_7$] salts, which are stable at elevated concentrations of acidic sulfur gases (SO_x) [39]. However, as recently discussed, typical SO_x levels produced with current operating practices are not, under almost any circumstances, high enough to promote corrosion by the formation of these molten acidic sulfate salts [34].

Superheater design for low pressure (<6,000 kPa), (LP) recovery boilers traditionally has been governed by the need to achieve a balance between performance (steam temperature and pressure) and plugging. Relative to other boilers, recovery boilers have a much higher particulate flux through the superheater section, and, consequently tend to plug more easily [45]. Side-to-side spacing (across the bank), tube size and mechanical design (including support) has varied throughout the decades to accommodate overall boiler design [46,47]. Low alloy steels have been commonly used for superheater tubes in LP boilers, with the selection generally governed by similar design constraints as for other types of boilers, namely high temperature strength, creep resistance, oxidation resistance and economics. Table 3 identifies those low alloy steels most commonly used along with the recommended maximum allowable tube temperature.

Table 3. Typical superheater tube materials in LP/HP kraft recovery boilers

Specification		Nominal Composition (wt.%)						Max. T[1] (°C)
ASME	UNS	Fe	Cr	Ni	Mo	Cu	C	
SA-209T1A	K12023	Bal.	- - -	- - -	0.44-0.65	- - -	0.15-0.25	524
SA-213T11	K11597	Bal.	1.0-1.5	- - -	0.44-0.65	- - -	0.05-0.15	566
SA-213T22	K21590	Bal.	1.9-2.6	- - -	0.87-1.13	- - -	0.05-0.15	602
SA-213T91	K90901	Bal.	8.5-9.5	- - -	0.85-1.05	- - -	0.08-0.12	649
SA-213T304	S30400	Bal.	18.0-20.0	8.0-11.0	- - -	- - -	0.08 Max.	760
SA-213TP347H[2]	S34709	Bal.	17.0-20.0	9.0-13.0	- - -	- - -	0.04-0.10	760
SA-213TP310H[3]	S31009	Bal.	24.0-26.0	19.0-22.0	- - -	- - -	0.04-0.10	816
SB-407-800H	N08810	Bal.	19.0-23.0	30.0-35.0	- - -	0.75 Max	0.10 Max.	816
Sanicro™ 28[3]	N08028	Bal.	27.0	31.0	3.5	1.0	0.02 Max.	N/S[4]

[1] Recommended maximum use temperature for superheater tube use in fossil-fired boilers [48].
[2] Nb/Ta content of not less than eight times the carbon content and not more than 1.0 wt.%.
[3] Fabricated as a co-extruded composite tube; exterior layer over a SA-213T22 core.
[4] N/S = Not Specified

For superheaters in HP recovery boilers, a balance between performance, plugging and corrosion is required. With respect to corrosion, a key superheater design constraint is to maintain tube temperatures below the first melting point of the deposits. Temperatures are reduced by ensuring relatively low flue gas velocity, ensuring relatively high steam flow through each tube, arranging for the coolest steam to flow through tubes exposed to hottest flue gas, and locating the majority of the superheater sections behind the bull nose (furnace arch), shielded from radiation [46,47]. This design philosophy has permitted the widespread use of the less-expensive low alloy steels as superheater tube materials. However, such application has not been without problems.

Reported experience with HP superheaters fabricated entirely of low alloy steel, revealed rapid corrosion at the bottom bends, with measured rates ranging from 0.3-0.6 mm/y [33,39,44] to as high as 2.4 mm/yr [49]. The cause in each case was attributed to elevated temperatures of the lower bends. Based on the various resistances to heat transfer, the surface temperature of a superheater tube is expected to be about 30 to 50C° hotter, or higher if affected by direct radiation, than the steam temperature inside the tube [50,51]. In addition, the tube temperature may be 20C° hotter on the windward side than on the leeward side [43]. Note also that the individual tube steam temperature can vary ± 23C° from the average across the steam manifold [52]. The resultant combined increase may be beyond the FMT of the deposit depending upon the composition.

Replacing the low alloy steel lower tube bends with higher chromium-containing, more corrosion-resistant alloys has been one approach used to address the accelerated corrosion observed. A listing of the more typical alloys used is also provided in Table 3. The selection of these alloys was based largely on prior field testing using air-cooled probes [33,39-44]. Reported experiences of using these upgrades have been positive for the most part. A summary of preliminary experience (no more than seven years service) of austenitic stainless steel lower tube bends installed in Finnish HP recovery boilers (480°C/8,000 kPa superheater units) was published some time ago [53]. As reported, the corrosion rate of the installed tube bends, fabricated from Type 304, 304L, 321 and 347 stainless steel, was around 0.1 mm/yr, with no significant differences found between the various grades of stainless steel used. There are also limited reports of low corrosion rates observed on Alloy 800H lower tube bends installed in Canadian HP recovery boilers (482°C/6,200 kPa superheater units); one based on a little more than two years of service [40], and the other based on about twenty years of service [54].

However, there have been reported cases in which these alternatives have experienced accelerated corrosion. A summary of these cases is provided in Table 4. A reported case of accelerated corrosion exists for each of the major alloys used as replacement upgrades, with the exception of Alloy 28 for lower superheater tube bends. Alloy 28 tube bends have been installed in Swedish, Brazilian and Finnish HP recovery boiler since 1994 [55]. An elevated tube temperature was identified as the root cause of the accelerated corrosion in each of the reported cases. This conclusion is consistent with the findings of the air-cooled probe studies, which show corrosion of these alternative alloys increases rapidly when the first melting point of the deposit is exceeded [33,39-44].

In addition to the fireside corrosion issues noted above, the reliability of superheaters in recovery boilers is also strongly affected by stress-related problems. Given that the superheaters are suspended through the roof and hang freely in the flue gas environment, they are susceptible to a combination of mechanical and thermal static and/or cyclic stresses, during start-ups, operation and shut-downs. As recently discussed, these problems can results in distortion (in-plane and out-of-plane) of the assembly, cracks at attachments, or crack-induced tube leaks [57]. Another cause for concern is waterside stress corrosion cracking. As reported in the literature, the monolithic authentic stainless steel tube bends are likely more susceptible [58].

Table 4. Reported cases of accelerated lower tube bend corrosion of replacement alloys

Tube Alloy	Design Steam T (°C)	Design Steam P (kPa)	Tube T (°C)	Deposit FMT (°C)	Corrosion Rate (mm/yr)	Ref.
SA-213T304	480	8,000	N/R	N/R	N/R	[42]
SA-213T304	480	6,500	N/R	N/R	N/R	[42]
SA-213TP347H	480	8,000	N/R	N/R	2.4-3.6	[49]
SA-213TP347H	480	8,000	N/R	N/R	0.3-1.6	[49]
SA-213TP347H	480	8,000	N/R	N/R	1.5	[49]
SA-213TP347H	482	8,620	> 590	520	1.0-2.0	[43]
SA-213TP310H/SA-213T22	454	6,200	> 590	560	1.0-2.0	[56]
SB-407-800H	482	6,200	N/R	N/R	0-1.4	[54]

*N/R = Not Reported.

Superheater Corrosion And Control In Next Generation HT/HP Recovery Boilers

Next generation HT/HP recovery boilers, which are operated at a steam temperature of 500 to 515°C and a steam pressure of 9,900 to 10,900 kPa, already exist in Japan [59-62]. Key design features implemented that help control superheater tube corrosion are reported by the boiler manufacturer to include the installation of non-process element (NPE), namely potassium and chlorine, removal equipment downstream of the recovery boiler, use special austenitic (25Cr-14Ni) stainless steels, and a large number of sootblowers. Reducing the potassium and chlorine content in the liquor cycle helps to control corrosion by lowering the potassium and chlorine content in the deposits that form on the superheater tubes, which in turn increases the FMT [37] and decreases the proportion of the liquid phase present [38], respectively. The special stainless steels were developed with input from laboratory studies, as well as from operating experience [59,63,64]. Table 5 documents the nominal compositions of the three grades developed. The original grade YUS170 was used in early HT/HP recovery boilers. The latest grade MN25R was developed to improve the strength at high temperatures and to increase the (intergranular) corrosion resistance. Experience reported has been positive with these alloys, except when there has been contact with a high sulfur dioxide (SO_2) concentration in the flue gas, and with deposits enriched in chlorine (as chloride) [61]. There was no mention of a waterside stress corrosion cracking concern. It is noted that no independent confirmation of boiler operation and/or superheater tube performance has been reported in the public domain.

The recent interest in implementing the next generation HT/HP recovery boilers in Finland has also initiated laboratory-based research and development programs designed to identify more corrosion resistant alloys from which to fabricate superheater tubes [35,65-67], in addition to those conducted in Japan [59,63,64]. An overview of the alloys and testing conditions studied is provided in Table 6. As the summary shows, a wide range of alloys have been tested in a wide range of salt mixtures, exposed to a wide range of cover gas mixtures, for a wide range of times.

In spite of the many inconsistencies among the testing parameters, these studies have generated a reasonably consistent set of results, and thus conclusions regarding corrosion above the FMT. Major findings are summarized as follows.

- Corrosion increases significantly at temperatures above the FMT, the extent of which increases with the amount of molten phase present at a given temperature.
- The corrosion mode is mostly localized (pitting and intergranular attack), consistent with a mechanism involving attack by a molten chloride-containing salt, and does not require an interaction with SO_2 or HCl in an O_2-containing gas phase.
- Alloys with higher chromium contents have a higher corrosion resistance, more so, if molybdenum and nitrogen are present as additional alloying elements.
- Finally, the removal of non-process elements (NPE) (potassium and chlorine) from the chemical recovery process is a critical part of corrosion control.

In contrast, the conclusions drawn from these studies regarding the corrosion of alloys below the FMT are less consistent. There is a consensus that the risk of corrosion below the FMT by the so-called “active-oxidation” mechanism [68,69] is low for the set of alloys studied, with the exception of the low alloy steel grade SA-213T22. Active oxidation involves the formation of Cl_2/HCl gas within a chloride-containing deposit, which then migrates to the alloy/scale interface, where the partial pressure of oxygen is low, and then reacts to form volatile metallic chlorides. As the vapor pressure of the metallic chloride products is considerable at the typical heat transfer surface temperatures involved, continuous sublimation occurs, and the gaseous metallic chlorides diffuse towards the scale/flue gas interface. Upon reaching regions with high oxygen (O_2) partial pressures, the gaseous metallic chlorides react with O_2/water vapor (H_2O) to form solid oxides, releasing Cl_2/HCl. The resulting scale is almost detached from the substrate and offers little protection.

Table 5. Superheater tube materials in HT/HP recovery boilers in Japan

Grade	Nominal Composition (wt.%)							
	Fe	Cr	Ni	Mo	Mn	Si	N	C
YUS170	Bal.	23.0-26.0	12.0-16.0	0.5-1.2	< 2.0	< 1.5	0.25-0.40	< 0.06
HR-2EL	Bal.	21.0-23.0	12.5-15.5	1.0-2.0	2.5-3.5	< 0.5	0.10-0.25	< 0.02
MN25R	Bal.	23.0-26.0	13.0-16.0	0.5-1.2	< 2.0	< 0.7	0.25-0.40	< 0.025

Several studies [65,70] conclude that, below the FMT, KCl-containing recovery boiler deposits are more corrosive than NaCl-containing ones, whereas others report the opposite [71,72]. Another controversy involves the critical temperature at which active oxidation initiates for stainless steel alloys. Based on a laboratory test, corrosion of stainless steel by active oxidation was found to be moderately dependent on temperature in a range from 550 to 650°C, and strongly dependent on temperatures at temperatures in excess of 650°C [73]. However, a recent study documenting the corrosion of high alloy superheater tubes in a waste-wood fluidized-bed boiler shows the critical temperature may be as low as 500°C for stainless steel [74].

Table 6. Laboratory superheater tube corrosion testing for HT/HP recovery boilers

Alloys	Deposit Composition				FMT	Environment	Ref.
316, 321, 347 YUS170	NaCl	K	Cl	S		Gas: Not Reported Temperature: 480-520 °C Time: Not Reported	[59]
	10%	5%	N/R	N/R	N/R		
	5%	10%	N/R	N/R	N/R		
	10%	10%	N/R	N/R	N/R		
321 YUS170,MN25R	NaCl	K	Cl	S	550 °C	Gas: $0.005\text{-}1\%SO_2\text{-}5\%O_2\text{-}10\%CO_2\text{-}N_2$ Temperature : 500-600 °C Time: Not Reported	[63]
	N/R	5%	3%	N/R			
	[56%(Na,K)SO_4-6.5%NaCl]						
304, 316, 316L, 321, 347, 310,170, N71, HR3CL,A600, A800	Na	K	Cl	S	523 °C	Gas: $0.25\text{-}1\%SO_2\text{-}1\%O_2\text{-}15\%CO_2\text{-}N_2$ Temperature: 450-650 °C Time: 20 Hours	[64]
	34.3%	16.2%	3.9%	12.7%			
T22, 304L,HR3C, 170NBB,AC66,45TM SAN28, A625	Na_2SO_4	Na_2CO_3	NaCl	KCl		Gas: Air; Air + HCl, SO_2, CO_2 or H_2O Temperature: 525 °C Time: 2-65 Hours	[65]
	59%	0%	6.5%	34.5%	N/R		
	37.3%	28%	15.3%	19.3%	N/R		
T11 304L 310 A625	Na_2SO_4	K_2SO_4	NaCl	KCl		Gas: Air Temperature: 440-590 °C Time: 6-168 Hours	[66]
	49.5%	49.5%	0.5%	0.5%	525 °C		
	47.5%	47.5%	2.5%	2.5%	524 °C		
	45%	45%	5,%	5%	522 °C		
	40%	40%	10%	10%	518 °C		
	10%	10%	40%	40%	509 °C		
T11,T22,304,HR11N HR3C,SAN28,AC66 45TM,170TMB,A625	Na_2SO_4	Na_2CO_3	NaCl	KCl	N/R	Gas: Air Temperature: 520-530 °C Time: 0.2-44 Hours	[67]
	59.0%	0%	6.5%	34.5%			

As the literature points out, there are many critical factors that influence the corrosion resistance of superheater tube alloys, both above and below the FMT of a typical deposit in a HT/HP recovery boiler. In spite of the relevant field studies conducted in HP recovery boilers using air-cooled probes and laboratory studies conducted under controlled conditions, it remains difficult to directly compare the corrosion resistance of candidate tube alloys. Comparisons among the field test results reported are not reliable considering the variable, poorly-defined, albeit real, environmental conditions encountered within the various boilers under study. Comparisons among the controlled laboratory test results reported are not reliable as a consequence of the differences in the testing parameters. Among the documented lab tests, it is difficult to assess, in a quantitative manner, the relative effect of elevated temperature, time at temperature both below and above the FMT, and gas composition, for a given deposit composition and alloy. In addition, more information is required on the possible influence of water vapor on corrosion both above and below the FMT. This is important since sootblowing can increase the local H_2O concentration by 3.5 vol.% [75]. Dissolved H_2O in molten chloride-containing salts has been reported to enhance melt corrosivity [67,71]. Also, in recently reported corrosion tests, water vapor additions (2 vol.%) were found to increase the corrosion rate of chromium-containing, nickel-based alloys tested in a simulated reducing low nitrogen oxide (NO_x) coal-fired combustion environment [76,77]. This finding may be relevant in HT/HP recovery boilers under conditions of high carryover.

Based on these shortcomings, a field study employing an air cooled corrosion probe and a laboratory corrosion testing program were conducted to facilitate an evaluation of alloy suitability for superheaters in next generation HT/HP recovery boilers.

LABORATORY STUDIES OF SUPERHEATER CORROSION

Experimental Details Of Laboratory Tests

Laboratory tests were conducted in which alloy test specimens were placed in crucibles, each of which containing a simulated ash salt mixture, within a three zone horizontal tube furnace. They were exposed to a particular synthetic cover gas at temperature for a specified exposure time. Specific details pertaining to the alloys tested, environments tested and procedures utilized are provided in the following text.

Alloy Test Specimens And Test Environments

Test specimens (25 mm x 15 mm x 2 mm) were prepared from sheet, plate or tubular forms supplied in the mill annealed condition. The alloys tested and their compositions are listed in Table 7. The alloy set was limited because of geometric constraints associated with the furnace apparatus. High alloy steel T91 was included as a reference for corrosion resistance below the FMT. Stainless steel grades 347H and 310H were included since they are typical alloys used to fabricate lower superheater tube bends in HT recovery boilers. The higher chromium-containing Alloy 28 and Alloy 33 were included as candidate upgrade alloys from which to fabricate superheaters for HT/HP recovery boilers. The aluminum-containing Alloy 693 was included in the alloy set exposed at the highest temperature to permit a relative comparison of corrosion resistance above the FMT between an alumina-forming alloy and the traditional chromia-forming alloys. Specimens were machined to produce a 125 micro-inch surface finish and then burnished with alumina burnishing triangles suspended in de-ionized water for 48 hours at 100 revolutions per minute (RPM). After burnishing, the specimens were first mechanically cleaned

Table 7. Alloy test specimens

Alloys		Composition (wt.%)						
Name	UNS	Fe	Cr	Ni	Mo	Mn	Al	C
T91	K90901	Bal.	10.1	0.5	0.8	0.6	<0.2	0.18
347H	S34709	Bal.	17.5	11.8	<0.04	1.7	<0.2	0.04-0.10
310H	S31009	Bal.	24.6	18.8	0.2	1.4	<0.2	0.04-0.10
Alloy 28	N08028	Bal.	26.5	30.3	3.3	1.7	- - -	0.017
Alloy 33	R20033	Bal.	33.0	30.9	1.5	0.6	- - -	0.015
Alloy 693	N06693	5.1	29.0	Bal.	0.04	0.2	3.35	0.015

by scrubbing with a stiff plastic bristle brush in a soap solution, then chemically cleaned using several solvents (detergent solution, de-ionized water, and denatured ethanol) and ultrasound successively, and then dried in hot air. After cleaning, the specimens were placed in polyethylene bags and stored in a desiccator for a minimum of 24 h before weighing with a digital balance.

A systematic screening evaluation of salt deposit mixtures was completed. A "worst case" salt deposit, with the chemical composition and FMT tabulated in Table 8, was selected for each of the three furnace test runs completed. The first melting temperature was experimentally determined using DTA, which was conducted at the Alberta Research Council (Edmonton, AB). This "worst case" deposit simulates a typical superheater deposit that would form in a recovery boiler operated at a coastal or a closed cycle mill, and was estimated using data published elsewhere [37,70]. A quantity of the mixture sufficient for the entire test requirements was prepared using reagent grade chemicals (Na_2SO_4, Na_2CO_3, K_2SO_4, KCl). To enhance homogenization, the various chemicals were mixed using a ceramic ball mill. After milling, the mixture was passed through a 100 mesh screen.

Table 8. Essential characteristics of salt deposit

Deposit	**Chemical Composition (wt.%)**					FMT
	Na	K	Cl	CO_3	SO_4	(°C)
D1	28.9	7.3	4.9	6.5	52.4	525

Two gaseous environments were tested, namely nitrogen (N_2), as an inert environment, and a mixture comprised of 4 vol.% hydrogen (H_2), 1 vol.% hydrogen sulfide (H_2S), 25 vol.% H_2O and N_2 making up the balance. A dewar of pre-purified 99.998 wt.% liquid nitrogen (typical moisture content of 5 ppm and oxygen (O_2) content of 8 ppm) was utilized to supply N_2 gas. Additional gaseous reagents used in the mixture were supplied by separate cylinders, one containing a 15 vol.% H_2-N_2 mixture, and another containing H_2S (99.6 vol.%). The target partial pressure of sulfur gas (S_2) in the mixture was 10^{-8} bar for all three temperatures.

Testing Program

An overview of the testing program is provided in Table 9. The program was divided into three series. During each series, tests were conducted in three furnaces simultaneously. In series 1, the goal was to assess the influence of time on corrosion at a temperature below the FMT, under an inert gaseous environment (N_2). In series II, the goal was to assess the influence of temperature on corrosion, again under an inert gaseous environment (N_2). The goal of series III was to assess the influence of temperature on corrosion in the presence of a "worst-case" gaseous environment (simulating carry over and sootblowing).

Procedure

The apparatus required to perform the experiments has been described in detail elsewhere [78]. Several alterations were required and are summarized as follows. The three-zone furnaces were mounted horizontally and fitted with 76.2 mm (3-in.) outer-diameter quartz reaction tubes. Alloy test specimens were tested in duplicate. Each specimen was placed flat in a rectangular alumina crucible (40 mm x 30 mm x 22 mm with a 3 mm wall thickness) and subsequently covered with 8 grams of the synthetic salt mixture. The filled crucibles were placed on alumina D-shaped supports in two adjacent rows containing five crucibles each. Two extra salt-filled crucibles were placed at each end of the two columns to help ensure a reproducible gas flow and radiant

Table 9. Laboratory test program summary

Series I – Influence of Exposure Time (Corrosion Kinetics)						
Alloy Set	Salt Deposit	Cover Gas	Temperature	Furnace 1	Furnace 2	Furnace 3
T91 347H 310H Alloy 28 Alloy 33	D1	N_2	510 °C	24 Hours	168 Hours	336 Hours
Series II – Influence of Temperature						
Alloy Set	Salt Deposit	Cover Gas	Time	Furnace 1	Furnace 2	Furnace 3
T91 347H 310H Alloy 28 Alloy 33	D1	N_2	336 Hours	510 °C	530 °C	
347H 310H Alloy 28 Alloy 33 Alloy 693	D1	N_2	336 Hours			560 °C
Series III – Influence of Sulfidizing/Oxidizing Environment						
Alloy Set	Salt Deposit	Cover Gas	Time	Furnace 1	Furnace 2	Furnace 3
T91 347H 310H Alloy 28 Alloy 33	D1	1% H_2S 4% H_2 25% H_20 70% N_2	336 Hours	510 °C	530 °C	
347H 310H Alloy 28 Alloy 33 Alloy 693	D1	1% H_2S 4% H_2 25% H_20 70% N_2	336 Hours			560 °C

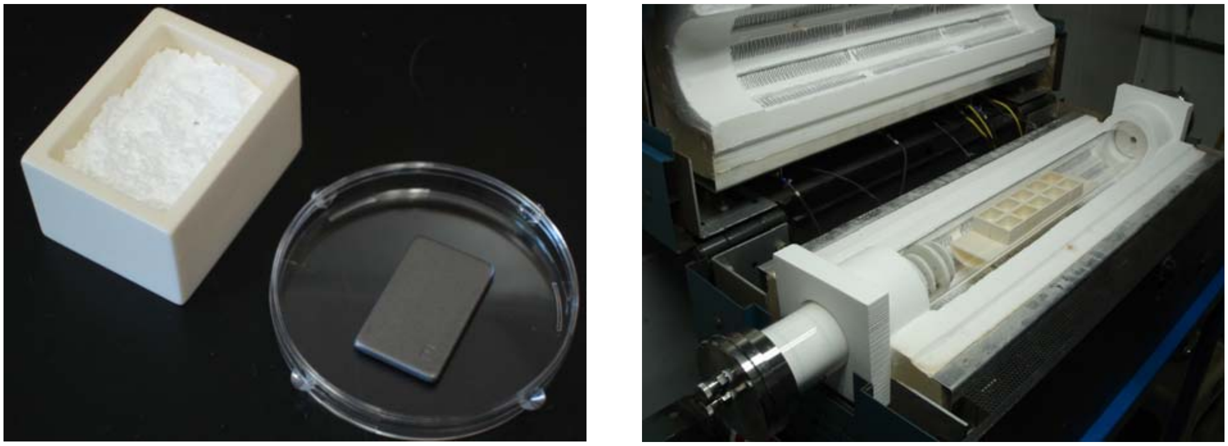

Alloy Test Specimen & Salt-Filled Crucible

Crucible Placement in Furnace

Figure 43 – Photographs documenting the test specimen geometry and the crucible containment system used and the placement of a set of crucibles into the isothermal zone in a horizontal three-zone furnace.

heat exposure for all crucibles. The D-shaped support was inserted into the furnace and centered in the 305 mm (12-in.) long isothermal region. The furnaces were held to the desired temperature within ±1C°. Four disk baffles, fabricated from 6.4 mm (¼-in.) thick ceramic fiber felt, were placed in the furnace tube inlet to help mix and equilibrate the gas mixture. Mass flow controllers, with stainless steel tubing, were used to supply N_2, H_2-N_2, and H_2S mixtures to the furnace. Water vapor was introduced directly into the first zone of the three zone furnace using a peristaltic pump and fine bore alumina tubing. A total gas flow rate of 200 SCCM was supplied to each furnace, which equates to a linear flow of approximately 34 cm/min over the crucibles. Prior to testing, furnace tubes were purged with N_2 gas overnight at ambient temperature.

Furnace temperatures were increased manually at approximately 55°C/15 minutes. For the series III tests, the flow of H_2-H_2S and water vapor was initiated after the desired test temperatures had stabilized, and was terminated just before the furnaces were cooled to ambient temperature. Photographs documenting the furnace apparatus are provided in Fig. 43.

After testing, one specimen was removed from the salt-filled crucible, separated from the salt mixture and photographed. After being photographed, specimens were first mechanically cleaned by abrasive blasting with walnut shells, then chemically cleaned using several solvents (inhibited dilute hydrochloric acid, detergent solution, de-ionized water, and denatured ethanol) and ultrasound successively, and then dried in hot air. After cleaning, the specimens were placed in polyethylene bags and stored in a desiccator for a minimum of 24 hours before final weighing using a digital balance. The other specimen from the duplicate set was extracted from the salt-filled crucible, with the salts adhered when possible, and vacuum impregnated with epoxy. In some cases where the salt was strongly adhered to the crucible, the alloy specimen was impregnated while still in the crucible. All of sample mounts were dry-sectioned and polished to 3-micron (diamond paste) surface finish using standard metallographic methods and water-free lubricants and consumables.

A power failure interrupted the series III tests after approximately 84 hours exposure. Consequences included a rapid cooling of the test specimens in a stagnant gaseous environment. This rapid cooling caused a fracture in the quartz tube housed in furnace 2 (530°C). It was decided to continue with the testing in furnace 1 (510°C) and furnace 3 (560°C), but not to continue the testing in Furnace 2 (530°C). Specimens were removed from that furnace and analyzed according to the procedure outlined above. Testing was re-started after an additional 36 hours. At approximately 72 hours of exposure after the re-start, the peristaltic pump supplying water to the furnaces stopped. It was re-started in less than 6 hours. The pump ceased working around the 264 hour mark. The testing continued without a supply of water for a period of about 48 hours, after which a replacement pump was installed and the flow of water re-started.

Results

Gravimetric analysis

Figure 44A shows a photograph of the cleaned alloy test specimens extracted from salt-filled crucibles after exposure to N_2 gas at 510°C, as a function of time. Each specimen tested formed a surface scale during the exposure, regardless of the exposure time. As shown by the photograph, the success of the post-exposure cleaning procedure in removing the scale formed on the specimen surface was highly variable. In general, the degree of scale removal tended to increase with the exposure time. Furthermore, scale color variations or patches toward the top and bottom edges left a distinct, roughly circular, central area on most of the specimens. These edge patches coincided with regions where the surface was not in direct contact with the salt deposit at the time specimens were extracted from the crucibles. The salt deposits tended to shrink, forming coherent blocks which pulled away from the top and bottom edges of the specimen. The mechanism responsible for this separation, or the significance, is not well understood at this time. Despite the variable success achieved from the post-exposure cleaning procedure, several observations were noted. First, the scales that formed during the short exposure (24 hours) were uniform and consistent in appearance, with the exception of the scale that formed on the T91 specimen, which was noticeably darker than the others. Secondly, the scale formed on the T91 specimens tended to be more resistant to the post-exposure cleaning procedure than the others, regardless of exposure time. Thirdly, a similar, relative change in scale appearance, and the degree of removal, upon post-exposure cleaning, was observed for the 347H and 310H specimens, as well as for the Alloy 28 and Alloy 33 specimens.

The corresponding weight loss measurements are plotted in Fig. 44B, as a function of time. All alloys exhibited a complex dependence on time, which is not surprising given the quantity of scale attached to the specimen surfaces. Correspondingly, not much can be inferred from the apparent time dependence. However, as reported in the next sub-section, the remaining scales were observed to be relatively thin in cross-section, and therefore, may not significantly alter the weight loss data reported. It is noted that the highest weight loss was measured on the T91 specimen at each exposure time considered, despite the fact that these specimens were still largely covered with scale. Another observation to note is the similarities between the apparent time dependence of 347H and 310H, and the apparent time dependence of Alloy 28 and Alloy 33. These apparently similar time dependencies coincide with the similar changes in scale appearance and degree of removal noted above.

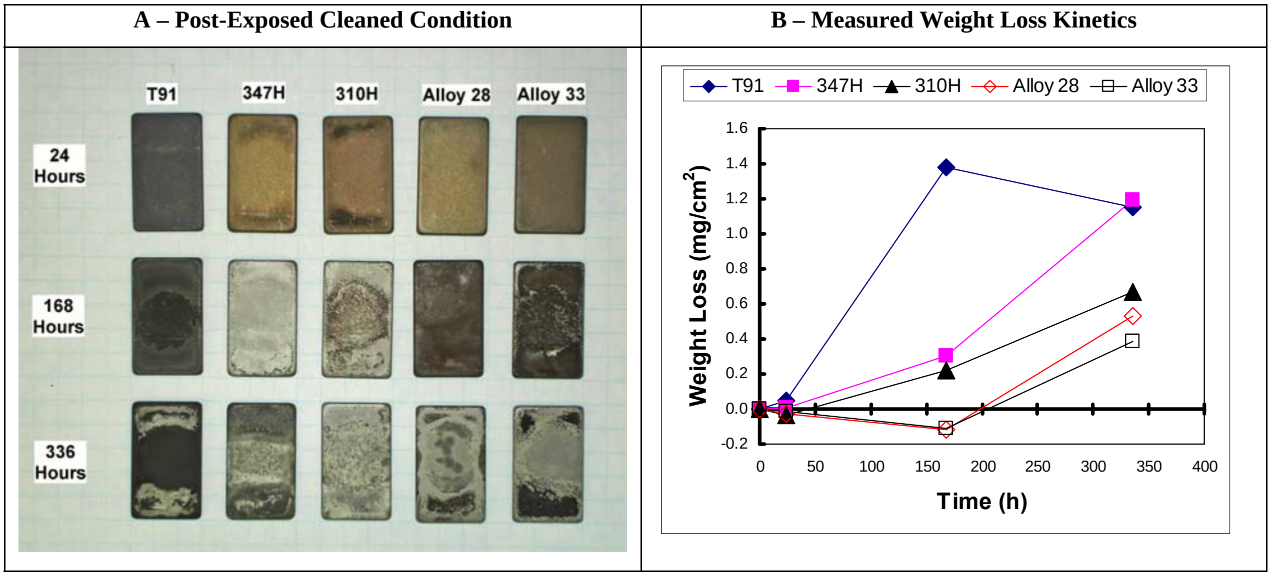

A – Post-Exposed Cleaned Condition

B – Measured Weight Loss Kinetics

Figure 44 – Results of corrosion tests conducted in N_2 gas at 510°C, as a function of time (series I). (A) Photograph documenting post-cleaned condition of the alloy test specimens extracted from salt-filled crucibles. (B) Plot showing the weight loss measured for each alloy, as a function of time.

Figure 45A shows a photograph of the cleaned alloy test specimens extracted from salt-filled crucibles after exposure to N_2 gas for 336 hours, as a function of temperature. Again, the success of the post-exposure cleaning procedure was variable. With this series, the degree of scale removal tended to decrease with an increase in temperature above the FMT of the salt mixture. Variations in the scale appearance leaving a central circular area were most apparent on specimens exposed below the FMT, and for the T91 and Alloy 33 specimens tested at 530°C. The scales that formed during the 336-hour exposure at temperatures above the FMT were reasonably uniform and consistent in their dark grey appearance. It is noted that the salt deposits tested above the FMT remained in contact with the specimen surface as observed at the time the specimens were extracted from their crucibles.

The corresponding weight loss measurements are compared in Fig. 45B, for each temperature tested. A consistent set of positive weight losses was observed only at the test temperature of 510°C, which is consistent with the relatively low quantity of scale that remained attached to the cleaned specimens exposed to this temperature. At this temperature, which is below the FMT of the deposit, T91 exhibited the highest apparent weight loss of the alloy set tested. The weight loss was some 88% higher than the next highest weight loss exhibited by the Alloy 33 specimen. An increase in temperature from 510°C to 530°C significantly increased the weight loss of T91 only. The weight loss of the four other alloys tested at both these temperatures decreased. A further increase in temperature from 530°C to 560°C had a less remarkable impact on weight loss. An increase in weight loss was measured for 347H and Alloy 33, whereas a decreased weight loss was measured for 310H, Alloy 28 and Alloy 693. Regardless of these relative changes, the weight loss measured on 347H, 310H, Alloy 28, Alloy 33 and Alloy 693 is small under these testing conditions.

A – Post-Exposed Cleaned Condition	B – Measured Weight Loss
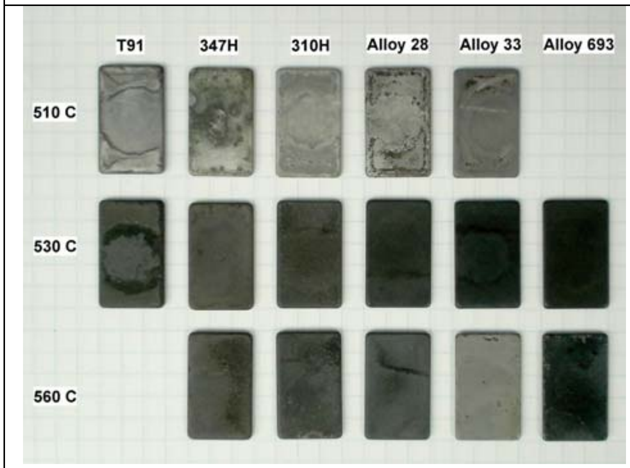	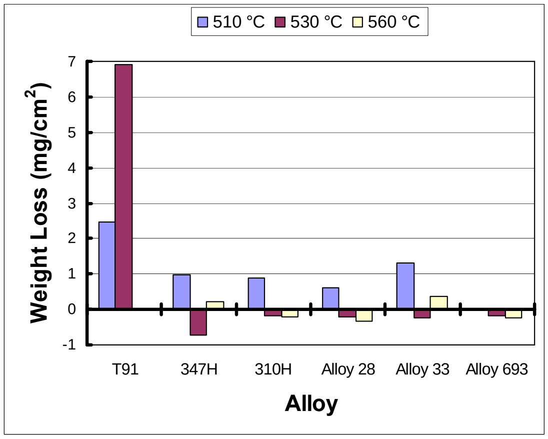

Figure 45 – Results of corrosion tests conducted in N_2 gas for 336 hours, as a function of temperature (series II). (A) Photograph documenting post-cleaned condition of the alloy test specimens extracted from salt-filled crucibles. (B) Plot showing the weight loss measured for each alloy, as a function of time.

Figure 46A shows a photograph of the post-cleaned alloy test specimens extracted from salt-filled crucibles after exposure to H_2S-H_2-H_2O-N_2 gas mixture for 84 hours (510°C) and for 336 hours (510 and 560°C). With this run, the post- exposure cleaning procedure was unsuccessful for the most part. The scales that formed during the 336-hour exposure at all three test temperatures were reasonably uniform and consistent in their dark grey appearance. It is noted there was evidence of scale spalling observed after exposure to this sulfidizing/oxidizing gas mixture. The color of the salt deposits ranged from dark brown to black in every case.

The corresponding weight loss measurements for each test temperature are shown in Fig. 46B. In contrast to the test results conducted in the inert N_2 gas, a positive weight loss was measured for each test specimen, regardless of temperature. An increase in temperature from 510°C to 530°C increased the weight loss measured on the five alloys tested at these temperatures. The increase was larger for T91 and 347H and was smaller for 310H, Alloy 28 and Alloy 33. Again, a further increase in temperature from 530°C to 560°C had a less remarkable impact on the measured weight loss. A decrease in weight loss was measured on 310H, Alloy 28, Alloy 33 and Alloy 693, whereas an increase was observed for T91.

SEM/EDS examination of alloy/scale interface

All mounted 347H and Alloy 28 test specimens were selected for further examination using a scanning electron microscope (SEM). These two alloys were selected on the basis that 347H and Alloy 28 represents the alloy with the leanest and richest chromium content, respectively, widely used to construct lower superheater tube bends in current generation HP recovery boilers. All of the micrographs taken of the mounted 347H and Alloy 28 test specimens are provided in Appendix 1. It is noted that the thickness and adherence of the scales varied along the length of

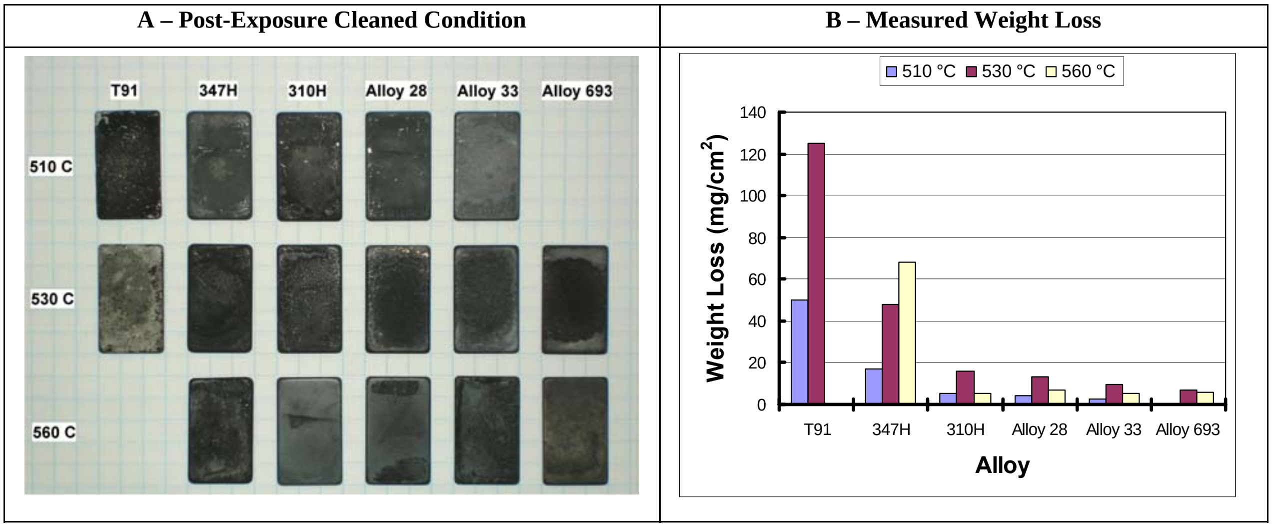

A – Post-Exposure Cleaned Condition

B – Measured Weight Loss

Figure 46 – Results of corrosion tests conducted in the H_2S-H_2-H_2O-N_2 gas mixture for 336 hours, as a function of temperature. (A) Photograph documenting post-cleaned condition of the alloy test specimens extracted from salt-filled crucibles. Note photographs of specimens exposed at 510°C taken after 84 hours. (B) Plot showing the weight loss measured for each alloy, as a function of time. Note data for 530°C extrapolated from the 84–hour weight loss measurement.

the test specimens. For this reason, it was decided to obtain a micrograph from the midpoint region along the length (region of contact with salt deposit), so as to impart some consistency on the position.

Several major observations were made from the collected micrographs. A subset of the micrographs obtained from 347H test specimens is provided in Fig. 47 to illustrate these observations.

- Scales that formed on both alloys during exposure to the inert N_2 gas were significantly thinner than those that formed during exposure to the H_2S-H_2-H_2O-N_2 gas mixture.
- An increase in temperature from 510°C to 560°C did not significantly affect the thickness of the scales formed on both alloys during exposure to the N_2 gas or that formed on the Alloy 28 specimens exposed to the H_2S-H_2-H_2O-N_2 gas mixture. In contrast, the same increase in temperature significantly increased the thickness, as well as the apparent structure of the scales formed on the 347H specimens during exposure to H_2S-H_2-H_2O-N_2 gas mixture.
- Scales that formed on the Alloy 28 specimens during exposure to the H_2S-H_2-H_2O-N_2 gas mixture were significantly thinner than those that formed on the 347H specimens at both 510°C and 560°C.
- No evidence of any internal penetration was found on any of the specimens, regardless of the environmental condition tested.

The scale/alloy interface region of this subset of 347H specimen mounts was further analyzed using energy dispersive spectroscopy (EDS). The corresponding elemental maps obtained by EDS are shown in Fig. 48. Maps were obtained for the major alloying elements, namely iron, chromium and nickel, and for the environment components expected to play a role in the corrosion process, namely sodium, potassium, chlorine, sulfur and oxygen. The scale that formed during exposure to the N_2 gas environment was rich in oxygen, chromium and iron, regardless of temperature. This is not surprising considering that residual oxygen gas level of 8 ppm expected in the liquid nitrogen supply is more than adequate to stabilize the native chromium-containing oxide film present on the specimens prior to exposure. Chlorine enrichment was noticeably absent from the alloy/scale interface at both temperatures tested in the N_2 gas environment, as well as from the salt mixture itself adjacent to the alloy. As expected, the scales that formed during exposure to the H_2S-H_2-H_2O-N_2 gas mixture were rich in sulfur and chromium at the alloy/scale interface, regardless of temperature. Interestingly, sodium, but not potassium, was also enriched in these scales. At 560°C, an outer scale consisting of a chromium-containing oxide was also observed in addition to the inner chromium-sodium-sulfur-containing scale noted. Again, chlorine enrichment was noticeably absent from the alloy/scale interface at both temperatures tested, as well as from the salt mixture itself adjacent to the alloy.

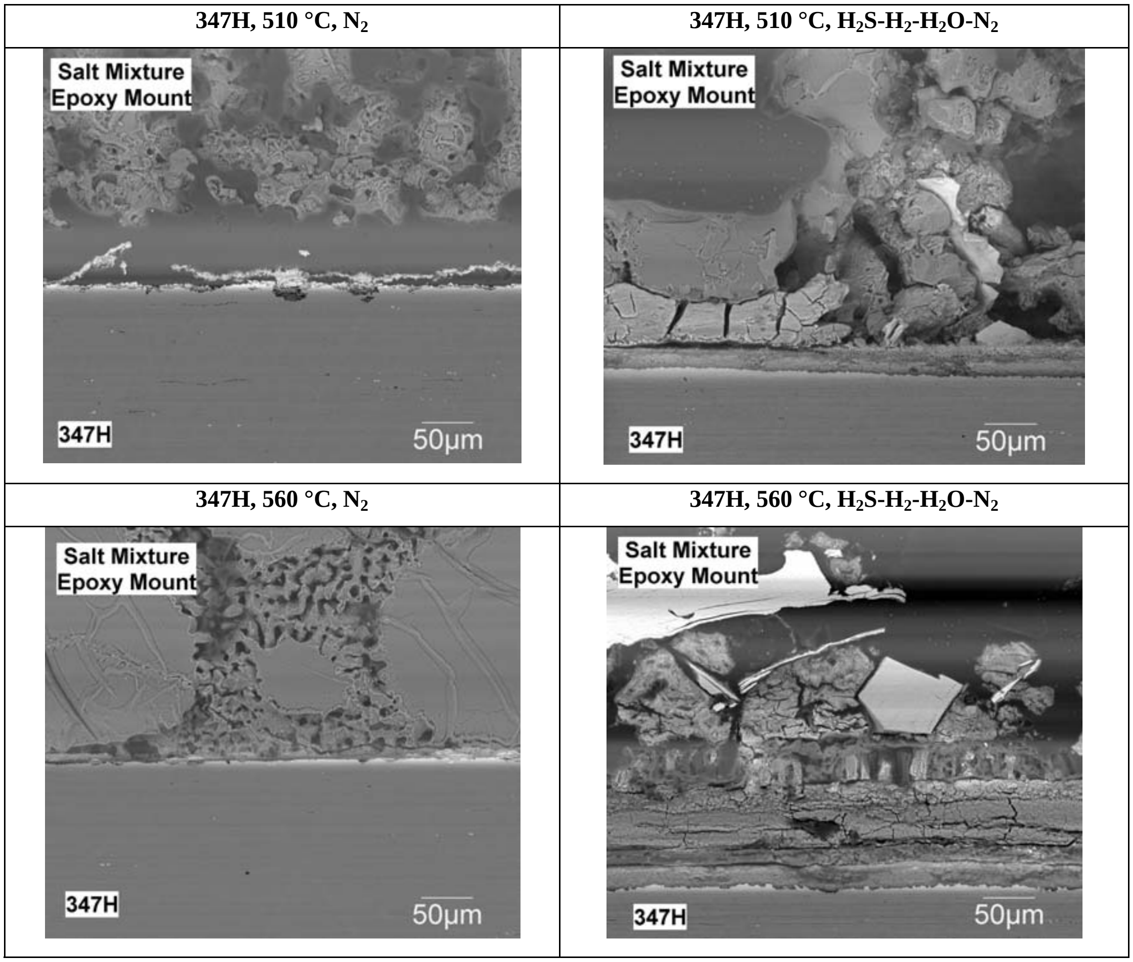

347H, 510 °C, N_2

347H, 510 °C, H_2S-H_2-H_2O-N_2

347H, 560 °C, N_2

347H, 560 °C, H_2S-H_2-H_2O-N_2

Figure 47 – Subset of micrographs obtained from 347H specimens mounted in cross-section documenting the appearance of the scale/alloy interface as observed at the midpoint region along the length of the specimens.

347H, 510 °C, N_2 | **347H, 510 °C, H_2S-H_2-H_2O-N_2**

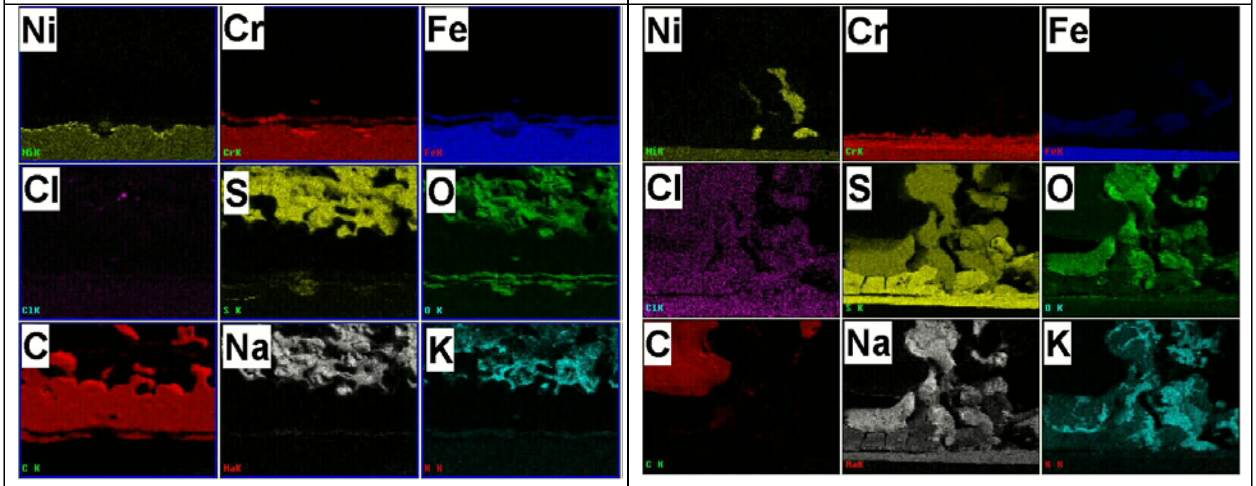

347H, 560 °C, N_2 | **347H, 560 °C, H_2S-H_2-H_2O-N_2**

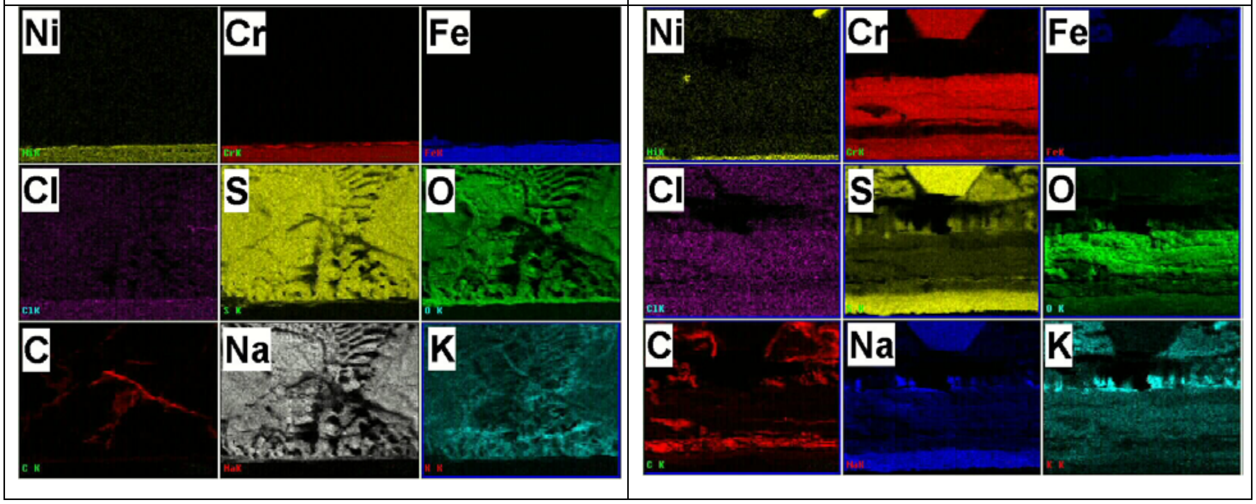

Figure 48 – Elemental maps of the scale/alloy interface obtained by EDS from the subset of 347H specimens mounted in cross-section documenting the distribution of major alloying elements (Fe, Cr, Ni) and major corrosion product elements (O, S, Cl, Na, K).

Discussion

The laboratory testing in simulated environments reported above was conducted in order to perform a preliminary evaluation of alloy suitability for superheaters in the next generation HT/HP recovery boilers. The evaluation required a reliable measurement of corrosion to form a comparative basis. Corrosion measurements traditionally used for comparative purposes include weight gain (before cleaning/descaling), weight loss (after cleaning/descaling), scale thickness and depth of attack (external and internal). The interpretation presented below utilized the weight loss measurements as the comparative basis, despite the obvious misrepresentation resulting from the presence of tightly adhering, compact scales remaining on many of the samples. The use of scale thickness or depth of attack was not practical given the relatively thin and non-uniform nature of the adhering scales and the lack of internal attack observed, respectively. Weight gain measurements were not attempted due to expected variations in scale density (composition), and the possible formation of volatile corrosion products.

Relative corrosion resistance and alloy suitability

A duplicate test condition (N_2 gas at 510°C for 336 hours) was included to evaluate the reproducibility of the testing procedure. Figure 49 compares the expected annual corrosion rate (extrapolated from the 336-hour weight loss measurement) for the various alloys tested in this duplicate condition. Reasonable agreement between the two measurements was obtained for 347H, 310H and Alloy 28. For T91 and Alloy 33, a greater weight loss was measured on those specimens exposed in series II. Considering the reasonably good agreement among the other specimens, it is unlikely that this discrepancy is solely related to the misrepresented measured weight loss resulting from remaining scale attached to the surface. Despite this disagreement, there is a consistent general trend in the data, namely the corrosion rate tended to decrease with a corresponding increase in the chromium content of the alloy (note the alloys are listed in terms of increasing chromium content). This trend is consistent with reported data from corrosion tests conducted in chloride-containing salts at temperatures below the corresponding FMT [63-66,74]. Note that although it is the highest relative corrosion rate of the alloys tested, the T91 corrosion rate of 0.06 mm/yr (2.4 mpy) is significantly lower than the minimum corrosion rate (0.3 mm/y) reported for corroded 347H tube bends in existing HT recovery boilers [79].
A plot comparing the influence of gas mixture on the expected annual corrosion rate (extrapolated from the 336-hour weight loss measurements) of these alloys at 510°C is provided in Fig. 50. Replacing the inert N_2 gas with the more reactive sulfidizing/oxidizing gas mixture increased the corrosion rate of all alloys tested except for Alloy 33, which showed a slight decrease in corrosion rate. The relative difference in corrosion rate depended on the alloy, and it exhibited the same trend noted above, namely the corrosion rate tended to decrease with a corresponding increase in the chromium content of the alloy. This trend is consistent with reported data on the sulfidation resistance of chromium-containing alloys at a similar temperature [80]. The T91 corrosion rate of 1.57 mm/yr (62 mpy) and the 347H corrosion rate of 0.36 mm/y (14 mpy) measured in the presence of the sulfidizing/oxidizing gas mixture are both greater than the minimum corrosion rate [0.3 mm/y (12 mpy)] reported for corroded 347H tube bends in existing HT recovery boilers [79].

Figure 51 shows a plot of the expected annual corrosion rate (extrapolated from the 336-hour weight loss measurements) of the various alloys tested at 560°C in the H_2S-H_2-H_2O-N_2 gas mixture. Data corresponding to the test conducted in the N_2 environment at the same temperature are excluded from this plot since a negative weight loss was measured on three of the five alloys tested at this temperature, and the two positive weight losses measured were both less than 0.012 mm/yr (0.5 mpy). Again, replacing the inert N_2 gas with the more reactive sulfidizing/oxidizing gas mixture significantly increased the corrosion rate of all alloys tested. Unlike the trend in corrosion rate observed below the FMT (Fig. 50), the corrosion rate did not vary much among the alloys with the obvious exception of 347H, which had a significantly higher rate relative to that of the others. Note that the corrosion rate of the alumina-forming Alloy 693 was similar to chromia-forming 310H, Alloy 28 and Alloy 33 in this environment. The corrosion rate of 347H was greater than the minimum rate of 0.3 mm/y (12 mpy) reported for corroded 347H tube bends in existing HT recovery boilers [79]. In contrast, the corrosion rate of the other four alloys was lower than this minimum rate, ranging from 0.172 mm/yr (6.8 mpy) for 310H to 0.234 mm/yr (9.2 mpy) for Alloy 28.

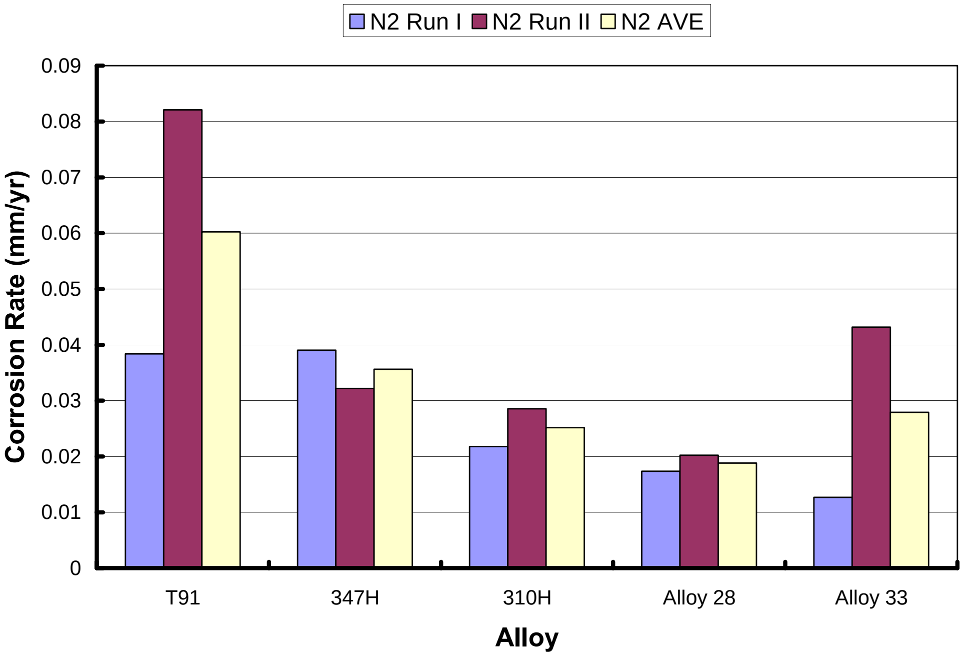

Figure 49 – Plot comparing the annual corrosion rate (extrapolated from the 336-hour weight loss measurement) for the various alloys tested after embedded in salt mixture and exposed to N_2 gas at 510°C. [1 mm/yr = 40 mpy]

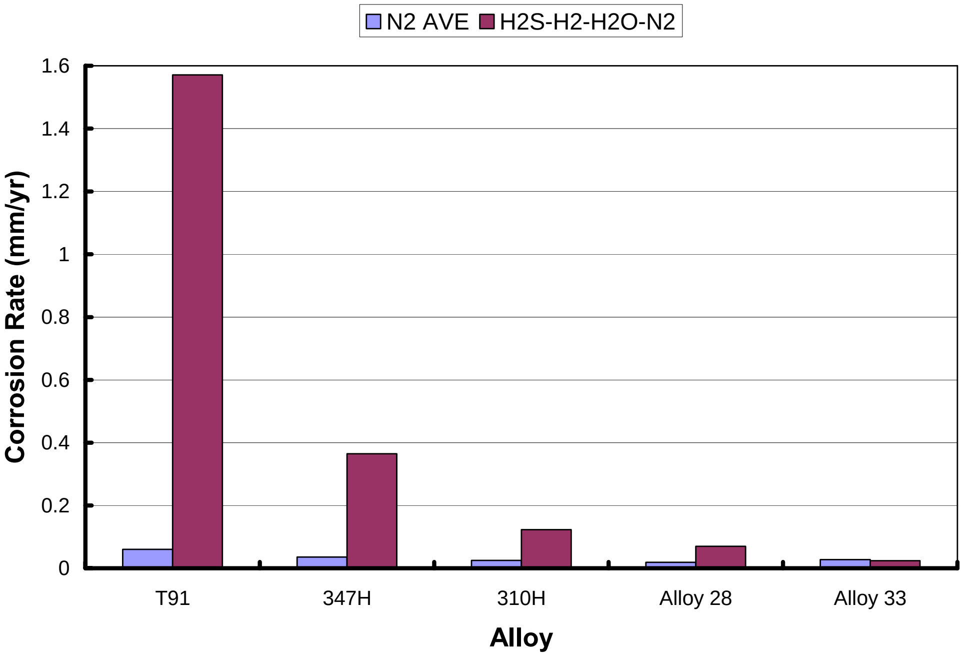

Figure 50 – Plot comparing the annual corrosion rate (extrapolated from the 336-hour weight loss measurement) for the various alloys tested after embedded in salt mixture and exposed to N_2 gas and to a H_2S-H_2-H_2O-N_2 gas mixture at 510°C. [1 mm/yr = 40 mpy]

The H_2S-H_2-H_2O-N_2 gas mixture was used on the basis that it simulated a possible worst-case scenario, one which involved an operating condition of high carryover combined with elevated moisture levels resulting from frequent sootblowing. The discussion of alloy suitability needs to take the corrosion resistance design criteria into consideration. If the criterion is acceptable corrosion resistance at temperatures below the FMT of the deposit, then, from Fig. 50, it appears as though 3347H would be the minimum alloy (of those tested) suitable, albeit marginal, for use as superheater tubes in HP/HT recovery boilers. A better choice would appear to be 310H or Alloy 28. Note that Alloy 33 was not tested under these conditions. To minimize the risk of corrosion in practice, removal of non-process elements (potassium and chlorine) could become a critical part of corrosion control to assure that the FMT of the superheater tube deposits is well above the tube temperature, even with the associated expected degree of variation in deposit composition. If the criterion is acceptable corrosion resistance at temperatures above the FMT of the deposit, then, from Fig. 51, it appears as though Alloy 28 would be the minimum alloy (of those tested) suitable to control corrosion of superheater tubes in HT/HP recovery boilers. For use of this material to be practical, tight control of tube temperature would become critical to corrosion control in order to ensure that the time at temperatures above the FMT of the deposit is minimized.

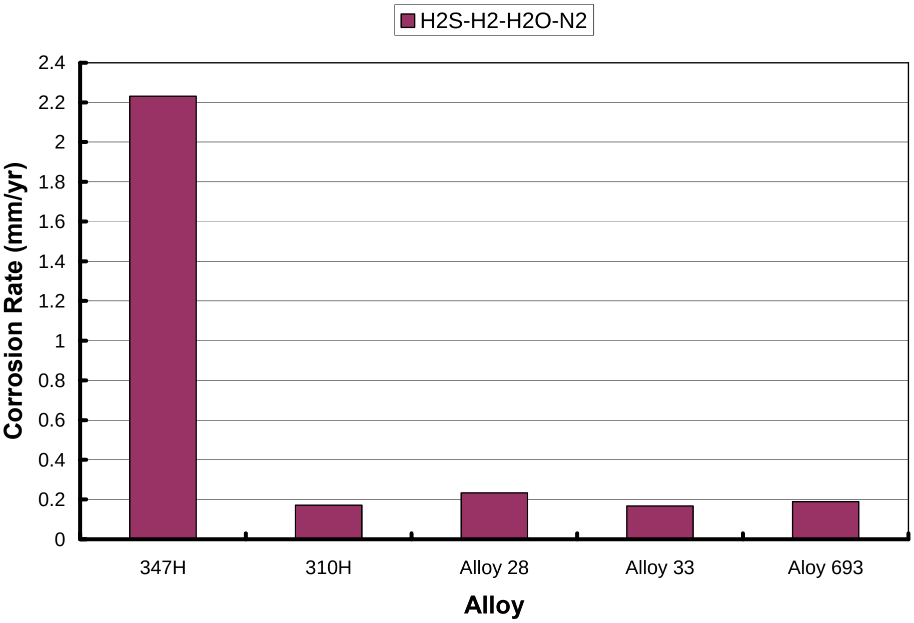

Figure 51 – Plot comparing the annual corrosion rate (extrapolated from the 336-hour weight loss measurement) for the various alloys tested after embedded in salt mixture and exposed to a H_2S-H_2-H_2O-N_2 gas mixture at 560°C. [1 mm/yr = 40 mpy]

As reported earlier, no evidence of internal attack was observed on any of the test specimens, regardless of the environmental conditions tested. This observation is inconsistent with those reported in related lab studies [64-67], as well as from field studies utilizing [33,39-44] air-cooled probes. It is quite possible that an exposure time longer than those considered in this lab study is required to initiate and/or propagate the corrosion process in alkali chloride-containing salt mixtures, both below and above the FMT. A lab study reporting on the corrosion resistance of commercial heat resistant alloys in contact with a synthetic recovery boiler superheater salt deposit (45%Na_2S-21%Na_2CO_3-21%Na_2SO_4-13%NaCl) in air at temperatures ranging from 550°C to 650°C clearly demonstrates the need for adequate exposure time to produce well-developed attack [81]. It is also quite possible that the testing in air or in the presence of excess oxygen is sufficient to produce the degree of internal attack expected. As documented in Table 5, most of the related lab studies were conducted in air or gas mixtures containing an oxygen

concentration similar to that typically present in a recovery boiler flue gas. Therefore, in order to support the suitability claims made herein and to provide a more reliable basis for a definitive ranking of alloys, testing at longer exposure times in an atmosphere with an oxygen concentration representative of boiler flue gas is recommended. Based on the findings of this study, it seems reasonable that a ranking based on time-to-failure basis, both below and above the FMT, would prove worthwhile in the attempt to specify superheater tube alloys for HT/HP recovery boilers.

Conclusions And Recommendations

Alloy selection for superheaters in recovery boilers is typically governed by the same design constraints as for other types of boilers, including high temperature strength, creep resistance and corrosion/oxidation resistance. Low alloy steels T11 and T22 are commonly used for superheater tubes in current generation LP and HP recovery boilers.

Accelerated corrosion of superheaters in current generation HP recovery boilers is usually caused by molten salt attack. As a corrosion control measure, monolithic corrosion-resistant alloy tubes (347H & 310H stainless steel, Alloy 800) and co-extruded composite tubes (310H/T22, Alloy 28/T22) have been used to fabricate the hottest tube bends. With the exception Alloy 28/T22 composite tube bends, accelerated corrosion has been reported in the open literature for each of these corrosion-resistant alloys.
There are two corrosion mechanisms that will influence alloy selection for superheater tubes in the next generation HT/HP recovery boilers, namely chlorine-induced active oxidation at temperatures below the FMT of the deposit, and molten salt attack at temperatures above the FMT of the deposit.

Alloy suitability likely depends upon the corrosion resistance design criterion. If the criterion is acceptable corrosion resistance at temperatures below the FMT of the deposit, then it appears as though 347H would be the minimum alloy (of those tested) suitable, albeit marginal, for use as superheater tubes in HP/HT recovery boilers. For this to be realized in practice, removal of non-process elements (potassium and chlorine) would become a critical part of corrosion control to assure that the FMT of the superheater tube deposit is well above the tube temperature, and the associated expected degree of variation.

If the criterion was to exhibit acceptable corrosion resistance at temperatures above FMT of the deposit, then it appears as though 310H would be the minimum alloy (of those tested) suitable to control corrosion of superheater tubes in HT/HP recovery boilers. For use of this material to be practical, tight control of tube temperature would become critical to corrosion control in order to ensure that the time at temperature above the FMT of the deposit is minimized.

Corrosivity of the potassium and chorine-containing deposit was significantly enhanced in the presence of the reactive gas mixture. There is a complex, yet poorly understood synergy between the reactants responsible for corrosion observed both below and above the FMT of the deposit.

Lab testing at both longer exposure times and with the presence of oxygen in the gas mixture is recommended to support the suitability claims made herein, and to provide a more reliable basis for a definitive ranking of alloys. Based on the findings of this study, it seems reasonable that a ranking based on time-to-failure basis, both below and above the FMT would prove worthwhile in the attempt to rank superheater tube alloys for HT/HP recovery boilers.

FIELD STUDIES OF SUPERHEATER CORROSION

Experimental Details Of Corrosion Probes And Testing Program

The alloys used for the corrosion probe samples were essentially the same as those used for the laboratory corrosion studies except that the Alloy 33 was used as a weld overlay on the corrosion probe samples. The alloys and their compositions are shown in Table 10. In addition to Alloy 33 being tested in the form of a weld overlay, the Alloy 28 was the outer layer of a co-extruded tube.

For the field exposure, 15 interlocking, air-cooled samples were assembled in a spring loaded assembly that provided for two thermocouples per sample. The samples were arranged in a repeating pattern based somewhat on the anticipated corrosion rate. The exception was the omission of T91 and the addition of weld overlaid alloy 33 in the set of five samples exposed at the hottest end of the probes Using the abbreviated descriptions listed in Table 10, the order of the samples, from the coolest to hottest positions, was: T91, 347, 310, 28, 693, T91, 347, 310, 28, 693, 347, 310, 28, 33, 693. Figures 52 to 57 show the components and the assembly of one of the two identical probes. Figure 52 shows a schematic of the corrosion probe, and in Fig. 53 the base of the probe with the thermocouples in place can be seen along with most of the samples sitting on the cart on the right side of the figure. Figure 54 shows the probe being assembled. Four of the samples are in place, and the thermocouples for the remaining samples along with the support rods can be seen extending above the samples. The arrangement of the spacer inserted inside the sample along with the support rods and thermocouples are shown in Fig. 55. Figure 56 shows how two thermocouples per sample were held in place by a snap ring. One snap ring was used in each sample to hold the thermocouples in shallow holes that were drilled on the ID of each tubular sample (top and bottom of the horizontally inserted probe) so the effects on metal temperature of such things as radiant heating and deposit accumulation could be determined. An assembled probe is shown in Fig. 57.

Two probes were assembled with the plan of exposing one probe in the superheater section of a recovery boiler at the Domtar mill in Ashdown, Arkansas, and the other in a comparable area of the Weyerhaeuser mill in Columbus, Mississippi. In addition to the corrosion probe, the data processing instrumentation, a computer and the necessary cables were provided by ORNL and were delivered to the respective mills in August, 2006. The computer was provided with a program to collect data from each thermocouple on a regular basis, and this information was stored so that it could be subsequently downloaded by an operator in Oak Ridge. Unfortunately, the probe for the Mississippi mill was damaged when the cooling air was not properly connected and the probe was considerably overheated during installation. Consequently, only the probe from the Ashdown mill was exposed the full 1000 hour period under controlled conditions.

The probe was inserted horizontally into the superheater section of the recovery boiler under study through an inspection door modified to accommodate the probe. Figure 58 shows the

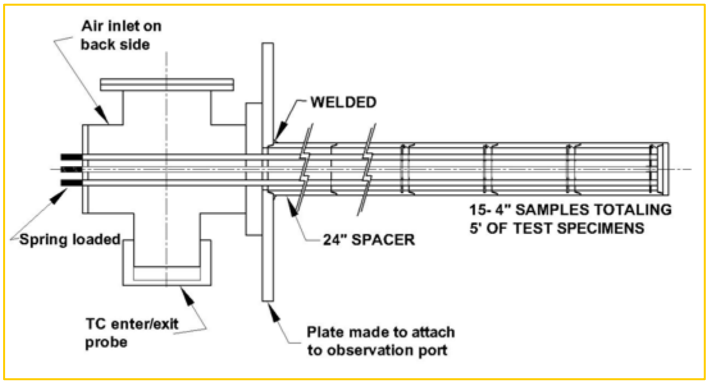

Figure 52. Schematic of superheater corrosion probe.

Figure 53. Base of corrosion probe prepared for sample assembly. Note tubular samples on cart in right rear of photo.

Figure 54. Corrosion probe being assembled. Thermocouples and support rods extend through the four samples already mounted.

Figure 55. The support rods, the internal spacer and the thermocouples are shown.

Figure 56. *Arrangement used to hold two thermocouples in place with a snap ring.*

Figure 57. Assembled superheater corrosion probe.

probe being inserted, and Fig. 59 shows the probe after installation was completed. In this figure, the air supply line and the remotely-controlled, variable flow valve are on the right side of the probe, and the 30 thermocouples that were attached to the samples can be seen coming into the bottom of the probe. The probe was aligned so that, for each sample, one thermocouple was at the 12 o'clock or top position and the other thermocouple was 180° away in the bottom position where it was subject to radiant as well as convective heating. The flue gas temperature in the vicinity of the probe was estimated to be about 650°C, and a temperature gradient along the probe ranging from 650°C to 316°C was expected. The probe was removed just before the boiler was water washed, and the exposure period was almost exactly 1000 hours. Because of deposits that had accumulated on the probe, removal of the probe through the small opening in the manway was difficult. Figure 60 shows the probe after removal.

Results

Temperature measurements

The computer that was provided as part of the data collection system recorded the temperature of each of the 30 thermocouples every 20 seconds. All data were regularly downloaded to a computer at ORNL through a phone line. Unfortunately, many of the thermocouples stopped working before the 1000 hour exposure was completed. Nevertheless, enough data were collected to provide a good indication of the top and bottom temperatures for each of the samples. The daily average measured metal temperatures are shown in Fig. 61, and the average temperatures for all 30 thermocouples are shown in Fig. 62. Because the thermocouples were a short distance below the surface of the tubular samples, it was assumed that the actual surface temperatures were about 17C° (30F°) higher than the measured temperatures.

Because some thermocouples failed and stopped providing data at random times throughout the exposure, a direct comparison between the top or bottom surface temperatures of the samples was not always possible. However, the data collected does provide useful information. With a first melting temperature (FMT) of the superheater deposits of about 547°C (1017°F), it is clear from Fig. 61 that samples #11 through #15 (Alloy 693, Alloy 33, Alloy 28, 310H and 347H) were exposed at temperatures above the FMT, while #1 through #10 (Alloy 693, Alloy 28, 310H, 347H, T91) were exposed at temperatures below this FMT for the majority of the exposure.

Figure 58. Corrosion probe being inserted through hole in manway door.

Table 10. Composition of alloys used for corrosion probe samples

Alloy	Designation	Fe	Cr	Ni	Mo	C	Other
T91	T91	Bal	8.4	0.1	1.0	0.11	0.2 V
347H	347	Bal	18.2	11.4	---	0.09	0.9 Ta
310H	310	Bal	24.2	20.1	0.3	0.05	-----
Sanicro 28	28	Bal	26.7	30.5	3.3	0.01	0.9 Cu
Alloy 33 weld	33	Bal	32.9	27.1	1.5	n/a	-----
Inconel 693	693	4.8	25.3	Bal	0.1	n/a	3.2 Al

n/a = not available

Figure 59. Corrosion probe installed in recovery boiler superheater. The air supply line and regulating valve are on the right and the 30 thermocouples extend from the bottom of the probe.

Figure 60. Corrosion probe after removal from recovery boiler.

considered to have been exposed at temperatures above the FMT for the majority of the

Considering that the external surface should be hotter than the internal surface, Alloy 33 was considered to have been exposed at temperatures above the FMT for the majority of the exposure. The increased variation in temperature observed in the second half coincides with changes made to the cooling air flow rate in order to maintain the temperatures at the tip of the probe. These changes were made in response to the loosening of samples in the probe and the subsequent leaking of air from the probe.

The results shown in Fig. 62 indicate the measured temperatures (not accounting for the difference between the inner and outer surface temperatures) for the thermocouples on the top and bottom of each sample and for the first two weeks and two weeks during the latter part of the exposure period. In almost all cases, the bottom thermocouple indicated a higher temperature than the top thermocouple, and for the hotter samples, the temperature was higher during the latter portion of the 1000 hour exposure period. The higher temperature on the bottom side of the probe samples was almost certainly a result of radiant heat resulting from combustion in the lower portion of the boiler.

Metallographic and electron microprobe examinations

Before the probe was disassembled, the orientation was carefully marked on each sample so that the top and bottom could be easily determined. A ring was cut from each tubular sample, and a metallographic examination was performed on samples cut from the top position and at 90° intervals around the ring. Consequently, 60 samples (15 rings x 4 locations per ring) were examined and photographed in the as-polished and etched conditions. Because of the heavy deposition on the surface of most samples, weight change measurements did not provide a meaningful indication of the extent of reaction of the samples with the environment. Ultrasonic thickness measurements were made on all the tubular samples before the probes were inserted in the superheaters of the boilers. However, the heavy deposition made post-exposure ultrasonic

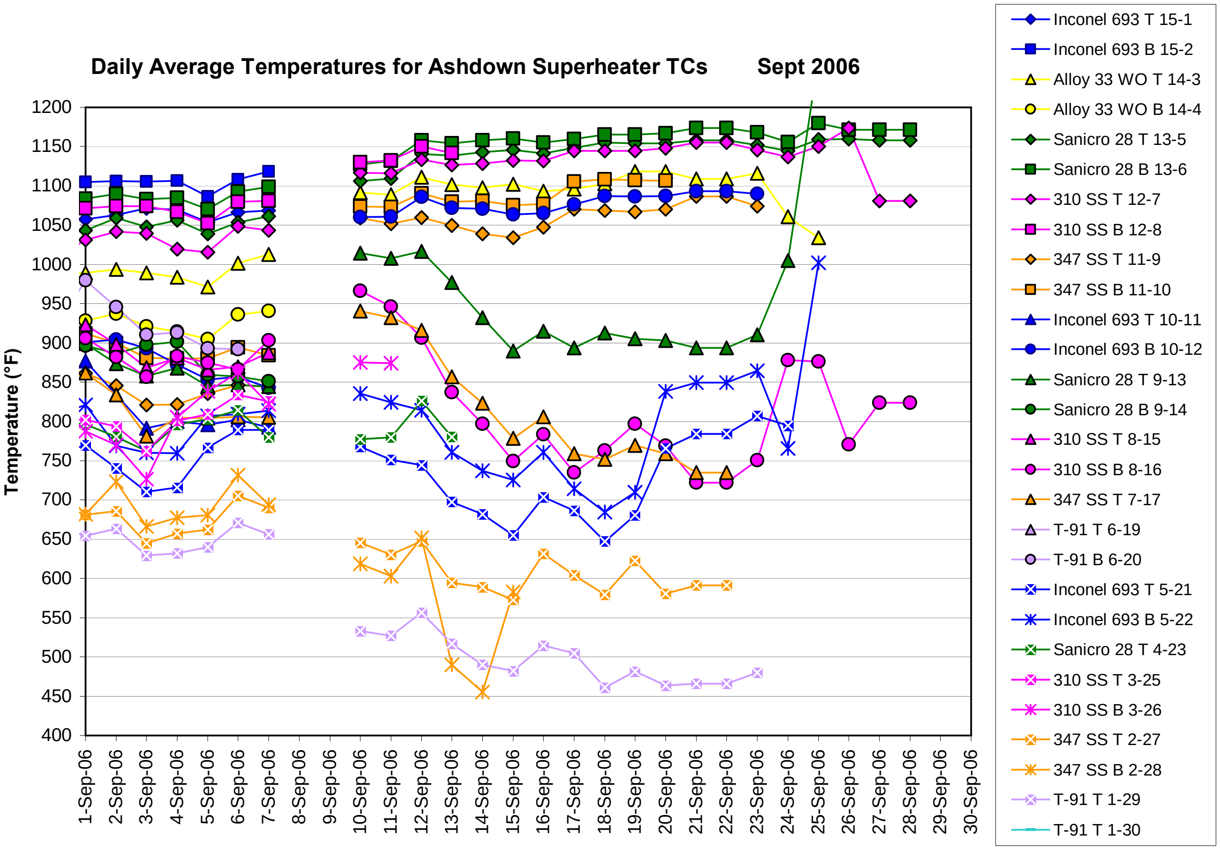

Figure 61. Daily average (measured) metal temperatures for the 30 thermocouples vs. date.

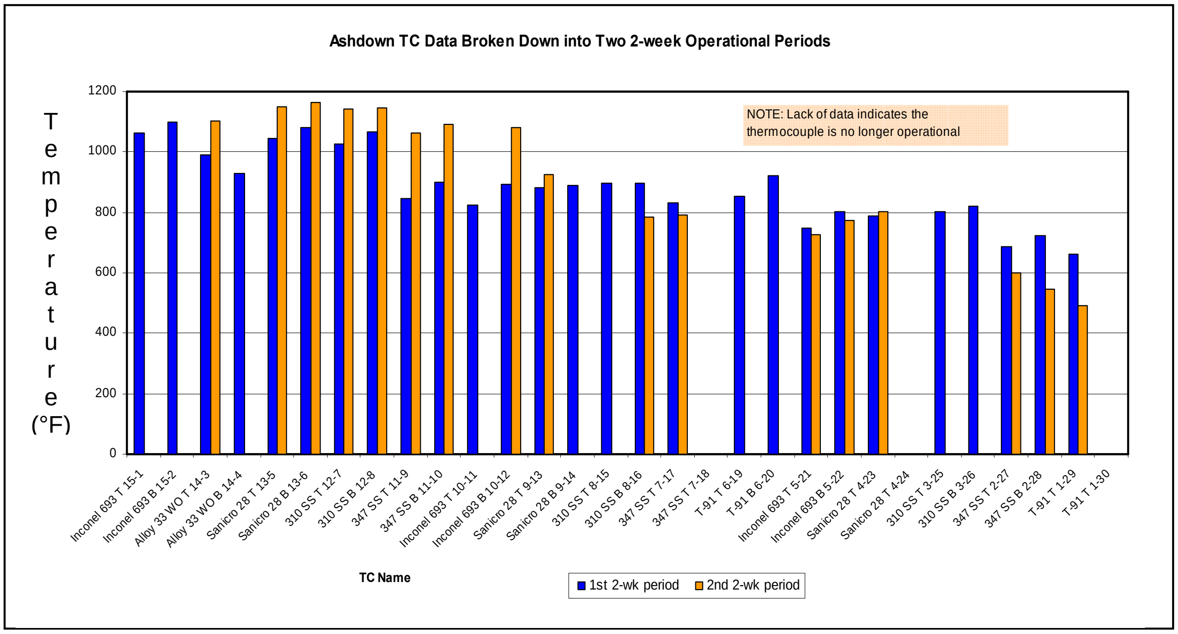

Figure 62. Thermocouple data for initial two week and later two week operating periods.

measurements impossible to make. As a result, the wall thicknesses measured from micrographs of the sample cross sections were compared to the pre-exposure thicknesses measured ultrasonically. Results of the thickness measurements are summarized in Table 11. There are many issues associated with interpretation of these results. First, the ultrasonic measurements were made after the probe was assembled, and the number reported for each sample was an average of at least a half dozen measurements. The post-exposure measurements were made on the 16X micrographs of the cross-sections. Errors could be introduced in the measurements or if the samples were not polished perpendicular to the axis of the tubular samples. Despite these shortcomings, there is some information to be gained from these results.

The six coolest samples showed no significant wall thickness changes. Stainless steel samples #7, #8, #11, and #12 as well as samples #14 and #15 all showed meaningful thickness losses. These measurements did not differentiate between unaffected metal and metal that suffered sub-surface attack, and as can be seen from the micrographs in Fig. 63, many of the samples exposed at the higher temperatures experienced sub-surface degradation.

The collection of micrographs in Fig. 63 shows the outer surface on the “bottom” side (180° position) of the tubular samples at an original magnification of 500X; additional micrographs are shown in Appendix 2. These micrographs show that for each alloy, the higher the temperature, the more extensive the degradation, particularly when the temperature exceeded the FMT. In addition, as a general rule, the lower the chromium content the more extensive was the degradation. Of the five samples at the highest temperature, the two stainless steels experienced external corrosion and some subsurface, probably intergranular attack. The other three samples had a more uniform subsurface degradation; the electron microprobe studies provided more information about the nature of this degradation. The more extensive collection of micrographs in Appendix 2 shows attack was generally worse on the bottom of the samples than on the top.

Table 11. Pre and post exposure thicknesses of corrosion probe samples

Sample number and ID	Average pre-exposure thickness measured ultrasonically (inches)	Post-exposure thickness from metallographic samples (inches)	
		90° from top	270° from top
1-1 T-91	0.225	0.229	0.221
1-2 347H stainless steel	0.183	0.183	0.183
1-3 310H stainless steel	0.259	0.258	0.258
1-4 Sanicro 28	0.213	0.214	0.216
1-5 Inconel 693	0.135	0.134	0.135
1-6 T91	0.225	0.228	0.231
1-7 347H stainless steel	0.184	0.182	0.180
1-8 310H stainless steel	0.263	0.254	0.256
1-9 Sanicro 28	0.215	0.213	0.216
1-10 Inconel 693	0.132	0.134	0.131
1-11 347H stainless steel	0.182	0.177	0.179
1-12 310H stainless steel	0.260	0.252	0.254
1-13 Sanicro 28	0.212	0.208	0.214
1-14 Alloy 33 weld overlay	0.202	0.190	0.185
1-15 Inconel 693	0.128	0.131	0.122

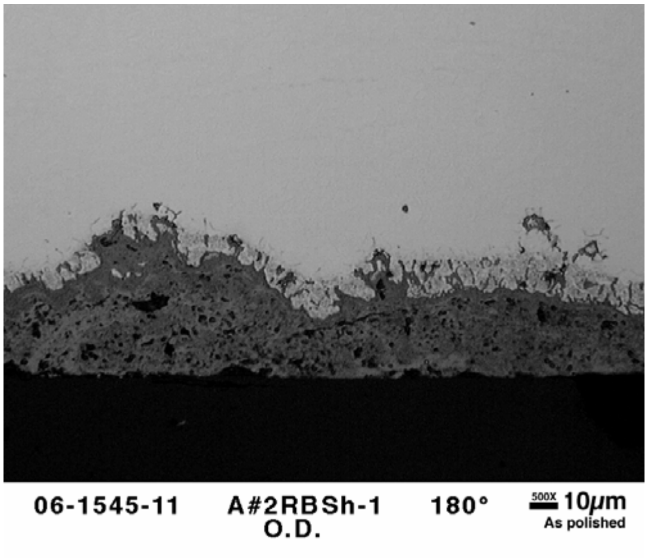

Figure 63a. T-91 - sample #1

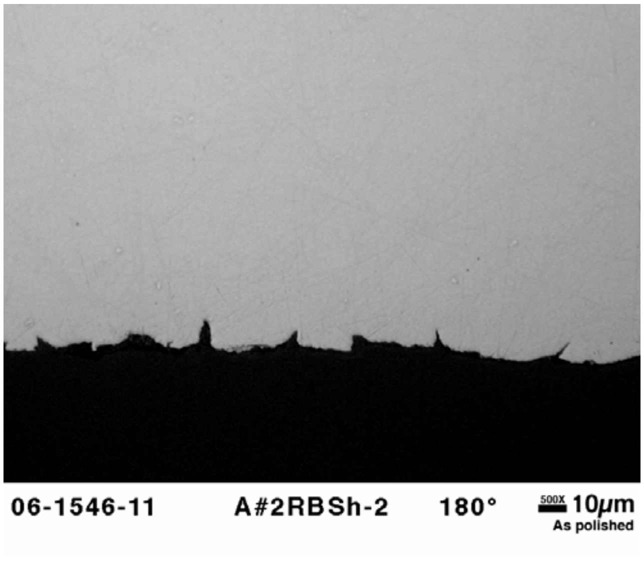

Figure 63b. 347H stainless steel – sample #2

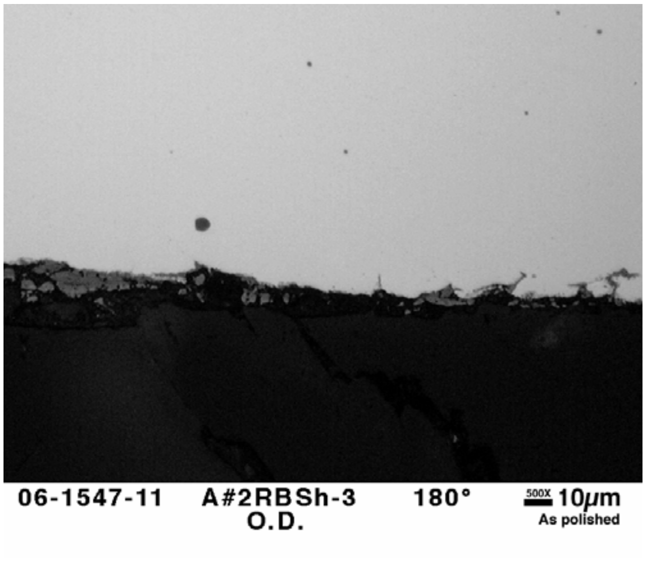

Figure 63c. 310H stainless steel – sample #3

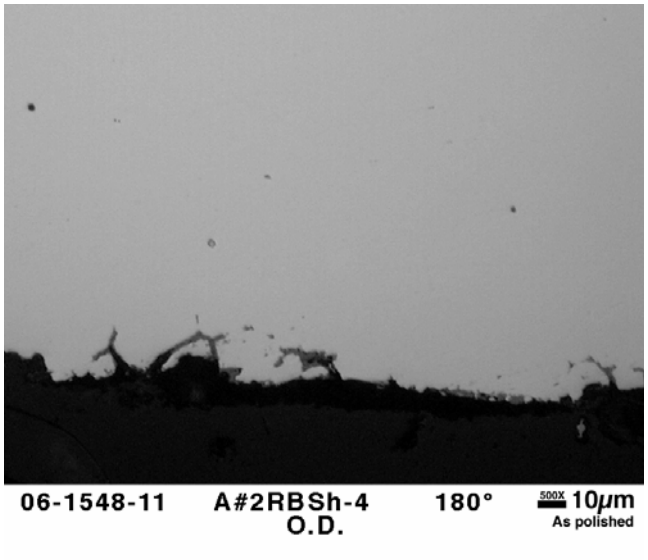

Figure 63d. Sanicro 28 – sample #4

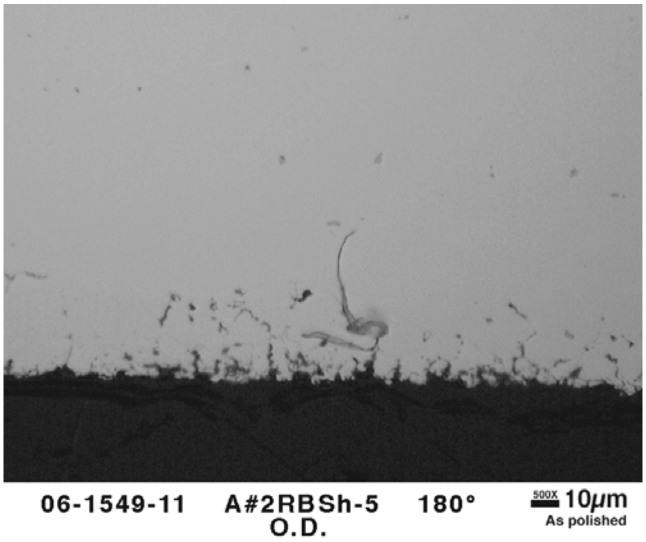

Figure 63e. Inconel 693 – sample #5

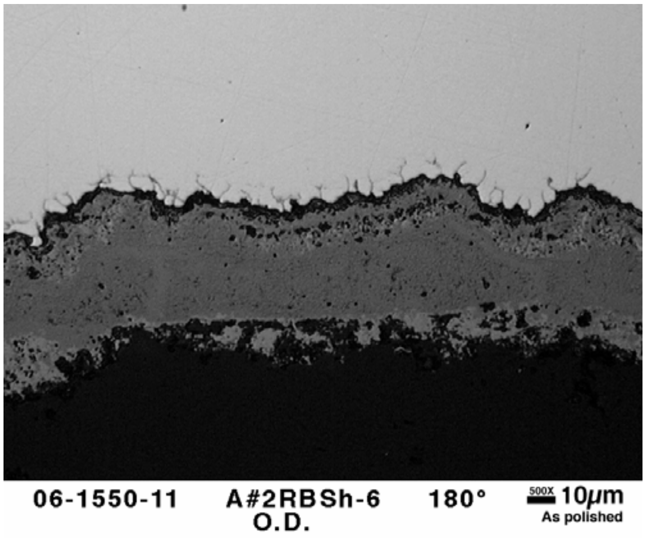

Figure 63f. T91 – sample #6

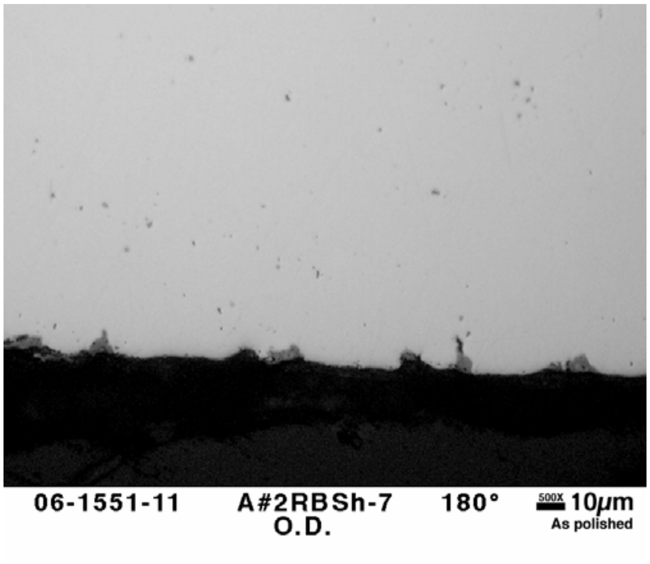

Figure 63g. 347H stainless steel – sample #7

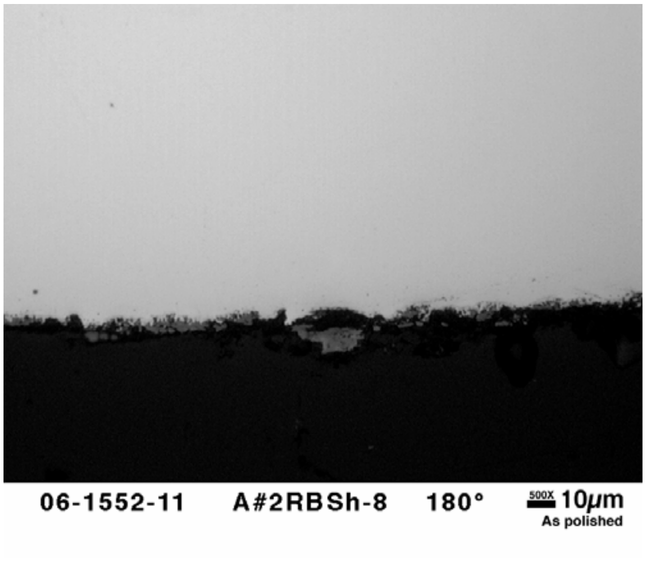

Figure 63h. 310H stainless steel – sample #8

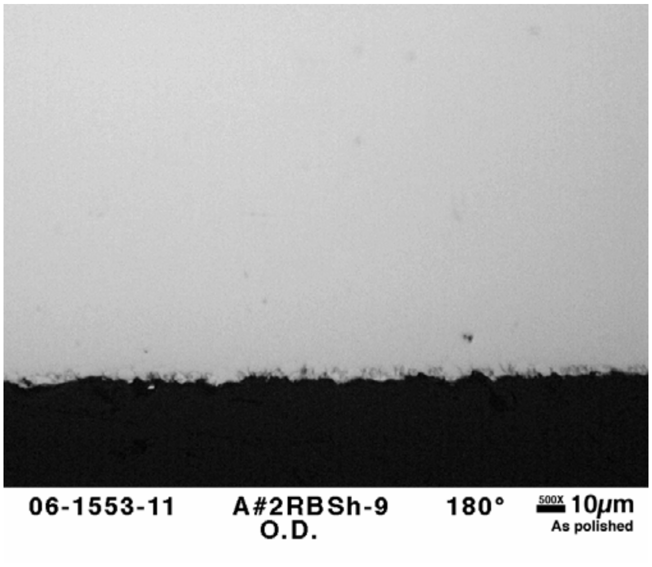

Figure 63i. Sanicro 28 – sample #9

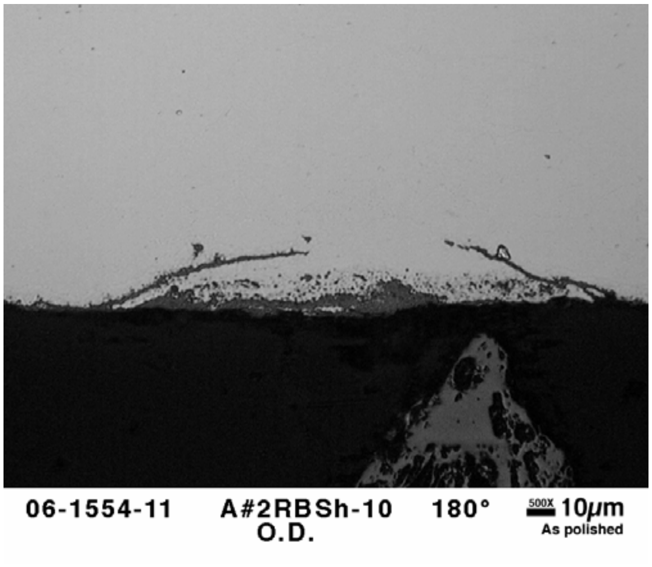

Figure 63j. Inconel 693 – sample #10

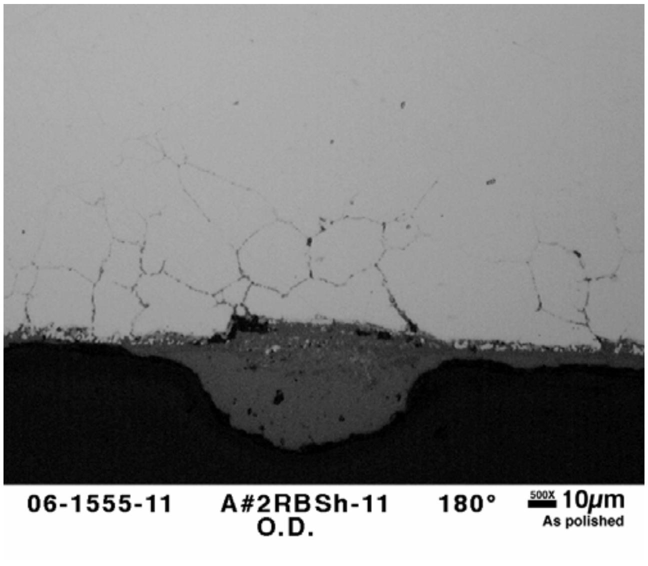

Figure 63k. 347H stainless steel – sample #11

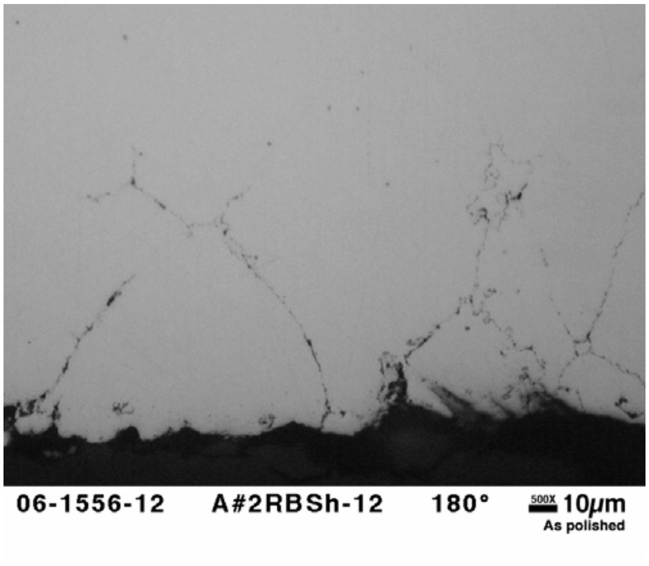

Figure 63l. 310H stainless steel – sample #12

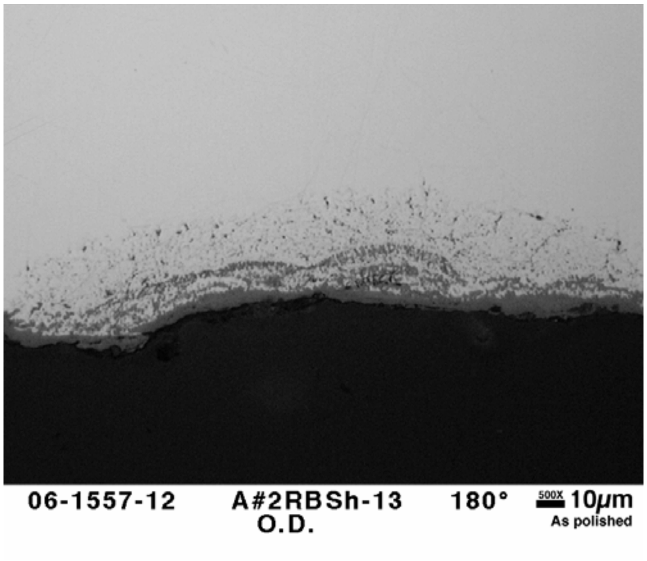

Figure 63m. Sanicro 28 – sample #13

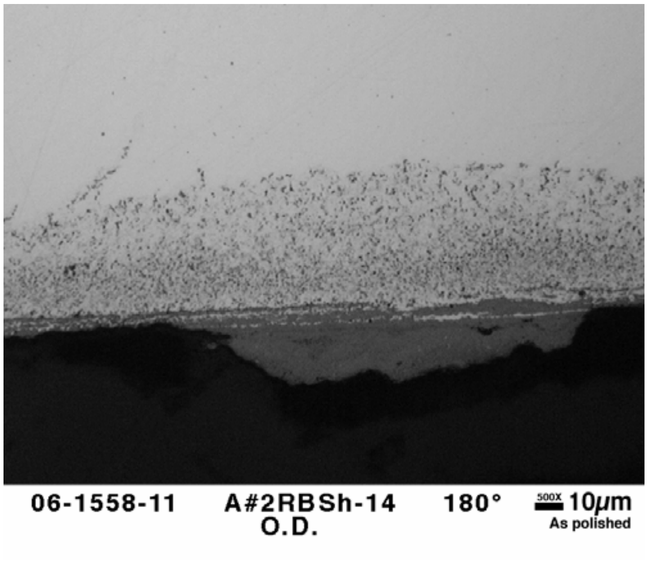

Figure 63n.Alloy 33 weld overlay–sample #14

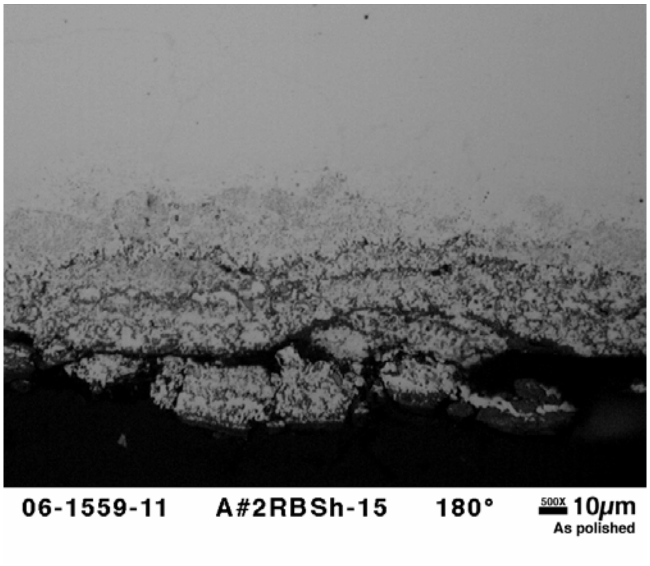

Figure 63o. Inconel 693 – sample #15

In order to better characterize the surface reactions that occurred on the samples exposed on the superheater corrosion probe, the electron microprobe was used to map the distribution of elements on and just below the outer surface of the ten samples exposed to the highest temperatures. A summary and description of the most significant microprobe results for each of the ten samples is given in the following text.

Sample #6 – T-91 steel
Figure 64 contains a series of micrographs that show the distribution of iron, chromium, molybdenum and oxygen in the sample that was exposed in the superheater at temperatures no higher than 510°C (950°F). This sample has a significant corrosion product layer on the surface, and the maps indicate the corrosion product is depleted in iron (compared to the base metal), enriched in chromium and molybdenum and contains a significant amount of oxide. This leads to the conclusion that the layer contains iron and chromium oxide.

Sample #7 – type 347H stainless steel

The micrographs in Fig. 65 show the reaction product on the 347H stainless steel sample exposed at temperatures definitely below the FMT of the superheater deposits. The corrosion product on the surface contains an outer layer richer in iron oxide and an inner layer containing primarily chromium oxide. The chlorine map shows appreciable chlorine content associated with the chromium oxide layer as well as the boiler material deposits that accumulated on the probe during operation.

Sample #8 – type 310H stainless steel

This stainless sample, as shown in Fig. 66, also has surface deposits of boiler material that contain oxygen but little or no iron and chromium. However, there are pits and subsurface penetrations that contain chromium oxide. There is a sulfur-containing layer on the metal surface and the surface deposits are enriched in sodium and oxygen.

Sample #9 – Sanicro 28

Although the thermocouples on this sample failed fairly early, based on temperatures reached by adjacent samples it appears the surface temperature of this sample probably did not exceed 538°C (1000°F). The micrographs in Fig. 67 show a thin oxygen-containing surface layer, primarily chromium oxide but with some iron oxide particularly where the chromium oxide appears to have separated from the surface of the sample. A layer of sulfur also appears to be present on the surface of the sample.

Sample #10 – Inconel 693

This alloy was included in the test series because of an interest in determining if a protective alumina layer would be formed on the surface of the alloy. It is generally thought that exposure to an oxidizing environment at temperatures of 900-1000°C is necessary to form the alumina layer, and this sample only reached about 600°C. The micrographs in Fig. 68 show this sample experienced a significant amount of subsurface attack. Some subsurface regions were depleted in chromium and aluminum while other areas had elevated concentrations. Oxygen was present in these regions of elevated chromium and aluminum indicating the presence of chromium and aluminum oxides. Scattered regions of increased sulfur concentration were also present, and these regions included areas where subsurface oxides were observed.

Sample #11 – 347H stainless steel

The microprobe images in Fig. 69 show this sample suffered considerable intergranular attack as well as having some surface corrosion products. Sulfur was particularly evident on the grain boundaries while no evidence of grain boundary enrichment of chromium was found. A thin chromium layer was present on the outer surface, and some enrichment of iron and chromium was also seen in the surface layers. The surface enrichment of iron and chromium corresponded to areas of high oxygen concentration, and oxygen was also seen on some of the grain boundaries.

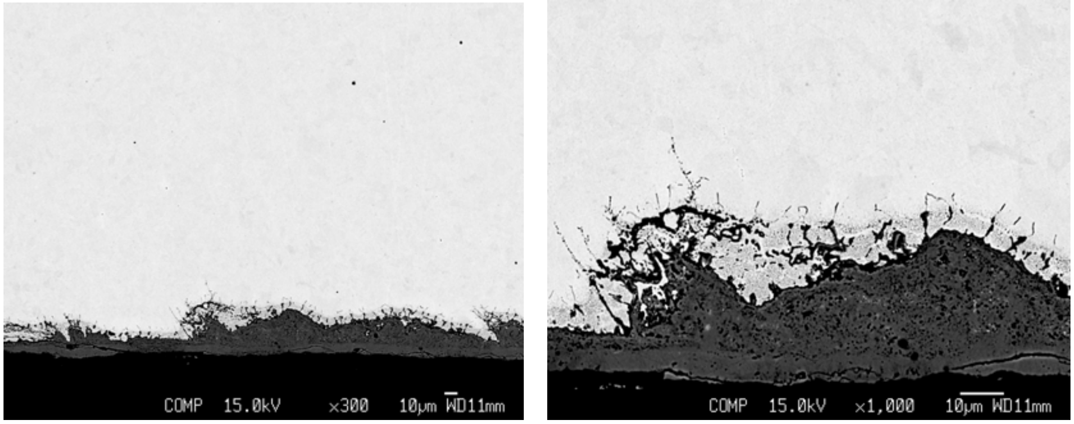

BSE 300 X BSE 1000 X

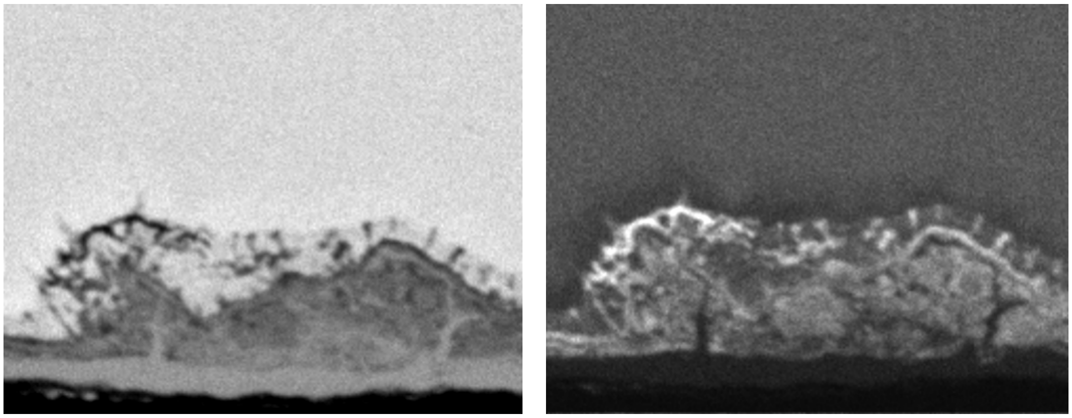

Fe map - 1000 X Cr map – 1000 X

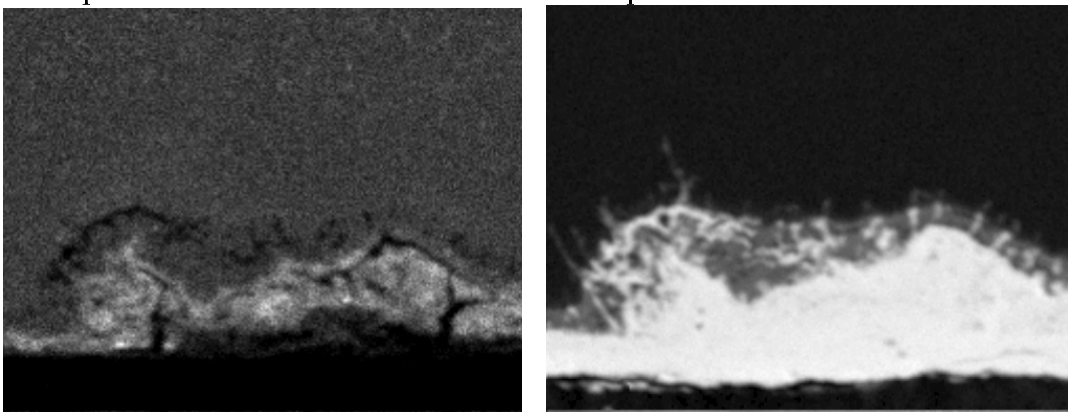

Mo map – 1000 X O map – 1000 X

Figure 64. Electron microprobe images from T-91 sample #6.

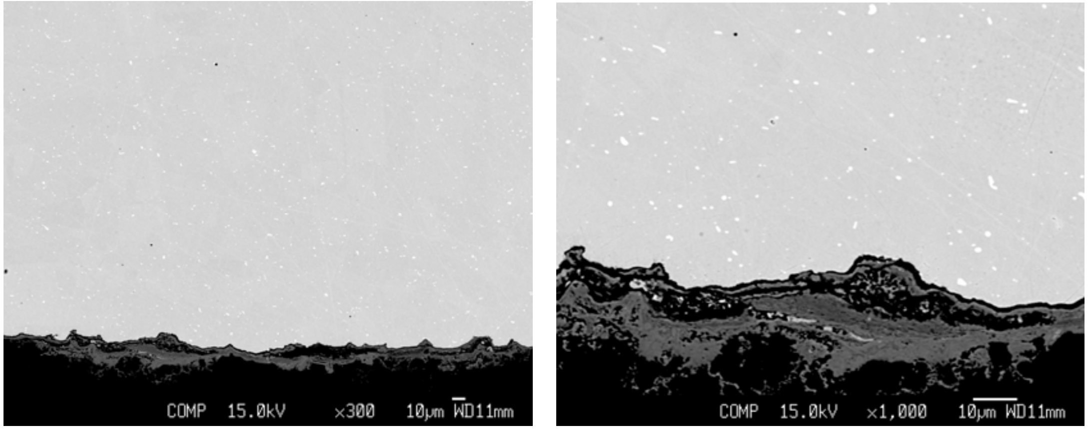

BSE 300 X BSE 1000 X

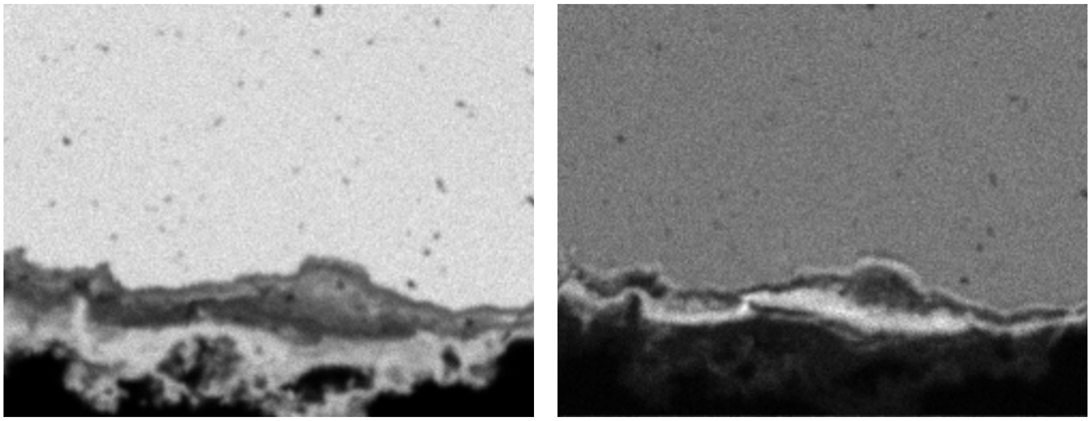

Fe map – 1000 X Cr map – 1000 X

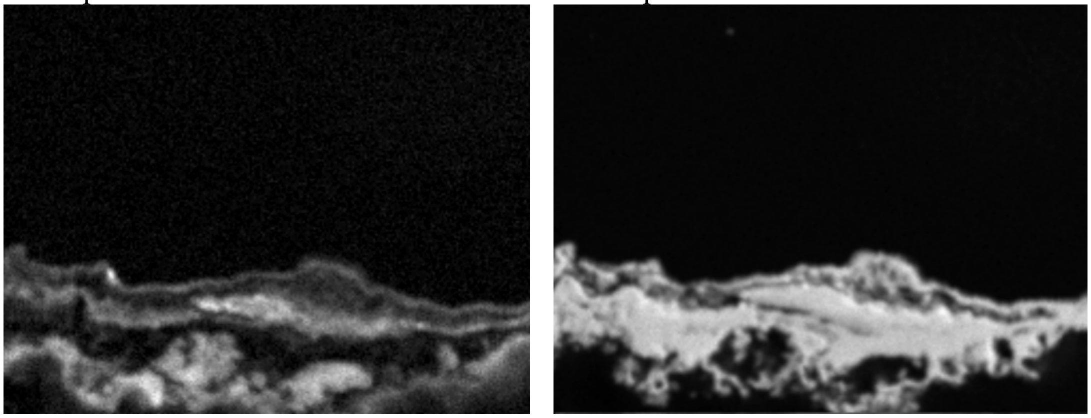

Cl map – 1000 X O map – 1000X

Figure 65. Electron microprobe images from 347H stainless steel sample #7

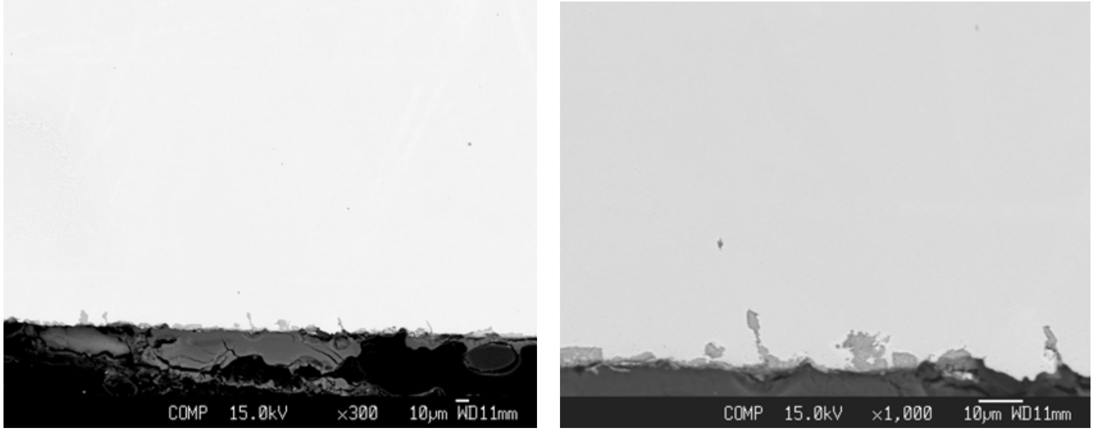

BSE 300 X BSE 1000 X

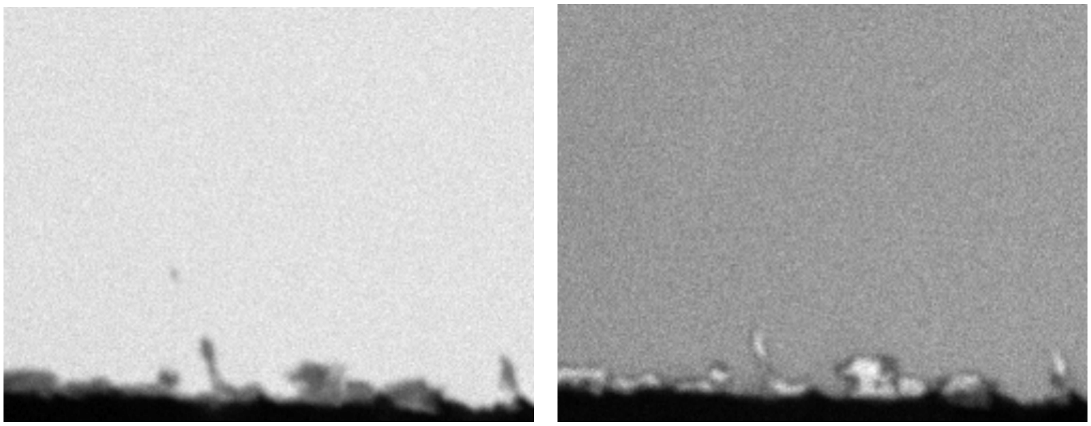

Fe map – 1000 X Cr map – 1000 X

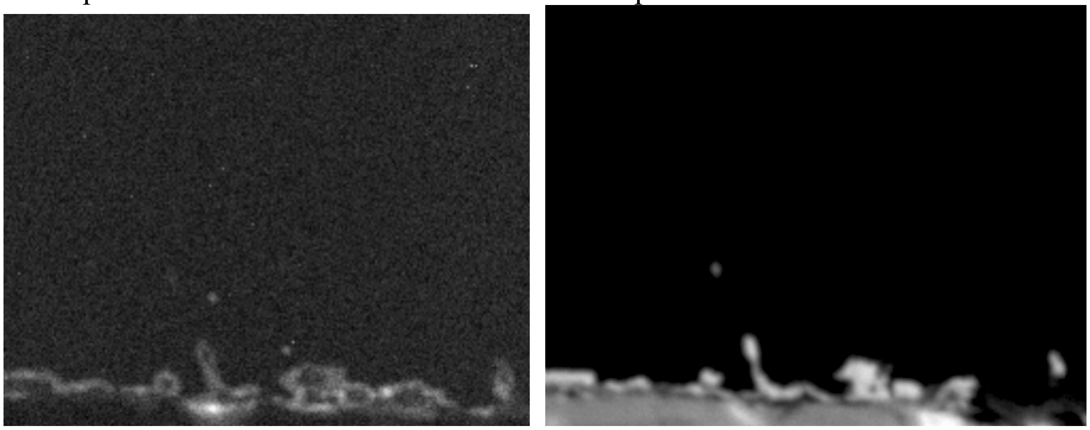

S map – 1000 X O map – 1000 X

Figure 66. Electron microprobe images from 310H stainless steel sample #8

Sample #12 – type 310H stainless steel

Like the 347H sample #11, this stainless steel sample suffered subsurface attack of the base metal. The micrographs in Fig. 70 show what are likely transgranular cracks that originate at the surface and advance a significant distance into the sample. A chromium oxide layer is present on the surface, and this layer appears to be continuous. Chlorine and sulfur are also present in this layer, and oxygen, sulfur and chlorine are concentrated on the cracks that advance into the base material. However, potassium and sodium were not present in significant amounts in the cracks into the base metal. Note that the magnification on these micrographs is 600X rather than 1000X as is the case for the elemental maps shown for 8 0f the other 9 samples examined.

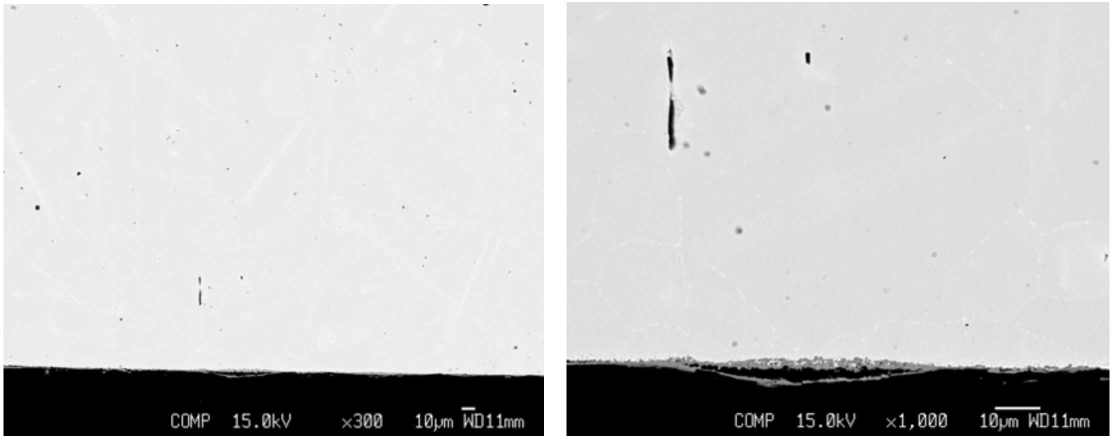

BSE 300 X BSE 1000 X

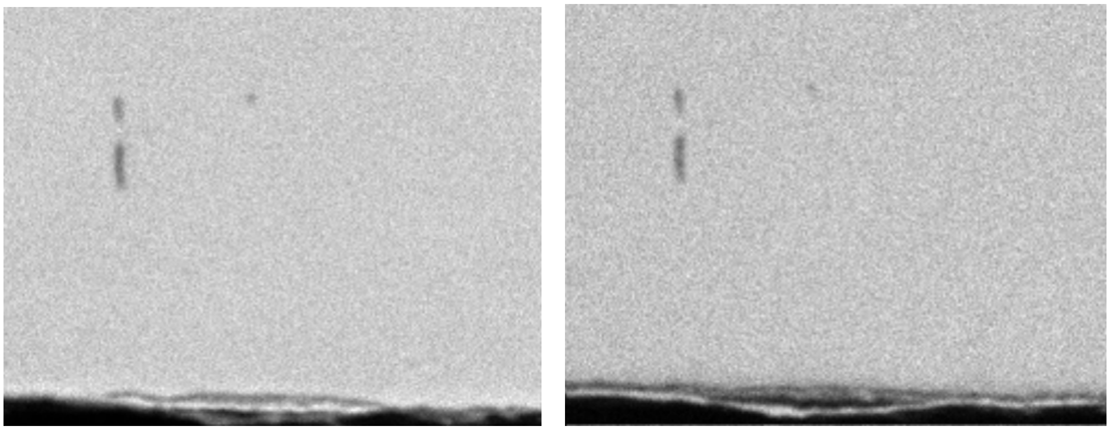

Fe map – 1000 X Cr map – 1000 X

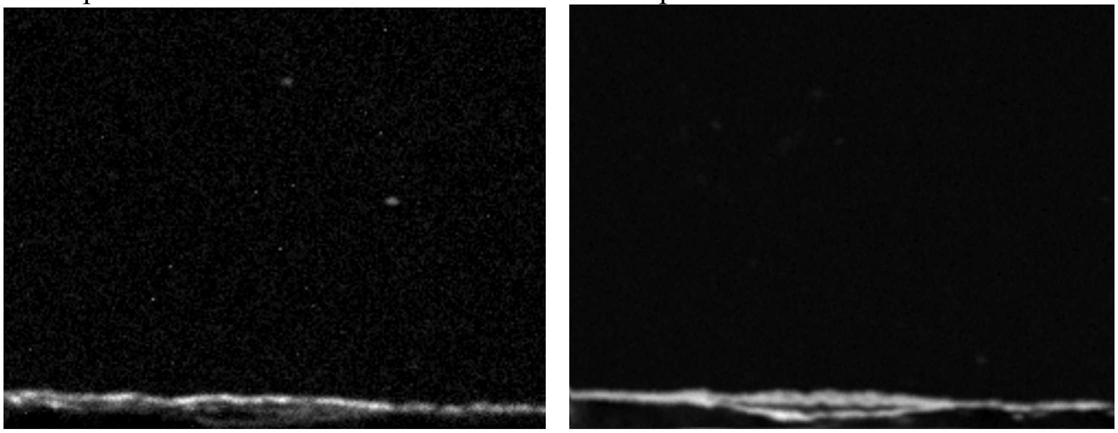

S map – 1000 X O map – 1000 X

Figure 67. Electron microprobe images from Sanicro 28 sample #9

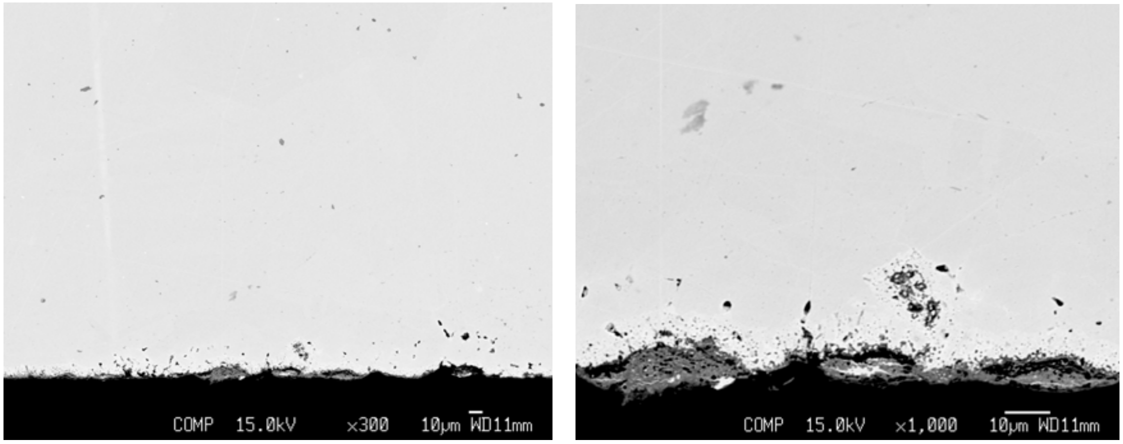

BSE 300 X BSE 1000 X

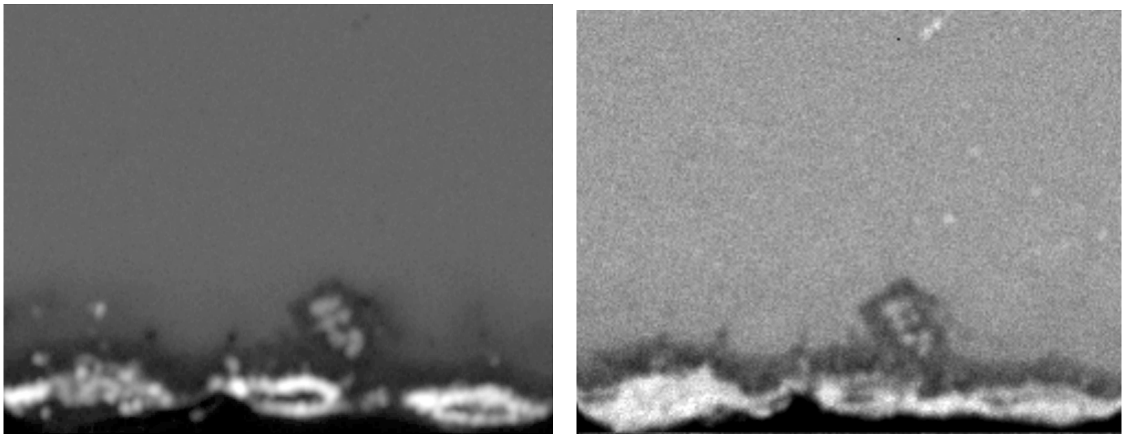

Al map – 1000 X Cr map – 1000 X

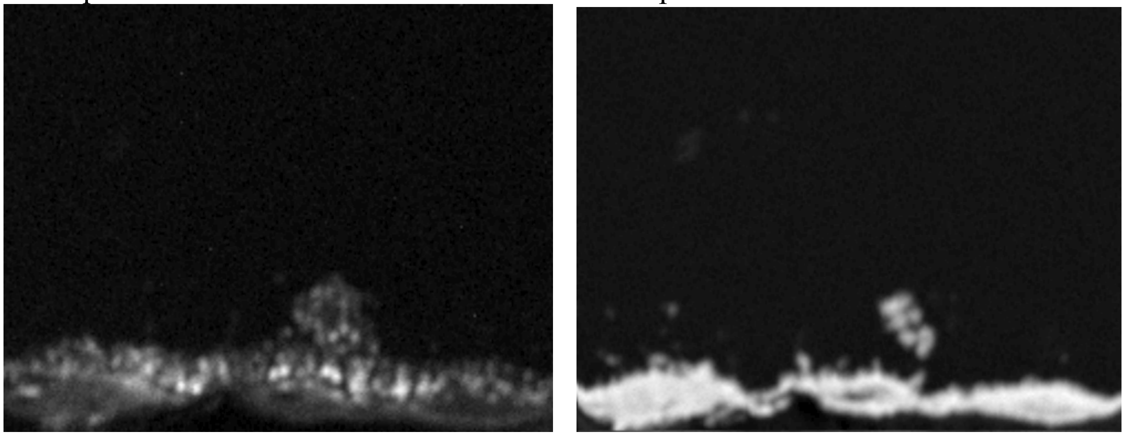

S map – 1000 X O map – 1000 X

Figure 68. Electron microprobe images from Inconel 693 sample #10

Sample #13 – Sanicro 28

This sample was exposed at temperatures as high as 645°C (1193°F) which is well above the FMT. The sample shows evidence of subsurface attack, but the extent is less than on the adjacent type 310H stainless steel sample and, as shown in Figs 72 and 73, than the two samples exposed at higher temperature. The elemental maps for this sample, which are given in Fig. 71, show there is a nearly continuous enrichment of chromium and oxygen along the surface indicating the presence of a chromium oxide layer. There is depletion of chromium in the sample just below the surface and a corresponding increase of iron in the area where chromium is depleted. In these subsurface, chromium-depleted regions, some sulfur and, to a lesser extent, chlorine, is present.

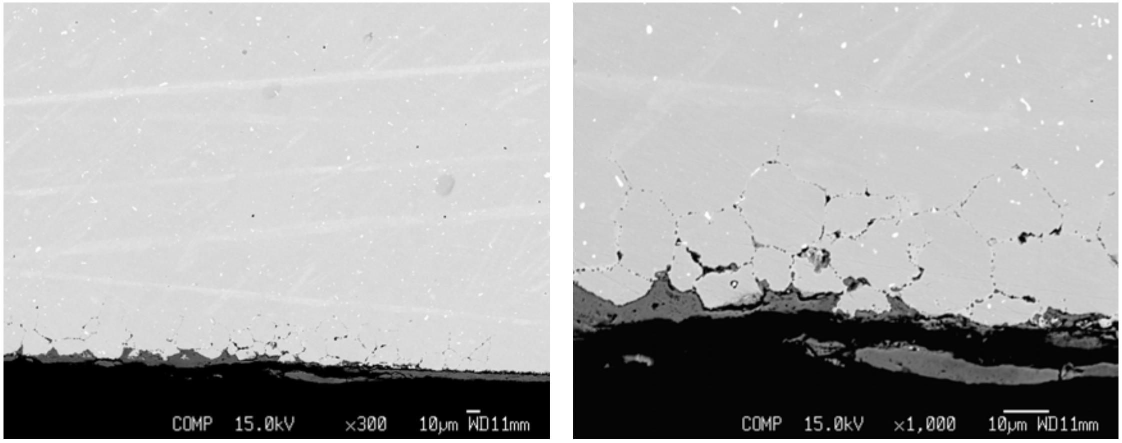

BSE 300 X BSE 1000 X

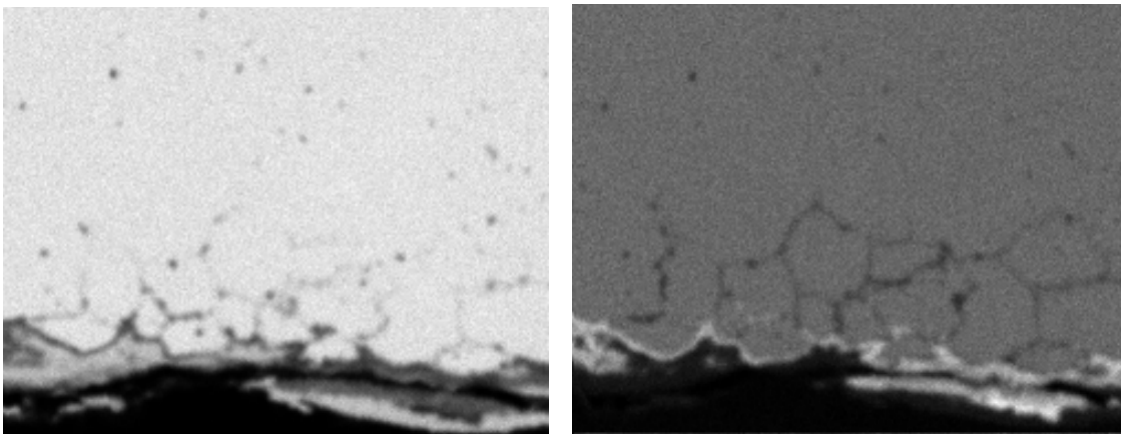

Fe map – 1000 X Cr map – 1000 X

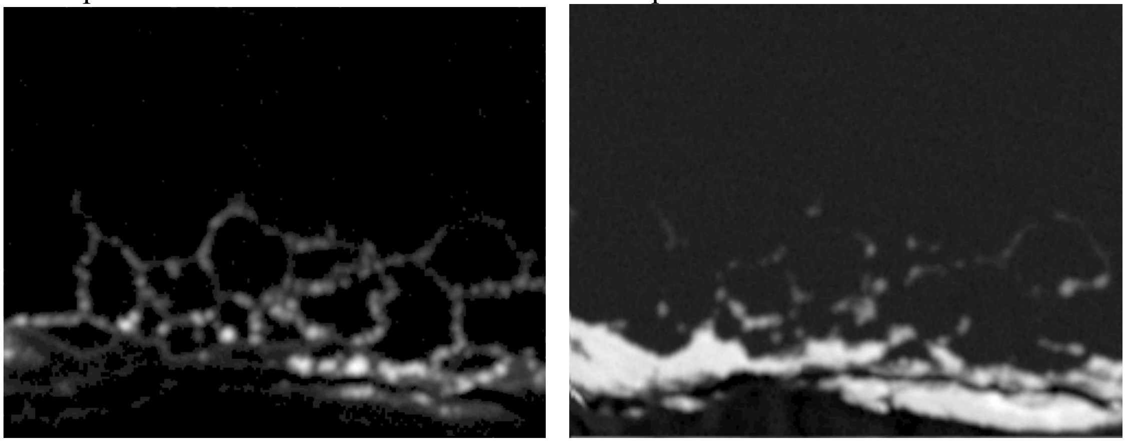

S map – 1000 X O map – 1000 X

Figure 69 Electron microprobe images from 347H stainless steel sample #11

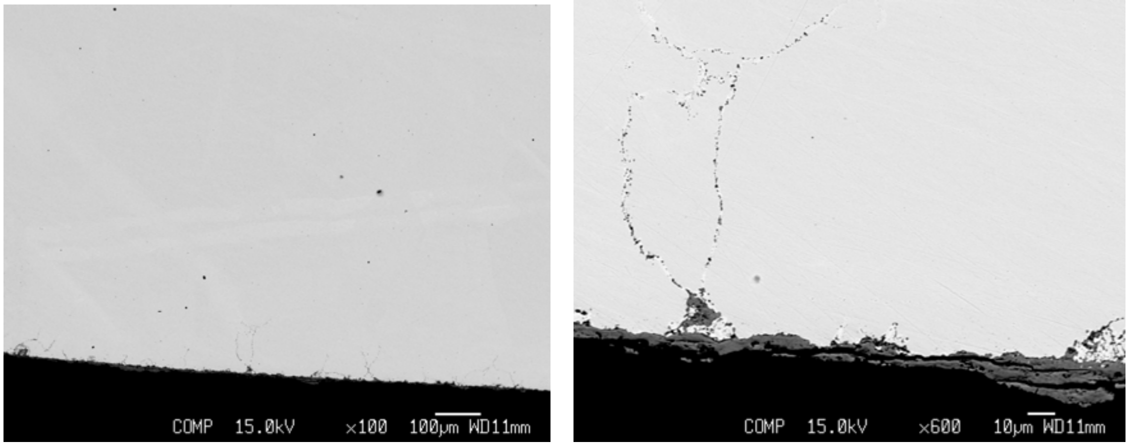

BSE 100 X BSE 600 X

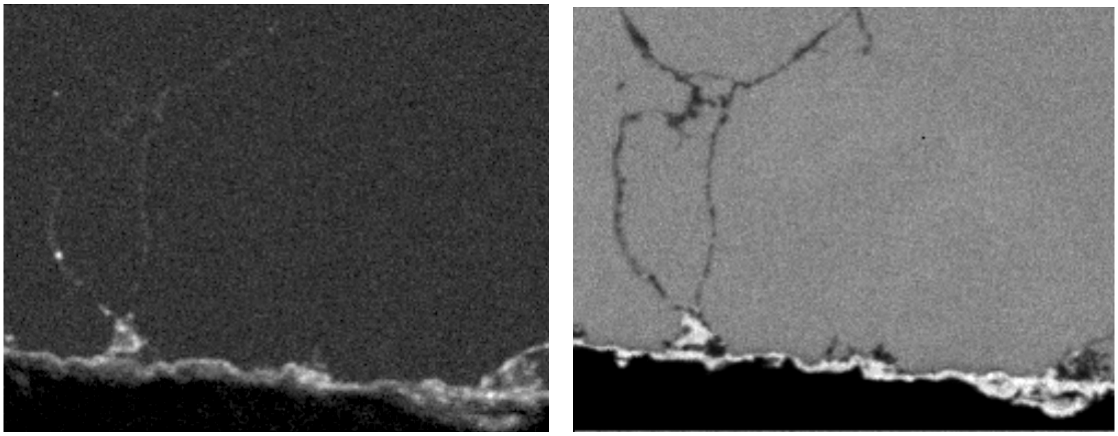

Cl map – 600 X Cr map – 600 X

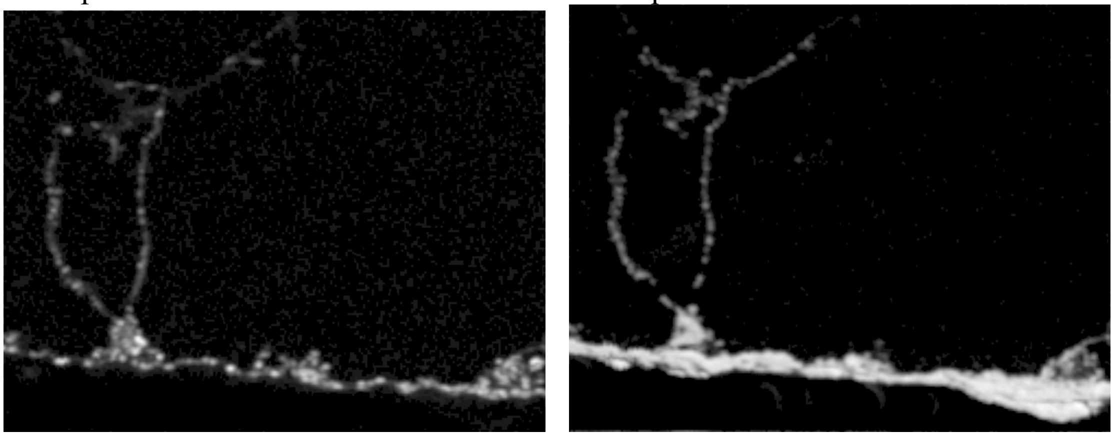

S map – 600 X O map – 600 X

Figure 70 Electron microprobe images from 310H stainless steel sample #12

Sample #14 – Alloy 33 weld overlaid on carbon steel
Figure 72 shows micrographs taken with the electron microprobe of the carbon steel sample that had an Alloy 33 weld overlay. Note that the elemental maps are shown at 400 X because of the size of the corrosion product on the surface and the volume of the affected subsurface region. The corrosion product on the surface is primarily chromium oxide, but there are detectable

amounts of chlorine and sulfur in the corrosion product. Sodium and potassium are also present in the corrosion product. In the subsurface area, there appear to be at least two distinct layers where the chromium, iron and nickel content vary. The sulfur content seems to be higher in the outermost of the subsurface layers and this may be due to development of some porosity in this sample. Clearly, this sample has undergone significant degradation.

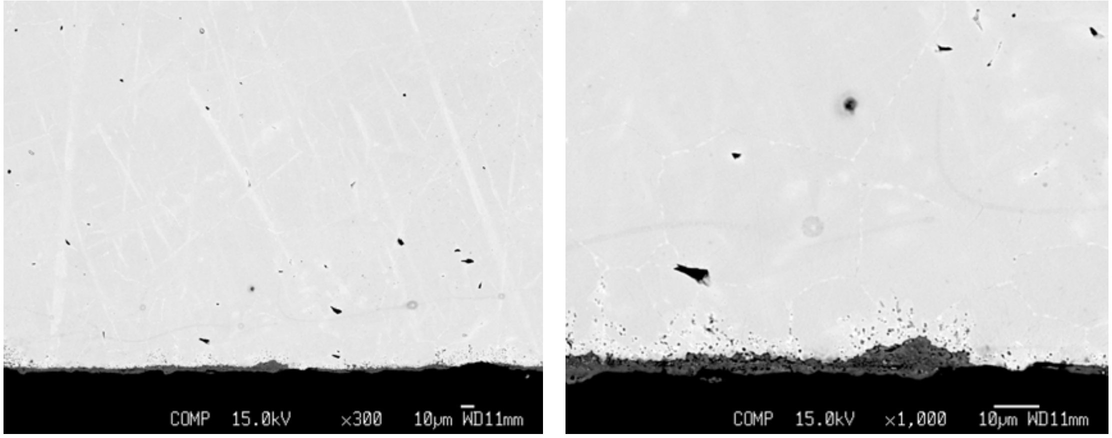

BSE 300 X BSE 1000 X

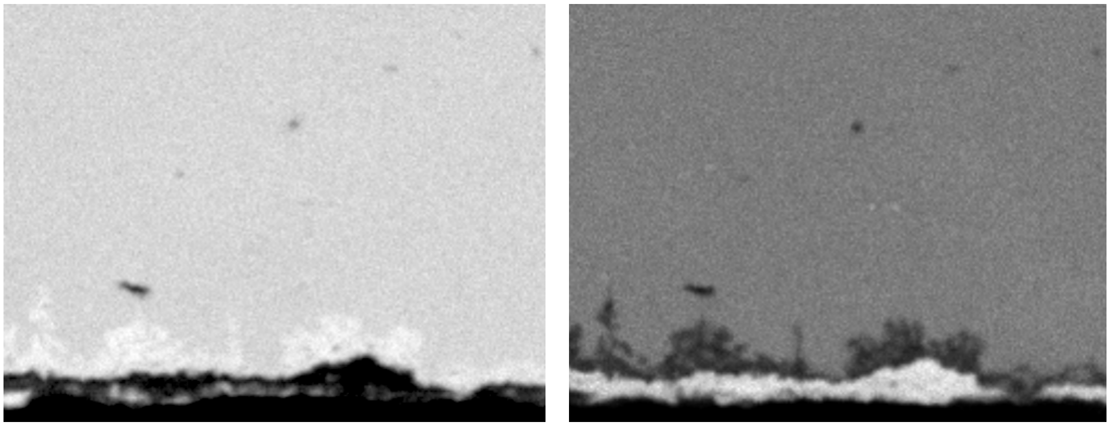

Fe map – 1000 X Cr map – 1000 X

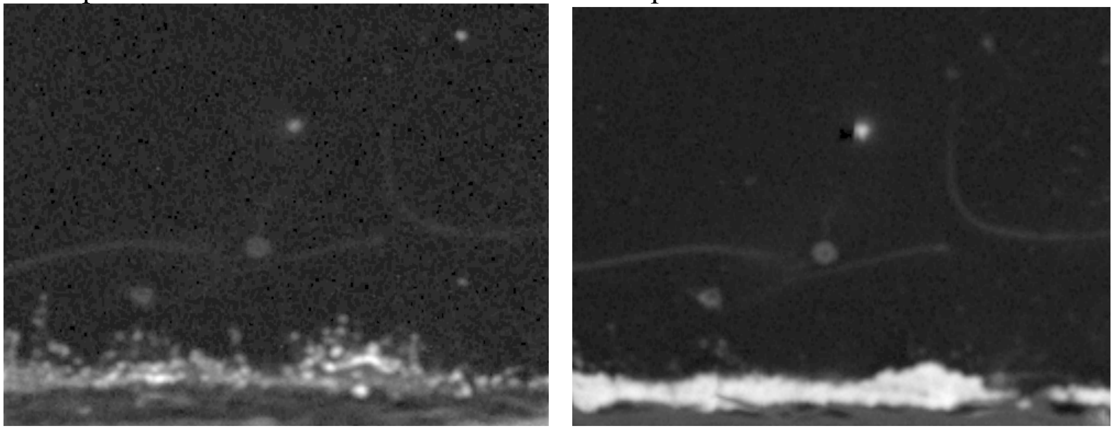

S map – 1000 X O map – 1000 X

Figure 71 Electron microprobe images from Sanicro 28 sample #13

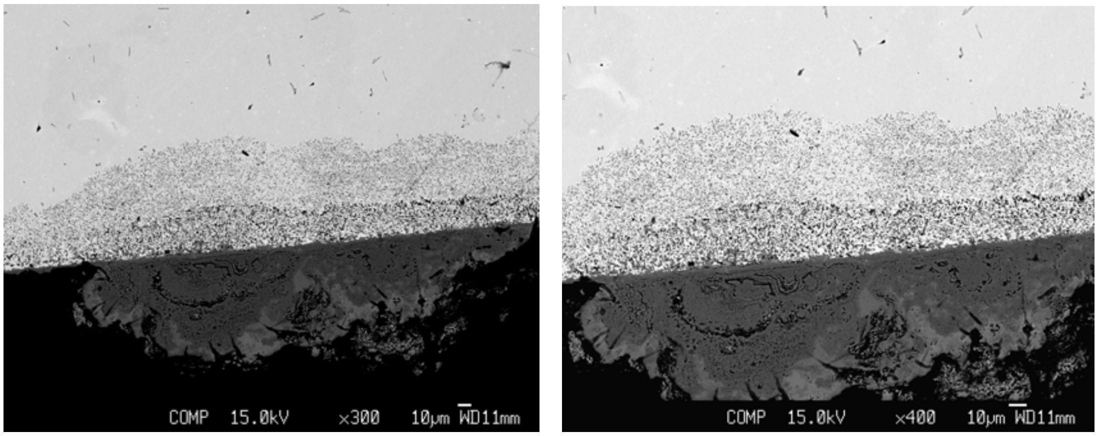

BSE 300 X BSE 400 X

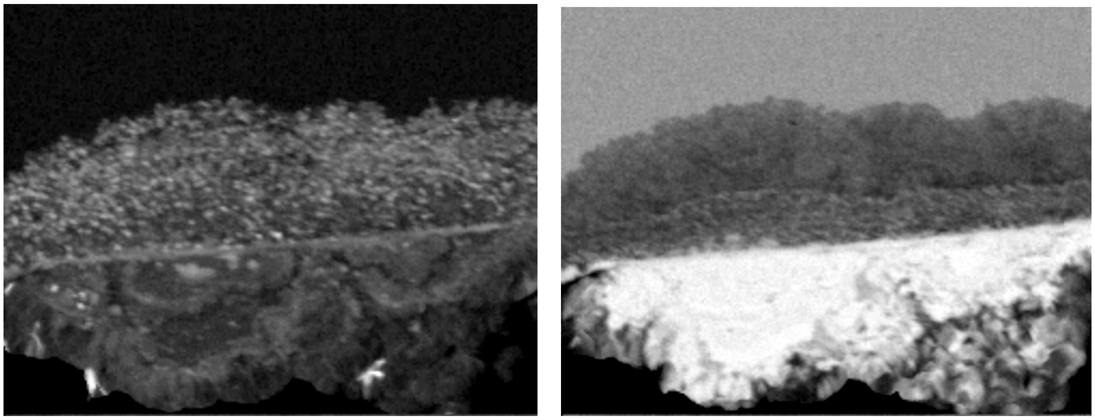

Cl map – 400 X Cr map – 400 X

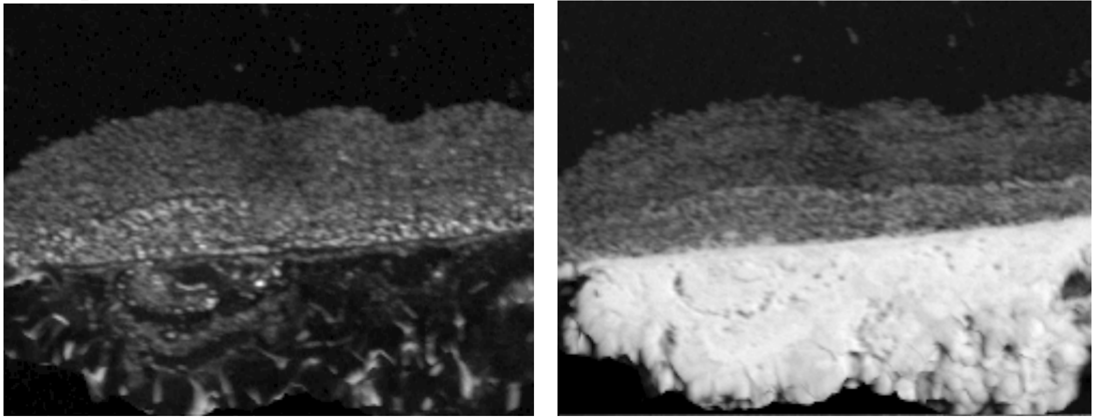

S map – 400 X O map – 400 X

Figure 72 Electron microprobe images from Alloy 33 weld overlay sample #14

Sample #15 – Inconel 693

As noted previously in this report, this alloy was chosen because of its ability to form a protective layer of alumina when exposed in an oxidizing environment at a sufficiently high temperature. Even though the surface of this sample probably reached temperatures in excess of 650°C (1200°F), it is very likely the temperature did not reach the level where a continuous and protective alumina layer could form. The elemental maps show the presence of a nearly continuous aluminum layer on the surface with an aluminum-enriched layer just below the surface. This same region appears depleted in chromium. Significant oxygen is present in this aluminum enriched region, but there apparently is not a continuous, protective layer developed. There is also sulfur present in this first subsurface, aluminum-enriched layer suggesting this may be a porous layer. However, potassium and sodium do not appear to be particularly enriched in this layer. The extent of degradation of this sample is not as extensive as on sample #14, but it significant enough that this alloy does not have enough corrosion resistance for this application.

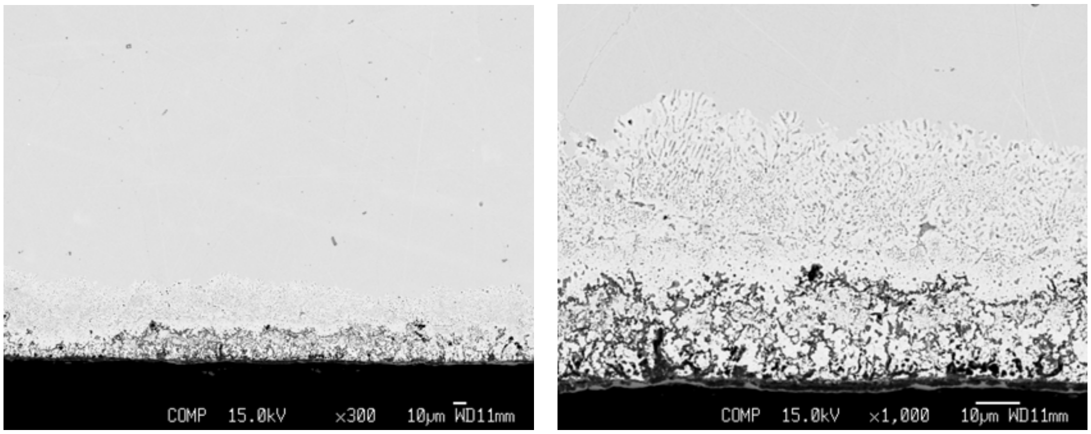

BSE 300 X BSE 1000 X

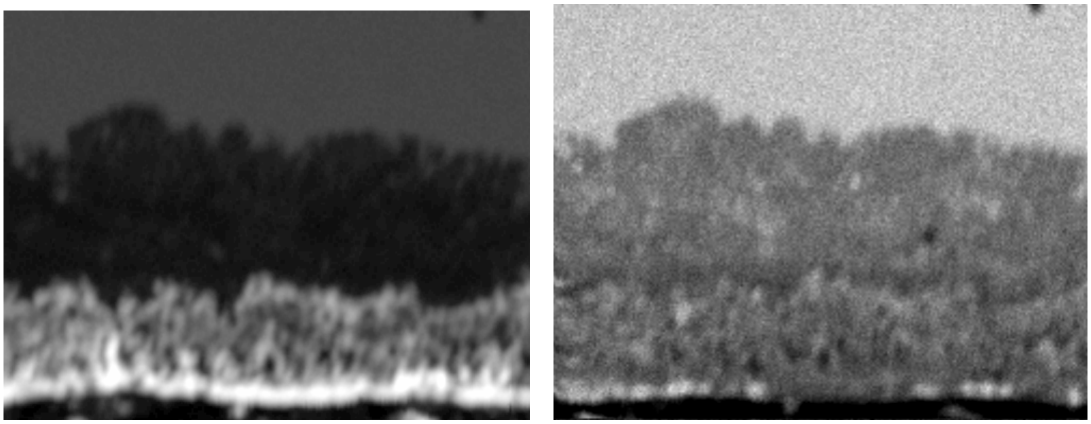

Al map – 1000 X Cr map – 1000 X

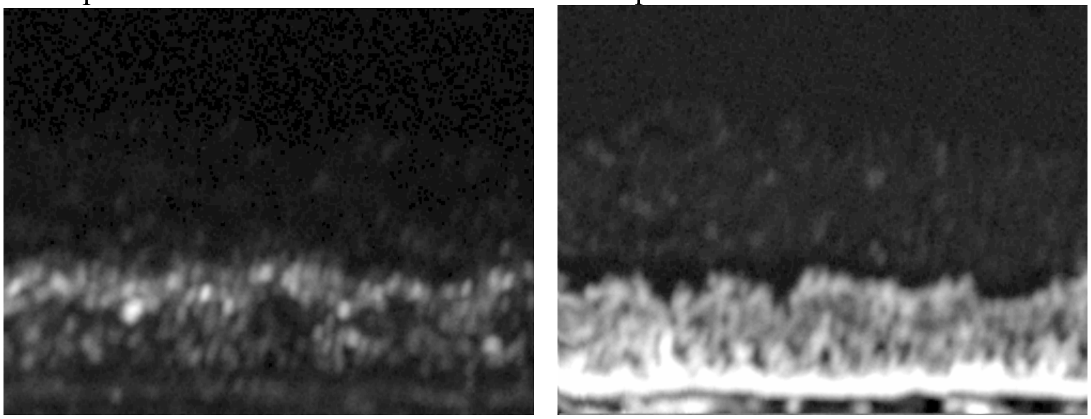

S map – 1000 X O map – 1000 X

Figure 73 Electron microprobe images from Inconel 693 sample #15

Discussion

The superheater corrosion probe exposure and examination that constituted the field study portion of this task provided information that complemented the laboratory corrosion studies. Examination of the probe samples provided information about the extent of wall thinning, the protective layers that did (or did not) form on the surface of the samples, the extent of subsurface attack and the extent of subsurface depletion of alloying elements. The two 300 series stainless samples exposed below the FMT showed wall thinning as did the samples of all alloys that were exposed above the FMT. A chromium oxide layer was observed on most of the samples examined with the electron microprobe although in a few cases, there was some doubt as to whether the layer was continuous and protective. The alumina-forming Inconel 693 was exposed at a temperature below that generally thought to be necessary to form a continuous alumina layer, and, not unexpectedly, it appeared the layer formed on the probe samples was not sufficient to protect the samples from significant degradation.

The six samples exposed at the highest temperatures as well as stainless steel samples #7 and #8 experienced subsurface attack. In some cases this was in the form of cracking while in other cases it was general attack that resulted in the depletion of selected elements from just below the surface of the samples. From the examinations several observations can be made.

- The attack mode consisted of external scaling and internal penetration, both above and below the expected FMT.
- The attack was generally most severe at the 180° (bottom) position.
- For a given alloy, the scale thickness and the depth of internal penetration observed were greater for the sample exposed at temperatures above the FMT.
- The depth of internal penetration observed varied among the set of alloys exposed at temperatures above and below the expected FMT.

An attempt was made to quantify the extent of corrosion by measuring the scale thickness and the depth of internal penetration observed on each sample at one of the four documented positions. Figure 74 shows the results of that attempt. Superimposed onto the bar chart is an estimated average exposure temperature for the outside surface of each sample. This estimated average is simply the average inside surface temperature, calculated from the data plotted in Fig. 61, plus an allowance to compensate for the expected temperature drop across the sample tube wall. Of the four alloys exposed at temperatures above the FMT, which includes the alumina-forming Alloy 693, Alloy 28 exhibited the lowest scale thickness and the lowest depth of internal penetration. Alloy 28 also exhibits the smallest total depth of attack of the four alloys exposed at temperatures just below the FMT. It exhibited the lowest scale thickness and the second lowest depth of internal penetration. Interestingly, this lowest total depth of attack exhibited by Alloy 28 occurred at the highest relative exposure temperature below the FMT.

Both the lab and field exposures were conducted in order to perform an evaluation of alloy suitability for superheaters in high energy-efficient HT/HP recovery boilers. The evaluation required a reliable corrosion measurement to form a comparative basis. Measurements of corrosion traditionally used for comparative purposes include weight gain (before descaling), weight loss (after descaling), scale thickness and depth of attack (external and internal). The interpretation presented below utilized the weight loss measurements for the lab exposure and depth of attack for the field exposure as the comparative basis. The use of scale thickness or depth of attack was not practical for the lab exposure given the relatively thin and non-uniform nature of the adhering scales and the lack of internal attack observed, respectively. Conversely, the use of a weight loss measurement for the field exposure was not practical for the field exposure given tightly adherent scales and the extent of internal attack observed.

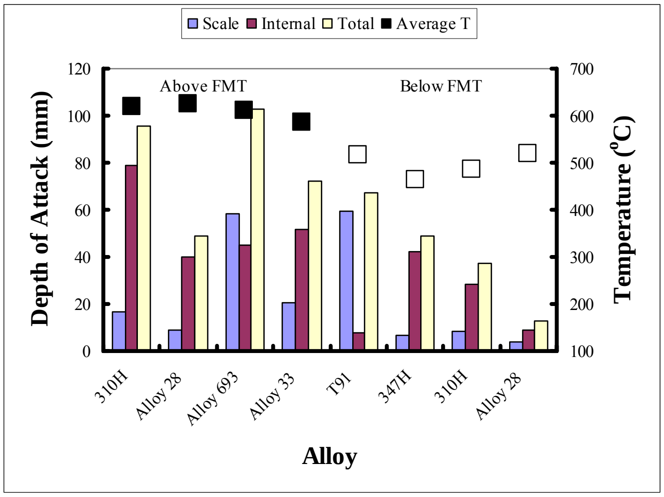

Figure 74. Depth of attack for alloys tested. Superimposed (as squares) is the estimated average exposure temperature for the outside surface of each sample.

In the lab exposure, the reactive cover gas mixture (H_2S-H_2-H_2O-N_2) was used on the basis that it simulated a possible worst-case scenario, one involving an operating condition of high carryover combined with elevated moisture levels resulting from frequent sootblowing. However, since sulfur was present in corrosion scales formed during the field exposure, it seemed reasonable to consider results obtained from a reactive cover gas environment in lab exposures along with results of the field exposure as part of the evaluation.

A plot comparing the extrapolated annual corrosion rate for the various alloys exposed at temperatures below the FMT in the lab (reactive cover gas mixture) and field exposure is shown in Fig. 75. superimposed on this plot, as a limit, is the minimum corrosion rate (0.3 mm/y) reported for corroded 347H tube bends in existing HT recovery boilers.[49] With the exception of T91, the field exposure appeared to be slightly more aggressive to the alloys than the lab exposure with the reactive cover gas mixture. Interestingly, both exposures yield the same relative ranking of alloys in terms of increasing corrosion rate at temperatures below the FMT, namely,

Alloy 28 < 310H < 347H < T91

which is consistent with the expected trend of lower corrosion rates for higher chromium-containing alloys. Of the alloys tested, only Alloy 28 exhibited a lab and field exposure corrosion rate lower than the minimum rate of 0.3 mm/y (12 mpy). (Alloy 33 was not exposed in the field test below the FMT.)

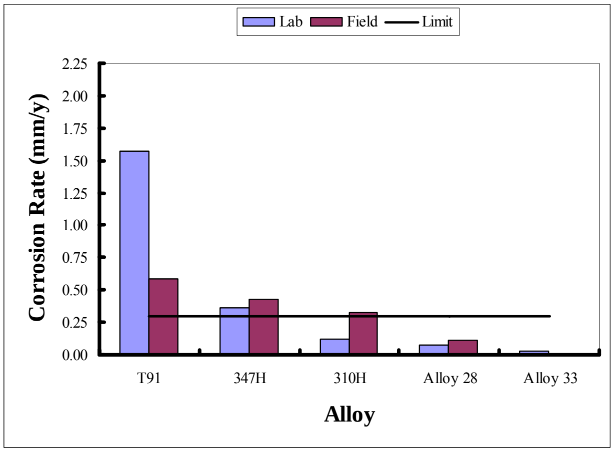

Figure 75. Annual corrosion rate extrapolated from lab (reactive cover gas mixture) and field exposure for alloys tested at temperatures below the FMT. Superimposed, as a limit, is the minimum corrosion rate (0.3 mm/y) reported for corroded 347H tube bends in existing HT recovery boilers.[49] Lab exposure based on 336 h and field exposure based on 1000 h.

A plot comparing the extrapolated annual corrosion rate for the various alloys exposed at temperatures above the FMT in the lab (reactive cover gas mixture) and field exposure is shown in Fig. 76. Also superimposed on this plot, as a limit, is the minimum corrosion rate (0.3 mm/y) reported for corroded 347H tube bends in existing HT recovery boilers.[49] The field exposure appeared to be moderately more aggressive to the alloys than the lab exposure using the reactive cover gas mixture. Unlike the trend in corrosion rate observed for the lab exposure below the FMT (Fig. 75), the corrosion rate did not vary much among the alloys, with the obvious exception of 347H, which had a significantly higher rate. Note that the corrosion rate of the alumina-forming Alloy 693 was similar to that of the chromia-forming 310H, Alloy 28 and Alloy 33 in the lab test environment. The corrosion rate of 347H was significantly greater than the minimum rate of 0.3 mm/y (12 mpy) reported for cases involving accelerated corrosion in HP recovery boilers. The lab exposure corrosion rates of the other four alloys were lower than this rate, ranging from 0.17 mm/y (6.8 mpy) for 310H to 0.23 mm/y (9.2 mpy) for Alloy 28. In contrast, the field exposure corrosion rates for 310H, Alloy 28, Alloy 33 and Alloy 693 were all greater than this limiting rate. Of the alloys tested at temperatures above the FMT in the field, which includes the alumina-forming Alloy 693, Alloy 28 exhibited the lowest corrosion rate. Based on the field exposure, the relative ranking of alloys in terms of increasing corrosion rate at temperatures above the FMT is,

Alloy 28 < Alloy 33 < Alloy 693 < 310H < 347H

which is not totally consistent with the expected trend of lower corrosion rates for higher chromium-containing alloys.

The discussion of alloy suitability needs to take the corrosion resistance design criterion into consideration. If the criterion is acceptable corrosion resistance at temperatures below the FMT of the deposit, then, from Fig. 75, it appears as though 347H would be the minimum alloy (of those tested) suitable, albeit marginal, for use as superheater tubes in HT/ HP recovery boilers. A better choice would appear to be 310H or Alloy 28 (Note Alloy 33 was not tested under these conditions). To minimize the risk of corrosion in practice, removal of non-process elements (potassium and chlorine) would become a critical part of corrosion control to assure that the FMT of the superheater tube deposit is well above the tube temperature and the associated expected degree of variation.

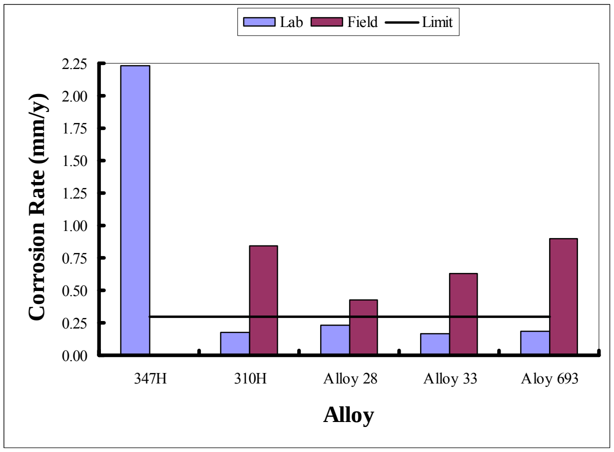

Fig. 76. Annual corrosion rate extrapolated from lab (reactive cover gas mixture) and field exposure for alloys tested above the FMT. Superimposed, as a limit, is the minimum corrosion rate (0.3 mm/y) reported for corroded 347H tube bends in existing HT recovery boilers.[49] Laboratory exposure is based on 336 h and field exposure is based on 1000 h.

If the criterion is acceptable corrosion resistance at temperatures above FMT of the deposit, then, from Fig. 76, it appears as though Alloy 28 would be the minimum alloy (of those tested) suitable to control corrosion of superheater tubes in HT/HP recovery boilers. For this to be realized in practice, tight control of tube temperature would become critical to corrosion control to assure that the time at temperature above the FMT of the deposit is minimized. Based on the various resistances to heat transfer, the surface temperature of a superheater tube is expected to be about 30 to 50C° hotter, or higher if affected by direct radiation, than the steam temperature inside the tube.[50,51] In addition, the tube temperature may be 20C° hotter on the windward side than on the leeward side.[43] Note also that the individual tube steam temperature can vary another ± 23C° from the average across the steam manifold.[52]

As reported earlier, no evidence of any internal attack was observed on any of the samples tested in the lab exposure. This observation is inconsistent with those reported in the field exposure reported herein, as well as in related lab studies,[64-66, 82] and field studies.[33,39-44] Apparently, an exposure time longer than those used in this lab exposure is required to initiate and propagate corrosion processes in alkali chloride-containing salt mixtures, both below and above the FMT. A lab study reporting on the corrosion resistance of commercial heat resistant alloys in contact with a synthetic recovery boiler superheater salt deposit (45%Na_2S-21%Na_2CO_3-21%Na_2SO_4-13%NaCl) in air at temperatures ranging from 550°C to 650°C clearly demonstrates the need for adequate exposure time to produce well-developed attack.[81] Therefore, in order to support the suitability claims made herein, and to provide a more reliable basis for a definitive ranking of alloys, testing at longer exposure times, both in lab and field exposures, is recommended. Extending the testing time of the lab exposure may also improve the agreement between corrosion rates determined from the two exposures. Based on the findings of this study, it seems reasonable that a ranking based on time-to-failure, both below and above the FMT would prove worth-while in the attempt to specify superheater tube alloys for HT/HP recovery boilers.

Conclusions And Recommendations

1. Alloy suitability likely depends upon the corrosion resistance design criterion. If the criterion is acceptable corrosion resistance at temperatures below the FMT of the deposit, then it appears as though 347H would be the minimum alloy (of those tested) suitable, albeit marginal, for use as superheater tubes in HP/HT recovery boilers.
2. If the criterion is acceptable corrosion resistance at temperatures above FMT of the deposit, then it appears as though Alloy 28 would be the most suited alloy (of those tested) to control corrosion of superheater tubes in HT/HP recovery boilers.
3. Based on the findings of this study, the relative ranking of alloys in terms of increasing corrosion rate would be:

   Alloy 28 < Alloy 33 < Alloy 693 < 310H < 347H < T91

4. Corrosivity of the synthetic superheater deposit was significantly enhanced in the presence of the reactive gas mixture. The detrimental influence of sulfur and oxygen, in combination with chlorine, observed in the lab exposure is consistent with the observations from the field exposure. There is a complex, yet poorly understood synergy between the reactants responsible for corrosion observed both below and above the FMT of the deposit.

ACCOMPLISHMENTS

Publications

1. Vikas R Behrani, Jamshad Mahmood, Preet M Singh, Mid Furnace Corrosion - Role of Fluctuations in the Gas Composition, Proceedings International Chemical Recovery Conference, Published by PAPTAC, Quebec City, Canada, May 2007.
2. James R. Keiser, Joseph R. Kish, Laurie A. Frederick, Adam W. Willoughby, Kimberly A. Choudhury, Douglas L. Singbeil, François R. Jetté, and J. Peter Gorog, "Recovery Boiler Superheater Corrosion Studies", Proceedings International Chemical Recovery Conference, Published by PAPTAC, Quebec City, Canada, May, 2007.
Awarded 2007 International Chemical Recovery Conference Award for Best Paper on Corrosion
3. Jerry Yuan, Zhuzhi Xiao, Martha Salcudean, Preet M. Singh, Peter Gorog, Numerical Study on Mid-Furnace Corrosion in a Kraft Recovery Boiler, Proceedings International Chemical Recovery Conference, Published by PAPTAC, Quebec City, Canada, May 2007.
4. Vikas R Behrani and Preet M Singh, Corrosion Behavior of Aluminized and Chromized Carbon Steel in Fluctuating Oxidizing-Sulfidizing Environments, NACE International, CORROSION/2007, Paper # 07209, Nashville, TN, USA, March 2007.
5. Vikas R. Behrani, Jamshad Mahmood, Preet M Singh, Mid Furnace Corrosion in Kraft Recovery Boilers and its Control, NACE International, CORROSION/2006, Paper No. 06238, San Diego, CA, USA, March 2006.
6. James R. Keiser, Gorti B. Sarma, Kimberly A. Choudhury, François R. Jetté, Richard L. Emerson, Elizabeth F. Walker, Joseph R. Kish and Douglas L. Singbeil, "Investigation of a Superheater Tube Cracking Problem", 2005 TAPPI Engineering, Pulping and Environmental Conference, August 2005, Philadelphia, PA.
7. Preet M. Singh, Vikas R. Behrani, Fireside Corrosion of Carbon Steel Tubes in Kraft Recovery Boiler Mid-Furnace, NACE International, CORROSION/2005. Paper# 05197, Houston, TX, USA, April 2005.

Presentations

Oral presentations were made for all seven of the publications listed above. In addition, the following oral presentations were also made:

1. "Materials Issues In Black Liquor Recovery Boilers" James R. Keiser at the American Forest & Paper Association Recovery Boiler Meeting and Conference, February 14, 2007, Atlanta, GA
2. "Recovery Boiler Superheater Tube Corrosion and Cracking Studies" James R. Keiser at the 7th International Colloquium on Black Liquor Combustion and Gasification, July 31-August 2, 2006, Jyväskylä, Finland
3. "Materials Issues In Black Liquor Recovery Boilers And Gasifiers" James R. Keiser at the American Forest & Paper Association Recovery Boiler Meeting and Conference, February 7-8, 2006, Atlanta, GA
4. "Materials For Industrial Heat Recovery Systems" James R. Keiser at the American Forest & Paper Association Recovery Boiler Meeting and Conference, February 2005, Atlanta, GA

Graduate students

Dr. Vikas Behrani did his PhD at Georgia Institute of Technology with partial support from this project.

TECHNOLOGY TRANSFER AND COMMERCIALIZATION

A final project review meeting was held April 11-12, 2007 at the Oak Ridge National Laboratory. Approximately 45 people attended the meeting, and they represented secondary aluminum producers, pulp and paper companies, manufacturers of recovery boilers, producers of metals (particularly tubing), the research organizations participating in this project, and the Department of Energy’s Industrial Technology Program office.

The selection of alloys for the superheater corrosion studies was made with input from an advisory committee composed of representatives of paper companies, a boiler manufacturer, and an inspection company. In addition, an effort was made to coordinate the selection of materials and test conditions with the SOTU II project that was funded by the Finnish government and was carried out by universities, boiler manufacturers and paper companies in Finland.

Both the study of mid-furnace corrosion and the superheater corrosion and cracking study provided information on boiler operation and materials selection toward the objective of lessening the frequency and severity of component degradation. It is too early to determine the extent to which the material selection information will be utilized while it is apparent that some of the guidance on operational changes is being implemented.

ACKNOWLEDGEMENTS

The contributions of the advisory team members are gratefully recognized. The members include:
David Crowe, David N. French Metallurgists
Margaret Gorog, Weyerhaeuser Company
François Jetté, Domtar Incorporated
John Kulig, Babcock & Wilcox
W. B. “Sandy” Sharp, retired from MeadWestvaco

Staff members at three paper mills were very supportive and cooperative for both the mid-furnace and superheater studies. These mills include:
Domtar Incorporated, Ashdown, Arkansas
Weyerhaeuser Company, Flint River, Georgia
Weyerhaeuser Company, Columbus, Mississippi

The efforts of DOE Project Officer, Mahesh Jha, who provided oversight and guidance for the project and provided valuable review and editorial comments for the final reports are sincerely appreciated.

REFERENCES

1. James R. Keiser, Douglas L. Singbeil, Gorti B. Sarma, Joseph R. Kish, Jerry Yuan, Laurie A. Frederick, Kimberly A. Choudhury, J. Peter Gorog, François R. Jetté, Camden R. Hubbard, Robert W. Swindeman, Preet M. Singh, and Philip J. Maziasz, "Cracking and Corrosion Of Composite Tubes In Black Liquor Recovery Boiler Primary Air Ports", ORNL/TM-2006/112, October 2006.

2. James R. Keiser, Gorti B. Sarma, Arvind Thekdi, Roberta A. Meisner, Tony Phelps, Adam W. Willoughby, John Zeh, J. Peter Gorog, Shridas Ningileri, Yansheng, Liu and Chenghe Xiao, "Improved Materials And Operation Of Recuperators For Aluminum Melting Furnaces", Final Report for Task 1 of DOE award # DE-FC36-04GO14035 (available from OSTI; OSTI Report No. 919037).

3. A.L. Plumley, E.C. Lewis, and R.G. Tallent, "External Corrosion of Water Wall-Tubes in Kraft Recovery Furnaces," Tappi J, 49(1), 72A (1966).

4. R.G. Tallent, A.L. Plumley, "Recent Research on External Corrosion of Waterwall Tubes in Kraft Recovery Furnaces," Tappi J., 52(10), 1955 (1969).

5. D. Singbeil, L. Frederick, N. Stead, J. Colwell, G. Fonder, "Testing the Effects of Operating Conditions on Corrosion of Water Wall Materials in Kraft Recovery Boilers," 1996 TAPPI Engineering Conference, TAPPI Press, Atlanta, GA, 649 (1996).

6. P.M. Singh, S.J. Al-Hassan, S. Stalder, G. Fonder, "Corrosion in Lower Furnace of Kraft Recovery Boilers - *In situ* Characterization of Corrosive Environments", Tappi J., 3(2), 21 (2003).

7. A.L. Plumley, W.R. Roczniak, "Recovery Unit Waterwall Protection, A Status Report," Tappi J, 58(9), 118 (1975).

8. W.B.A. Sharp "Composite Furnace Tubes for Recovery Boilers – A Problem Solved," Tappi J., 64(7), 113 (1981).

9. H. Tran, Kraft Recovery Boilers, T.N. Adams, W.J. Frederick, T.M. Grace, M. Hupa, K. Iisa, A.K. Jones, H. Tran (Eds.), TAPPI Press, Atlanta, GA (1998).

10. H. Dykstra, "Recovery Boiler Waterwall Tube Failure Analysis with Implications for Furnace Replacement and New Construction," 1998 TAPPI Engineering Conference, Volume 2, TAPPI Press, Atlanta, GA , p. 431 (1998).

11. P.M. Singh, J. Perdomo, J. Mahmood, "Mid-Furnace Corrosion in Kraft Recovery Boiler," 11th International Symposium on Corrosion in the Pulp and Paper Industry, TAPPI Press, Atlanta, GA (2004).

12. P.M. Singh, V.R. Behrani, "Fireside Corrosion of Carbon Steel Tubes in Kraft Recovery Boiler Mid-Furnace," Corrosion/05, Paper # 197, NACE, Houston, TX (2005).

13. P. McKeough, M. Kurkela, H. Kyllonen, E. Tapola, "New Insights into the Release of Sodium, Sulphur, Potassium and Chlorine During Black-Liquor Combustion and Gasification," LIEKKI 2, Technical Review 1993–1998. Volume 2, M. Hupa (Ed.), Abo Akademi University, Turku, Finland, 855 (1998).

14. D.L. Feuerstein, J.F. Thomas, D.L. Brink, "Malodorous Products from the Combustion of Kraft Black Liquor. I. Pyrolysis and Combustion Aspects," Tappi J., 50(6), 258 (1967).

15. J. Li, A. R. P. Van Heiningen, "Sulfur Emission During Slow Pyrolysis of Kraft Black Liquor," Tappi J, 74(3), 237 (1991).

16. V. Sricharoenchaikul, W.J. Frederick, T.M. Grace, "Sulphur Species Transformations During Pyrolysis of Kraft Black Liquor," J. Pulp and Paper Sci., 23(8), J394 (1997).

17. P.J. Ficalora, T.G. Godfrey, "Technique to Study Corrosion in Fluctuating Gaseous Atmospheres", Oak Ridge National Laboratory Report ORNL/TM-8734 (5900469; DE83014565), Oak Ridge, TN, (1983).

18. M.F. Stroosnijder , W.J. Quadakkers, "Review of High Temperature Corrosion of Metals and Alloys in Sulfidizing/Oxidizing Environments II. Corrosion of Alloys", High Temp. Technol., 4 , 141 (1986).

19. J. Stringer, "Mixed Oxidant Corrosion in Coal Combustion and Conversion Systems: Manifestations and Mechanisms", High-Temperature Oxidation and Sulphidation Processes, J.D. Embury (Ed.), Pergamon Press, New York, 257 (1990).

20. B. Gleeson, "Alloy Degradation under Oxidizing-Sulfidizing Conditions at Elevated Temperatures", Mat. Res., 7(1), 61 (2004).

21. F. Gesmundo, D.J. Young, S.K. Roy, "The High-Temperature Corrosion of Metals in Sulfidizing-Oxidizing Environments: A Critical Review," High Temp. Mater. Proc., 8, 149. (2004).

22. H. J. Grabke, R. Lobnig, P. Papaiacovou, Johannesen, A.G. Andersen (Eds.), Selected Topics in High Temperature Chemistry: Defect Chemistry of Solids, Elsevier, New York, 263 (1989).

23. D.L. Douglass, P. Kofstad, A. Rahmel, G.C. Wood, "International Workshop on High Temperature Corrosion," Oxidation of Metals, 45(5-6), 529 (1996).

24. S.J. Al-Hassan, G.J. Fonder, P.M. Singh, "The Effect of Temperature Excursion on Sulfidation of Carbon Steel in 1% H_2S Environment," Pulp & Paper Canada, 100(10), 40 (1999).

25. S. Osgerby, "Oxide Scale Damage and Spallation in P92 Martensitic Steel," Materials at High Temperatures, 17(2), 307 (2000).

26. M. Schulte, M. Schutze, "The Role of Scale Stresses in the Sulfidation of Steels," Oxidation of Metals, 51 (1/2), 55 (2002).

27. M. Mäkipää, M. Oksa, P. Pohjanne, "Corrosion Testing of High-Nickel Alloy Composite Tube Materials in Simulated Recovery Boiler Lower Furnace Conditions," 10th International Symposium on Corrosion in the Pulp and Paper Industry, Vol. 1, T. Hakkarainen (Ed.), VTT, Espoo, Finland, 73 (2001).

28. A. Hendry, "The Oxidation Resistance of Nitrided Mild Steel," Corrosion Science, 18(6), 555 (1978).

29. James R. Keiser, Gorti B. Sarma, Kimberly A. Choudhury, François R. Jetté, Richard L. Emerson, Elizabeth F. Walker, Joseph R. Kish, and Douglas L. Singbeil, "Investigation of a Superheater Tube Cracking Problem", TAPPI Engineering, Pulping and Environmental Conference, Philadelphia, PA, August 28-31, 2005.

30. Boardman, B., "Fatigue Resistance of Steels," Metals Handbook, 10th Edition, Volume 1 Properties and Selection: Iron, Steels, and High-Performance Alloys, Lampnam, S.R, Zorc, T.B., Editors, p. 678, ASM International, Materials Park, OH (1990).

31. "SA-210/SA-210M Specification for Seamless Medium-Carbon Steel Boiler and Superheater Tubes," 2004 ASME Boiler and Pressure Vessel Code, Section II – Materials, American Society of Mechanical Engineers, New York, NY (2004).

32. T.N. Adams, Wm.J. Frederick, T.M. Grace, M. Hupa, K. Iisa, A.K. Jones, H. Tran, Editors., Kraft Recovery Boilers, TAPPI Press, Atlanta, GA: p. 310 (1997).

33. D.C. Crowe, W.C. Youngblood, "Recovery Boiler Superheater Corrosion," 9th International Symposium on Corrosion in the Pulp and Paper Industry, CPPA, Montreal, QC: 225 (1998).

34. F. Bruno, "Thermochemical Aspects on Chloride Corrosion in Kraft Recovery Boilers," Paper No. 01426, CORROSION/2001, NACE, Houston, TX (2001).

35. M.Mäkipää, E, Kauppinen, T. Lind, J. Pyykönen, J. Jokiniemi, P. McKeough, M. Oksa, Th. Malkow, R.J. Fordham, D. Baxter, L. Koivisto, K. Saviharju, E. Vakkilainen, "Superheater Tube Corrosion in Recovery Boilers," 10th International Symposium on Corrosion in the Pulp and Paper Industry, Volume 1, VTT, Espoo Finland: 157 (2001).

36. J. Tuiremo, K. Salmenoja, "Control of Superheater Corrosion in Black Liquor Recovery Boilers" 10th International Symposium on Corrosion in the Pulp and Paper Industry, Volume 1, VTT, Espoo Finland: 181 (2001).

37. H. Tran, M. Gonsko, X. Mao, "Effect of Composition on the First Melting Temperature of Fireside Deposits in Recovery Boilers," Tappi Journal, 82(9): 93 (1999).

38. K. Salmenoja, "Field and Laboratory Studies on Chlorine-Induced Superheater Corrosion in Boilers Fired with Biofuels", Report 00-01, Faculty of Chemical Engineering, Abo Akademi, Turku, Finland (2000).

39. K.W. Morris, A.L. Plumley, W.R. Roczniak, "The Effect of Chlorides on Recovery Unit Superheater Wastage: An R&D Progress Report," Pulp and Paper Industry Corrosion Problems, Volume 3, NACE, Houston TX: 47 (1980).

40. D.W. Reeve, H.N. Tran, D. Barham, "Superheater Fireside Deposits and Corrosion in Kraft Recovery Boilers," Tappi Journal, 64(5): 109 (1981).

41. H.N. Tran, D.W. Reeve, D. Barham, "Local Reducing Atmosphere – A Cause of Superheater Corrosion in Kraft Recovery Units," Tappi Journal, 68(6): 102 (1985).

42. R. Backman, M. Hupa, E. Uppstu, "Fouling and Corrosion Mechanism in the Recovery Boiler Superheater Area," Tappi Journal, 70(6): 123 (1987).

43. C. Dees, J. Simonen, H. Tran, "Experience of Recovery Boiler Superheater Corrosion at Willamette Hawesville, 7th International Symposium on Corrosion in the Pulp and Paper Industry, TAPPI Press, Atlanta, GA: 251 (1992).

44. W. Blakemore, M. Ellis, H. Tran, "Experience of Recovery Boiler Superheater Corrosion at Carter Holt Harvey Kinleith," 11th International Symposium on Corrosion in the Pulp and Paper Industry," TAPPI Press, Atlanta, GA: 217 (2004).

45. T.N. Adams, Wm.J. Frederick, T.M.Grace, M. Hupa, K Iisa, A.K. Jones, H. Tran, Editors, Kraft Recovery Boilers, TAPPI Press, Atlanta, GA: p. 247 (1997).

46. S.C. Stultz, J.B. Kitto, Editors, Steam/Its Generation and Use, 40th Edition, Babcock & Wilcox Company, Barberton, OH: 26-10 (1992).

47. M.P. LeBel, "CRU Superheater Experience," Alstom Power Inc., Correspondence to Paprican, May 11, 2005.

48. S.C. Stultz, J.B. Kitto, Editors, Steam/Its Generation and Use, 40th Edition, Babcock & Wilcox Company, Barberton, OH: 6-21 (1992).

49. A. Jaakkola, T. Rose, "Operational Experiences of Austenitic Superheater Tube Bends in Recovery Boilers," Pulp and Paper Industry Corrosion Problems, Volume 4, Swedish Corrosion Institute, Stockholm, Sweden: 82 (1983).

50. J.F. La Fond, A. Verloop, A.R. Walsh, "Engineering Analysis of Recovery Boiler Superheater Corrosion," Tappi Journal, 75(6): 101 (1992).

51. F. Bruno, "The Significance of Superheater Tube Corrosion on the Steam Temperature of Kraft Recovery Boilers," 8th International Symposium on Corrosion in the Pulp and Paper Industry, Swedish Corrosion Institute, Stockholm, Sweden: 138 (1995).

52. D.N. French, Metallurgical Failures in Fossil Fired Boilers, John Wiley & Sons, New York, NY: 248 (1983).

53. P-E. Ahlers, A. Jaakola, "Experiences of Austenitic Superheater Tube Bends in Finnish Recovery Boilers, Black Liquor Recovery Boiler Symposium 1982, Ekono Oy/Finnish Recovery Boiler Committee/Finnish Energy Economy Association, Helsinki, Finland: D7-1 (1982).

54. C. Reid, "Lower Bend Superheater Tube Experience in Coastal Recovery Boilers," Acuren, Correspondence to Paprican, November 5, 2001.

55. "Sandvik Sanicro 28 – Composite Tube for Steam Boiler Application," S-12111-ENG, Sandvik Steel, Sandviken, Sweden (1999).

56. B.K. Trask, "Superheater Corrosion at Scott Maritimes Limited," CPPA Atlantic Branch Conference 1992, CPPA, Montreal QC (1992).

57. J. McMillan, "Superheater Problems, Their Causes and Solutions," 2004 International Chemical Recovery Conference, Volume 2, TAPPI Press, Atlanta, GA: 953 (2004).

58. T. Odelstam, "Material Evaluation for BLRB Superheater Tubes," Black Liquor Recovery Boiler Symposium 1982, Ekono Oy/Finnish Recovery Boiler Committee/Finnish Energy Economy Association, Helsinki, Finland: D6-1 (1982).

59. A. Fujisaki, H. Takatsuka, M. Yamamura, "World's Largest High Pressure and Temperature Recovery Boiler," 1992 International Chemical Recovery Conference, TAPPI Press, Atlanta, GA: 1 (1992).

60. A. Fujisaki, H. Takatsuka, M. Yamamura, "World's Largest High Pressure and Temperature Recovery Boiler," Pulp & Paper Canada, 95(11): T452 (1994).

61. H. Tran, Y. Arakawa, "Recovery Boiler Technology in Japan," TAPPI 2001 Engineering/Finishing and Converting Conference, TAPPI Press, Atlanta, GA: 49 (2001).

62. Y. Arakawa, Y. Taguchi, T. Meda, Y. Bara, "Experience with High Pressure and High Temperature Recovery Boilers for Two Decades," Pulp & Paper Canada, 106(12): T269 (2005).

63. H. Matsumoto, A. Notomi, T. Nishio, "Advanced Technology for Corrosion Resistant Materials for Recovery Boilers," 1998 International Chemical Recovery Conference, TAPPI Press, Atlanta, GA: 51 (1998).

64. H. Fujikawa, H. Makiura, Y. Nishiyama, „Corrosion Behaviour of Various Steels in Black Liquor Recovery Boiler Environment," Materials and Corrosion, 50: 154 (1999).

65. M. Mäkipää, M. Oksa, L. Koivisto, "Superheater Tube Corrosion in Changing Operation Conditions of Recovery Boilers," CORROSION/2004, Paper No. 01424, NACE, Houston TX (2001).

66. R. Backman, M. Hupa, J. Lagerborn, T. Lepistö, "Influence of Partially Molten Alkali Deposits on Superheater Corrosion in Black Liquor Recovery Boilers," 10th International Symposium on Corrosion in the Pulp and Paper Industry, Volume 1, VTT, Espoo, Finland: 137 (2001).

67. M. Oksa, M. Mäkipää, "Comparative Laboratory Testing of Molten Salt Attack of Superheater Tube Materials," 10th International Symposium on Corrosion in the Pulp and Paper Industry, Volume 2, VTT, Espoo, Finland: 523 (2001).

68. H.J. Grabke, E. Reese, M. Spiegel, "The Effects of Chlorine, Hydrogen Chloride and Sulphur Dioxide in the Oxidation of Steels below Deposits," Corrosion Science, 37: 1023 (1995).

69. R.W. Byers, "Fireside Slagging, Fouling and High Temperature Corrosion of Heat Transfer Surface due to Impurities in Steam-Raising Fuels," Prog. Energy Combust. Sci., 22: 29 (1996).

70. T. Nishio, H. Matsumoto, M. Shinohara, Y. Arkawa, "Influence of Ash Composition on the Corrosion Rate of Superhetaer Tubes," TAPPI 2001 Engineering, Finishing and Converting Conference, TAPPI Press: CD-ROM (2001).

71. M. Mäkipää, T. Malkow, D.J. Baxter, "The Effect of Salt Composition on the Chlorine Corrosion of Low Alloy Steels," CORROSION/2001, Paper No. 01186, NACE, Houston, TX (2001).

72. S.C. Cha, M. Spiegel, "Local Reactions between NaCl and KCl Particles and Metal Surfaces," Corrosion Engineering, Science & Technology, 40(3): 249 (2005).

73. J.R. Kish, C. Reid, D.L. Singbeil, R. Seguin, "Corrosion of High Alloy Superheater Tubes in a Coastal Biomass Power Boiler," CORROSION/2007, Paper No. 07349. NACE, Houston, TX (2007).

74. Y. Shinata, F. Takahashi, K. Hashiura, "NaCl-Induced Hot Corrosion of Stainless Steels," Materials Science and Engineering, 87: 399 (1987).

75. H. Tran, N. Mapara, D. Barham, "The Effect of H_2O on Acidic Sulfate Corrosion in Kraft Recovery Boilers," Tappi Journal, 79(11): 155 (1996).

76. L. Paul, G. Clark, M. Eckhardt, "Laboratory and Field Corrosion Performance of a High Chromium Alloy for Protection of Waterwall Tubes from Corrosion in Low NO_x Coal Fired Boilers," CORROSION/2006, Paper No. 06473, NACE, Houston, TX (2006).

77. S.D. Kiser, E.B. Hinshaw, T. Orsini, "Extending the Life of Fossil Fired Boiler Tubing with Cladding of Nickel Based Alloy Materials," CORROSION/2006, Paper No. 06474, NACE, Houston, TX (2006).

78. D. Singbeil, L. Frederick, N. Stead, "Testing the Effects of Operating Conditions on Corrosion of Water Wall Materials in Kraft Recovery Boilers", TAPPI 1996 Engineering Conference, TAPPI Press, Atlanta, GA: 649 (1996).

79. R. Backman, M. Hupa, P. Hyoty, "Corrosion due to Acidic Sulphates in Sulphate and Sodium Sulphite Recovery Boilers," Pulp and Paper Industry Corrosion Problems, Volume 4, Swedish Corrosion Institute, Stockholm, Sweden: 76 (1983).

80. S. Mrowec, K. Przybylski, "Defect and Transport Properties of Sulfides and Sulfidation of Metals," High Temperature Materials and Processes, 6(1-2), 1 (1984).

81. J. Klower, F.E. White, "High Temperature Corrosion of Commercial Heat Resistant Alloys under Deposits of Alkali Salts; Recent Laboratory Data," 8th International Symposium on Corrosion in the Pulp and Paper Industry, Swedish Corrosion Institute, Stockholm, Sweden: 179 (1995).

82. Mäkipää, M., Kauppinen, E., Lind, T., Pyykönen, J., Jokiniemi, J., McKeough, P., Oksa, M., Malkow, T., Fordham, R.J., Baxter, D., Koivisto, L., Saviharju, K., Vakkilainen, E., "Superheater Tube Corrosion in Recovery Boilers," Proceedings of the 10th International Corrosion in the Pulp and Paper Industry, Volume 1, Hakkarainen, T. Editor, p. 157, VTT, Espoo, Finland (2001).

APPENDIX 1

SEM Micrographs of Laboratory Corrosion Samples

SEM micrographs of 347H and Sanicro 28 test specimens documenting typical scale formation as a function of exposure time after exposure in synthetic ash mixture with a nitrogen cover gas at a temperature of 510°C.

Time	Type 347H Stainless Steel	Alloy 28
24 Hours	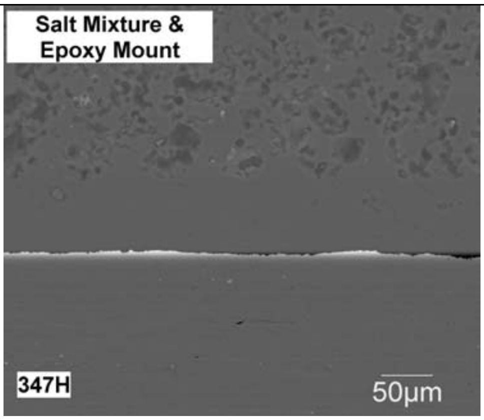	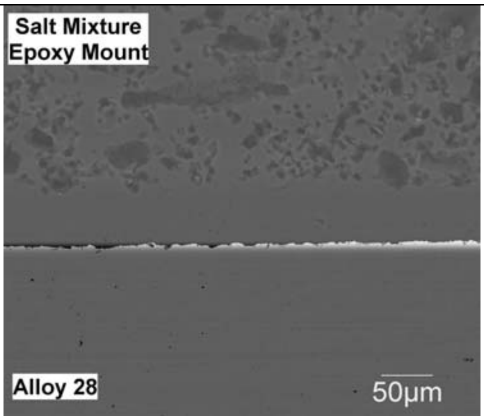
168 Hours	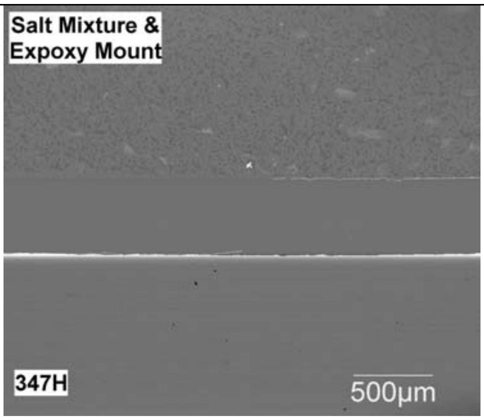	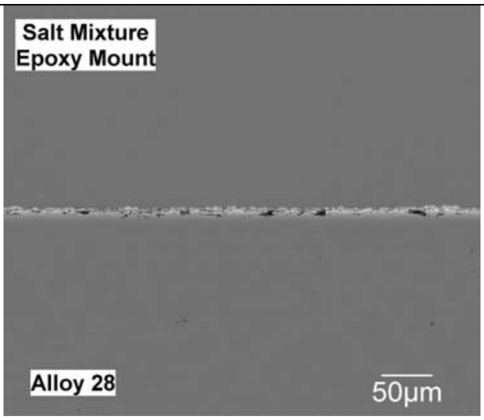
336 Hours	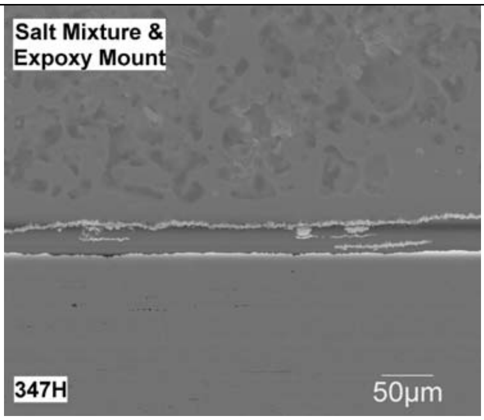	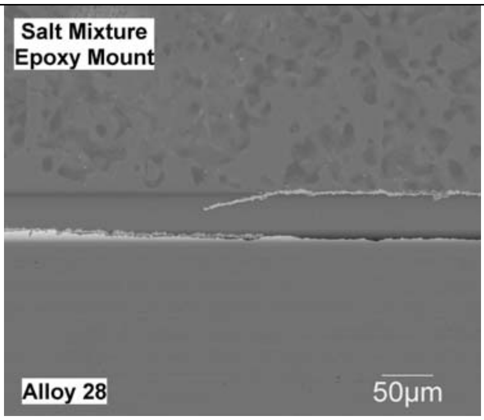

SEM micrographs of 347H and Sanicro 28 test specimens documenting typical scale formation as a function of temperature after exposure in synthetic ash mixture with a nitrogen cover gas for 336 hours.

T	Type 347H Stainless Steel	Alloy 28
510°C	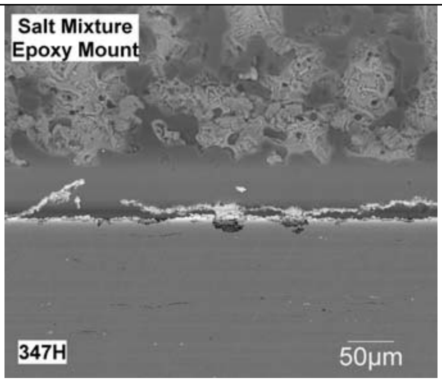	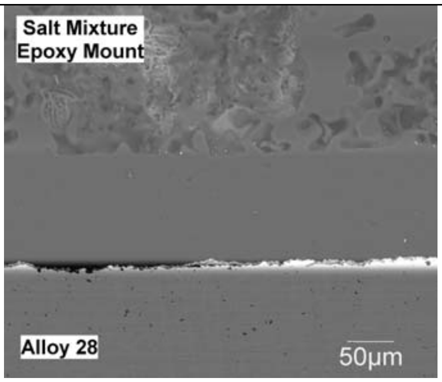
530°C	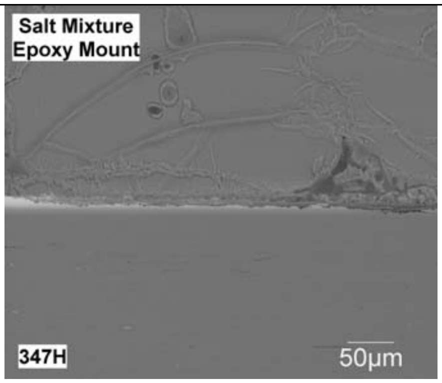	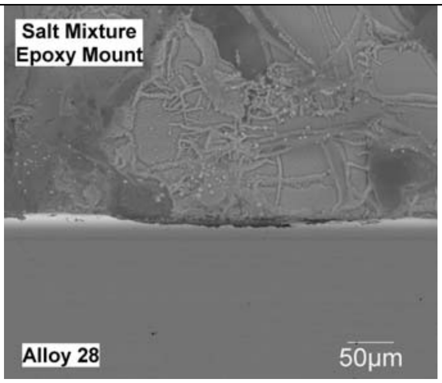
560°C	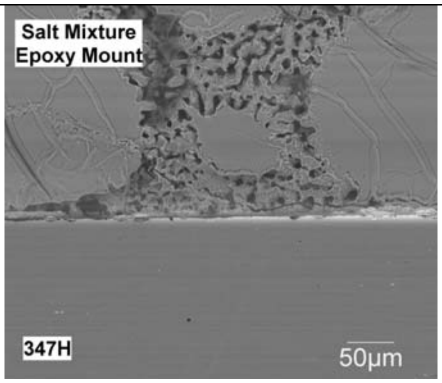	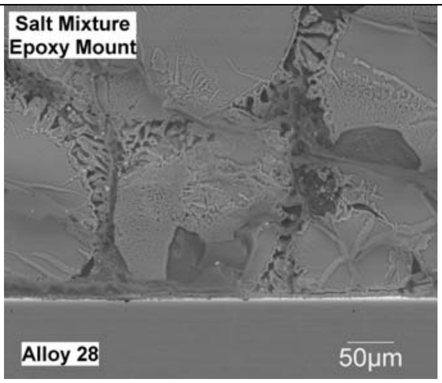

SEM micrographs of 347H and Sanicro 28 test specimens documenting typical scale formation as a function of temperature after exposure in synthetic ash mixture with a H_2S-H_2-H_2O-N_2 cover gas for 336 hours.

T	Type 347H Stainless Steel	Alloy 28
510°C	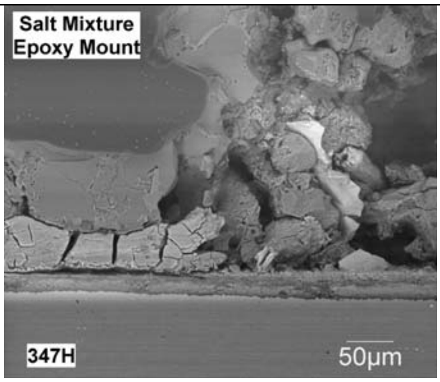	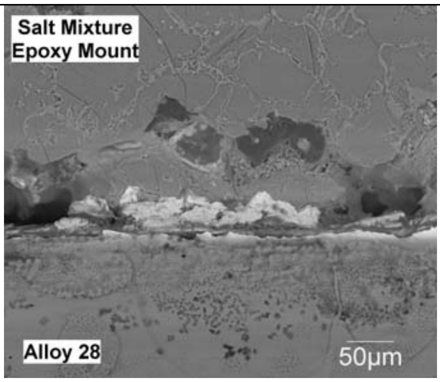
530°C	**Not** **Available**	**Not** **Available**
560°C	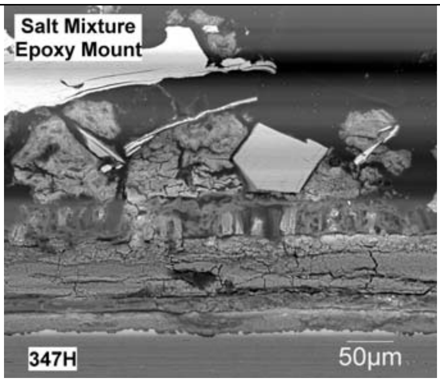	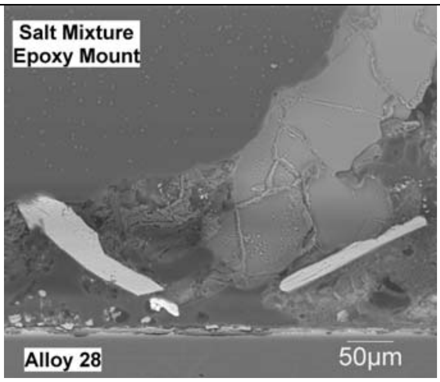

APPENDIX 2

Micrographs of Superheater Probe Corrosion Samples

Collections of four 500 X micrographs from the rings cut from each sample showing the as-polished microstructures at 90° spacings around the rings

T-91 – Sample #1

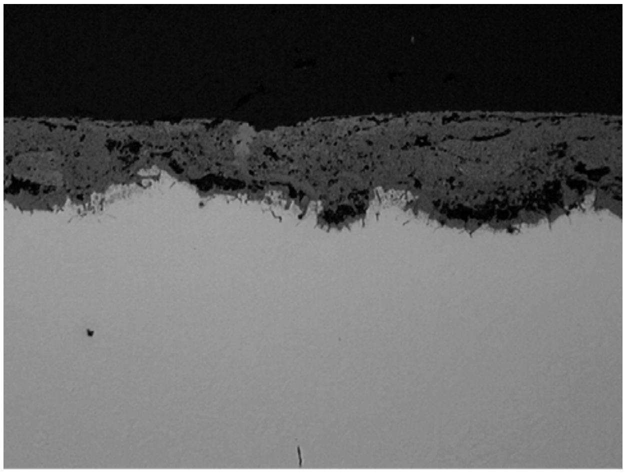
06-1545-03 A#2RBSh-1 O.D. 0°

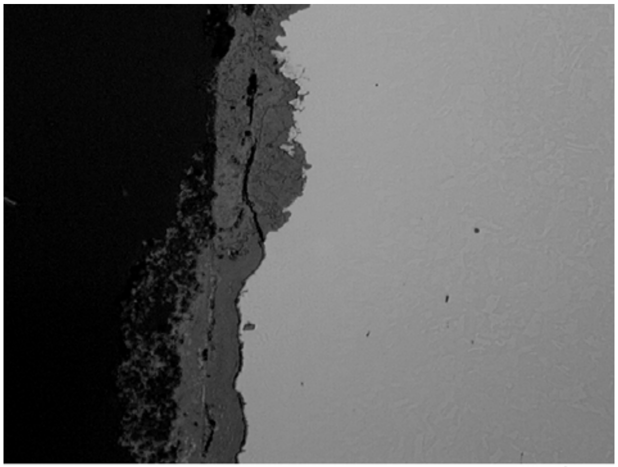
06-1545-15 A#2RBSh-1 O.D. 270°

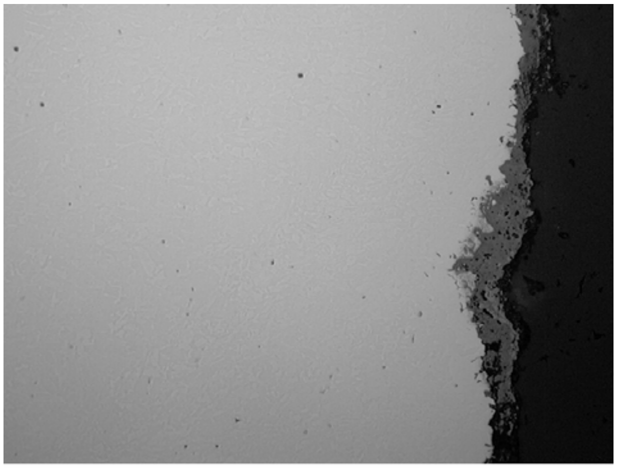
06-1545-08 A#2RBSh-1 O.D. 90°

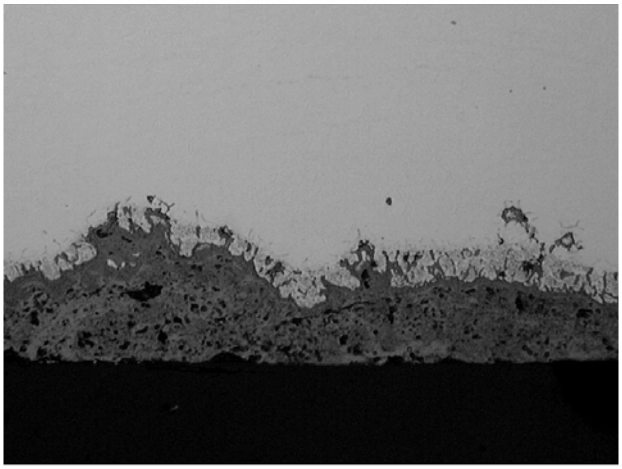
06-1545-11 A#2RBSh-1 O.D. 180°

347H – sample #2

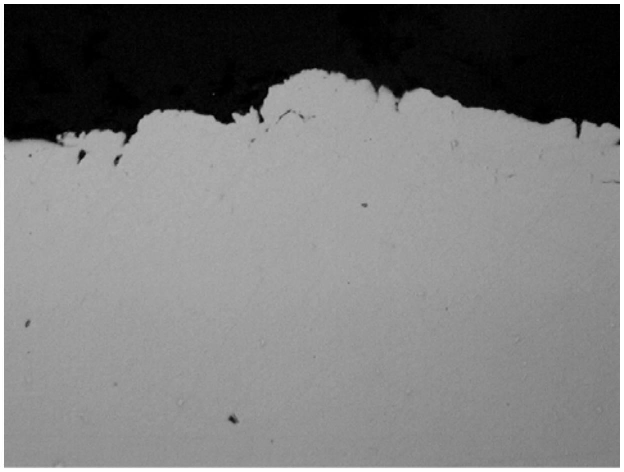

06-1546-04 A#2RBSh-2 0° 500X 10μm As polished

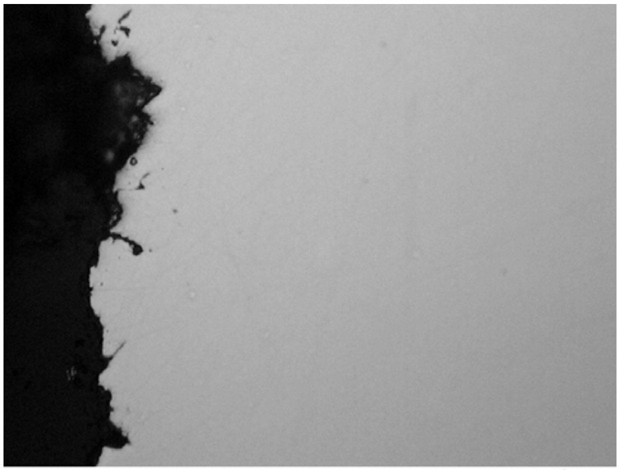

06-1546-15 A#2RBSh-2 270° 500X 10μm As polished

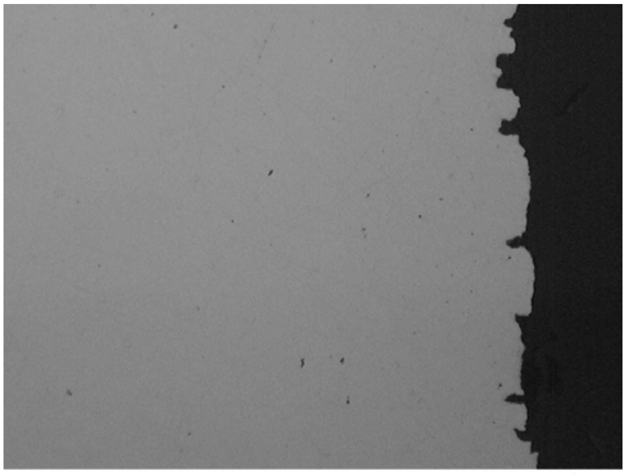

06-1546-07 A#2RBSh-2 90° 500X 10μm As polished

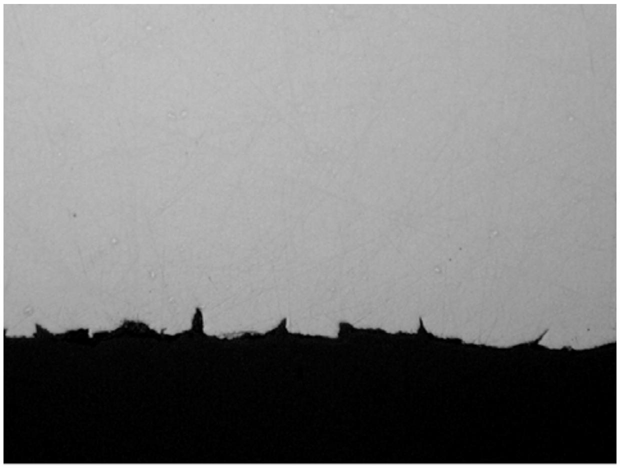

06-1546-11 A#2RBSh-2 180° 500X 10μm As polished

3310H – sample #3

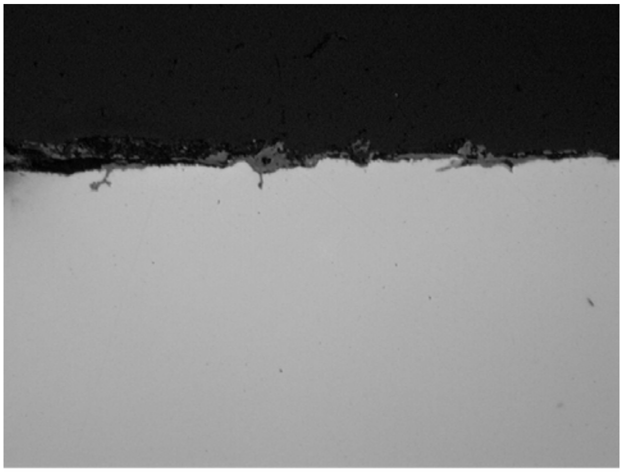

06-1547-04 A#2RBSh-3 O.D. 0° 500X 10μm As polished

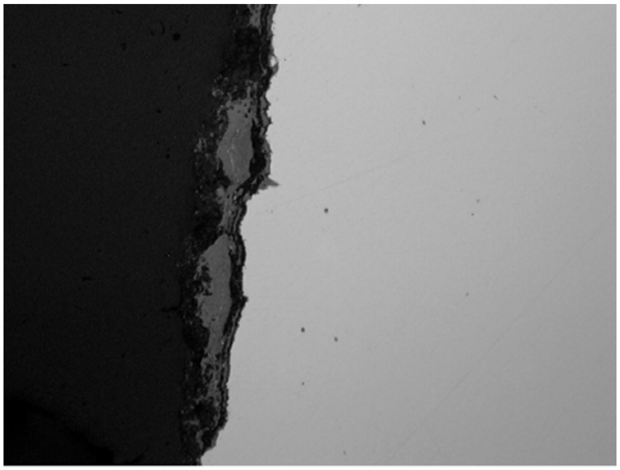

06-1547-15 A#2RBSh-3 O.D. 270° 500X 10μm As polished

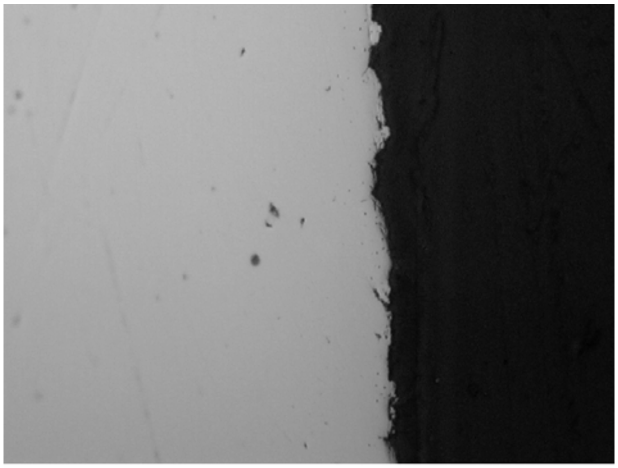

06-1547-07 A#2RBSh-3 O.D. 90° 500X 10μm As polished

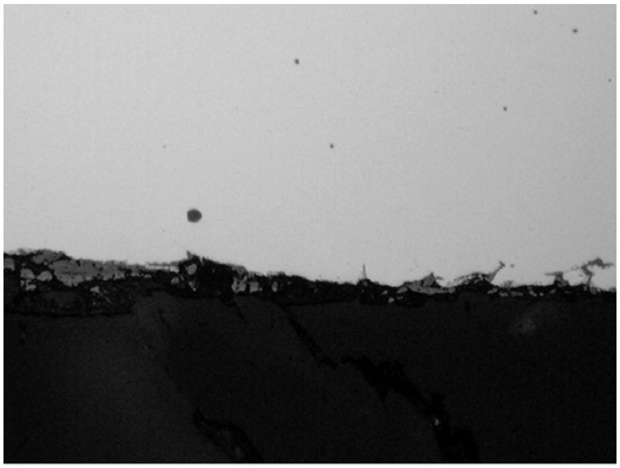

06-1547-11 A#2RBSh-3 O.D. 180° 500X 10μm As polished

Sanicro 28 – sample #4

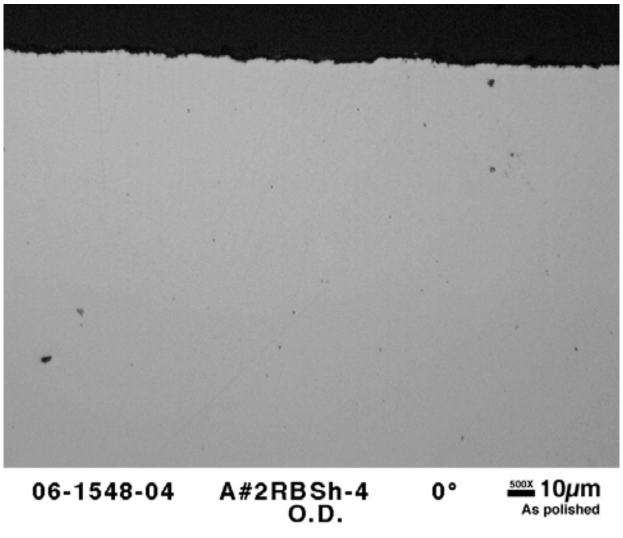

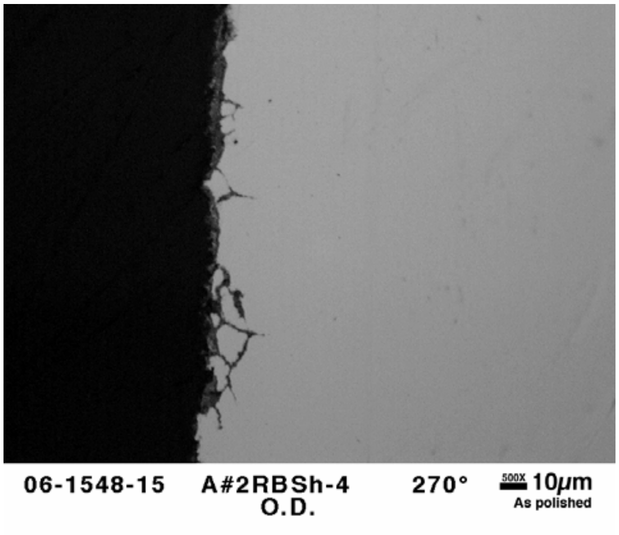

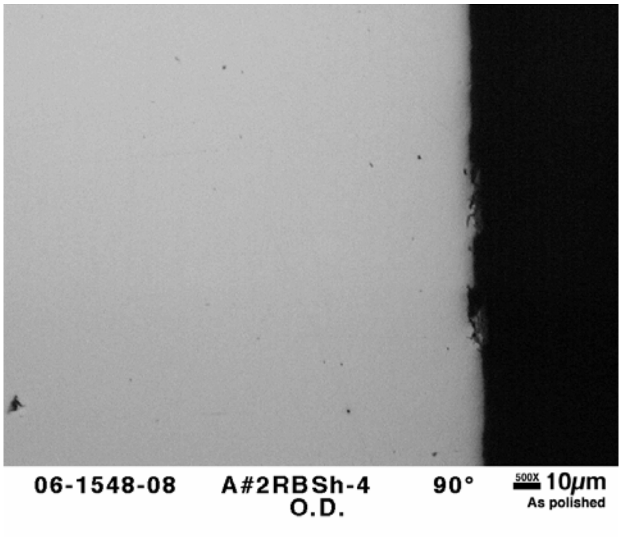

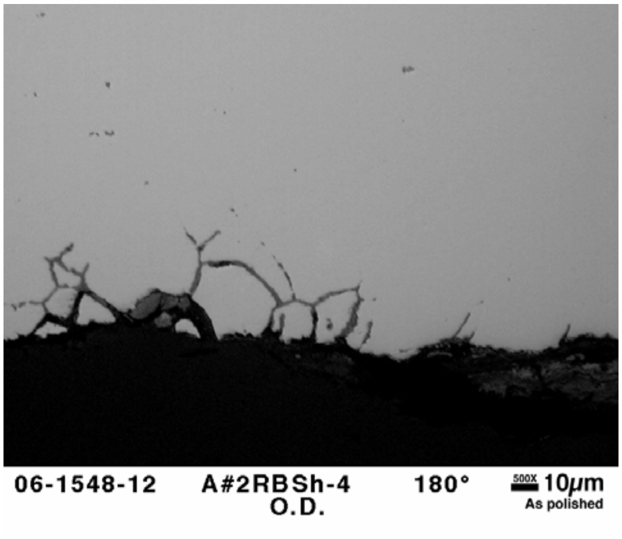

Inconel 693 – sample #5

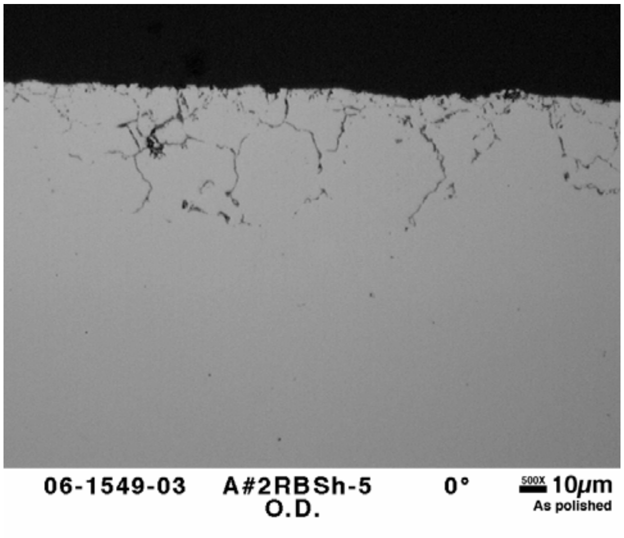

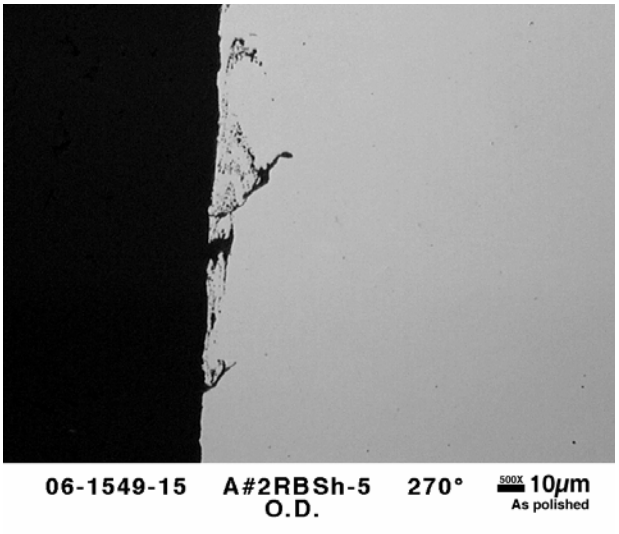

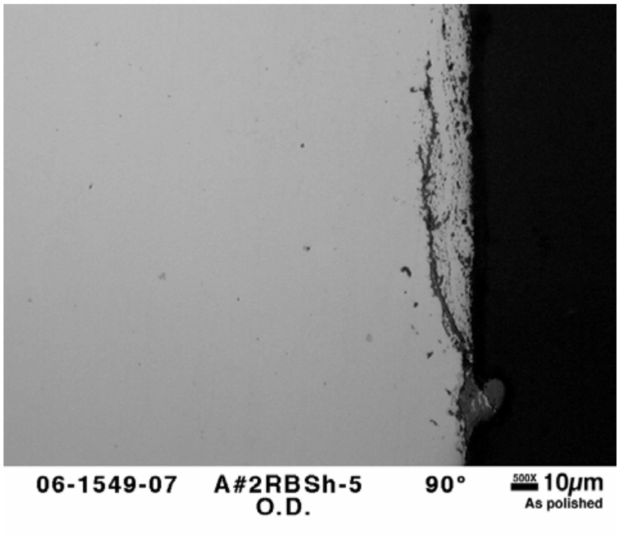

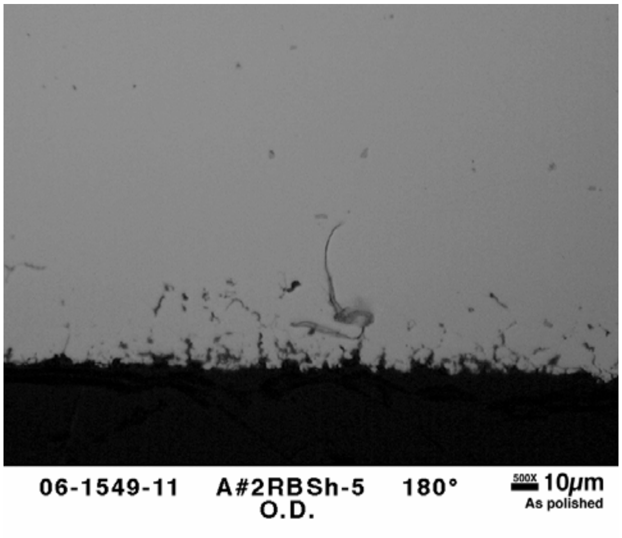

T91- sample #6

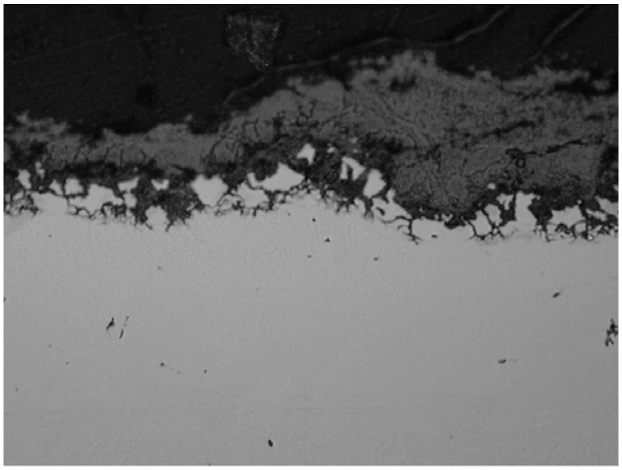
06-1550-03 A#2RBSh-6 0° 500X 10μm
O.D. As polished

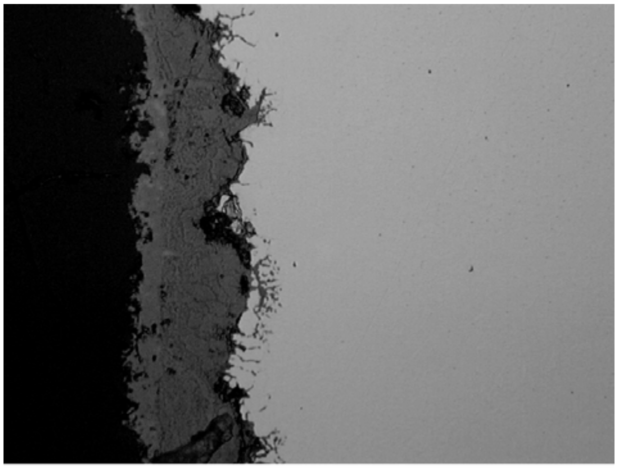
06-1550-16 A#2RBSh-6 270° 500X 10μm
O.D. As polished

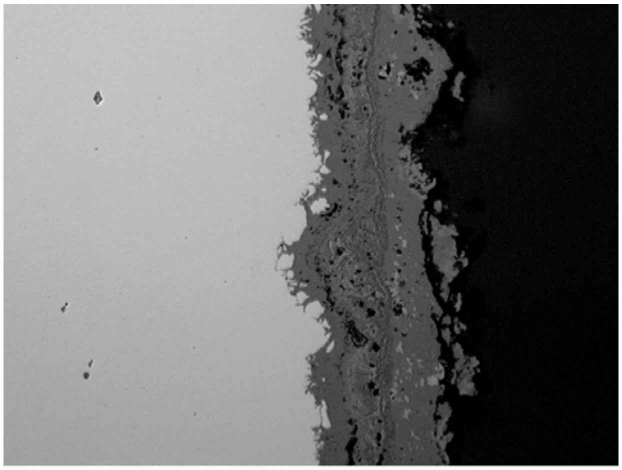
06-1550-07 A#2RBSh-6 90° 500X 10μm
O.D. As polished

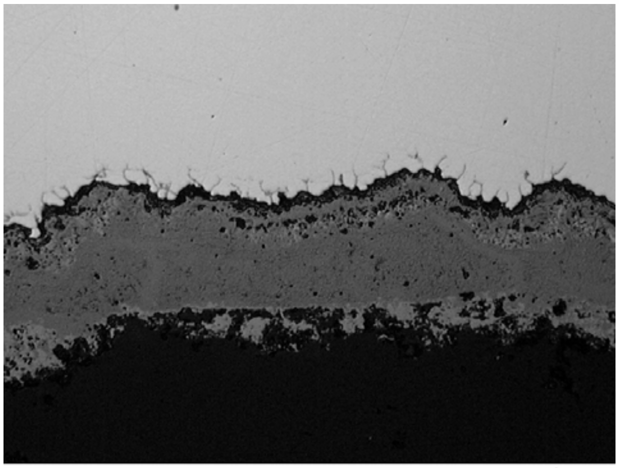
06-1550-11 A#2RBSh-6 180° 500X 10μm
O.D. As polished

347H stainless steel – sample #7

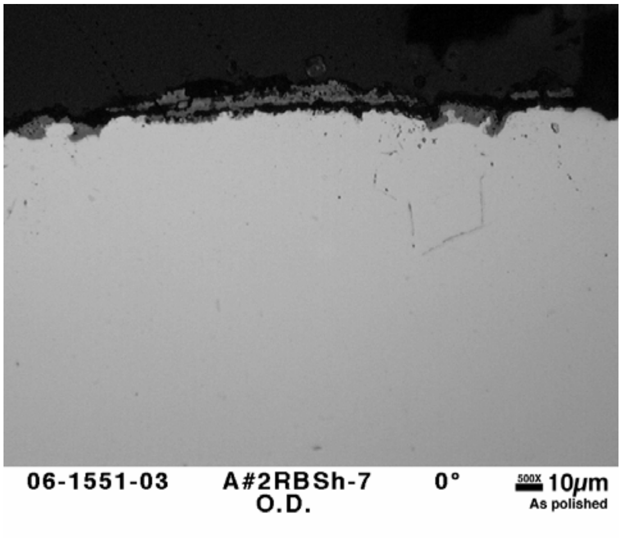

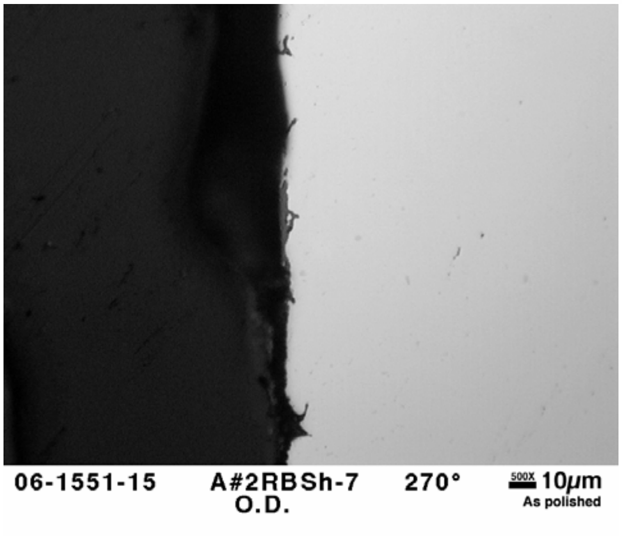

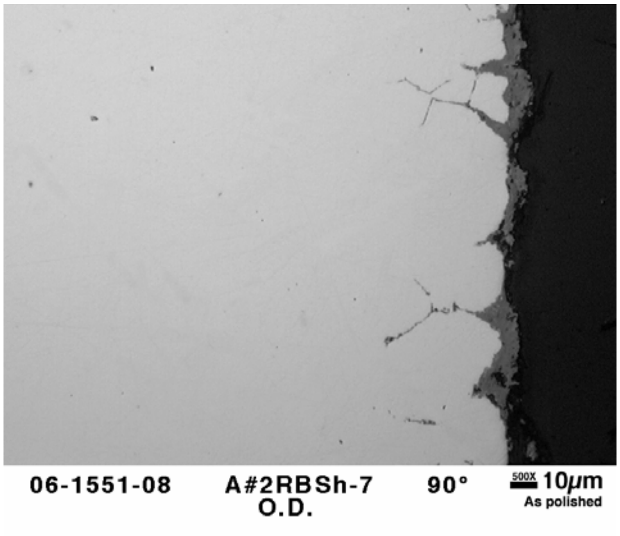

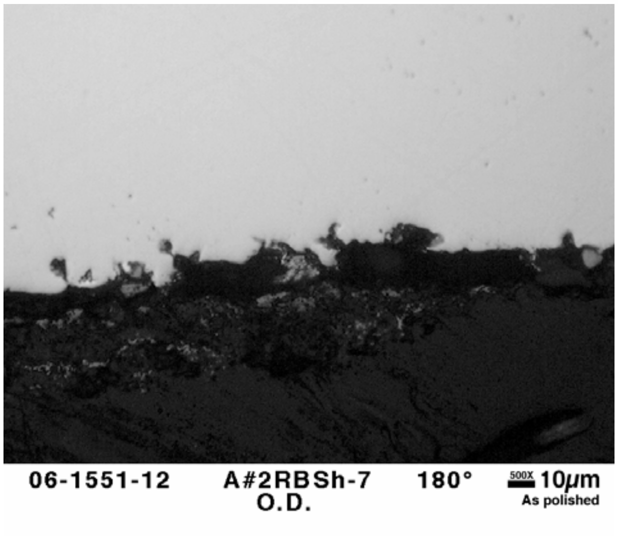

310H stainless steel – sample #8

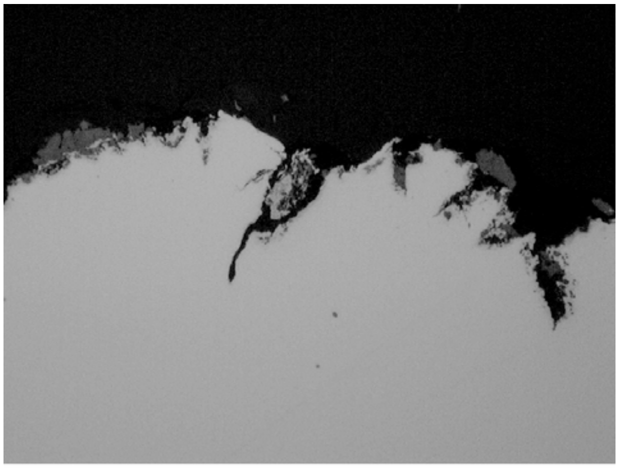
06-1552-03 A#2RBSh-8 0° 500X 10μm As polished

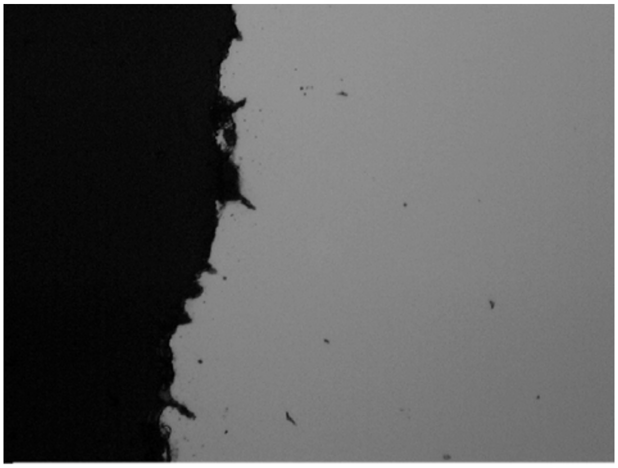
06-1552-15 A#2RBSh-8 270° 500X 10μm As polished

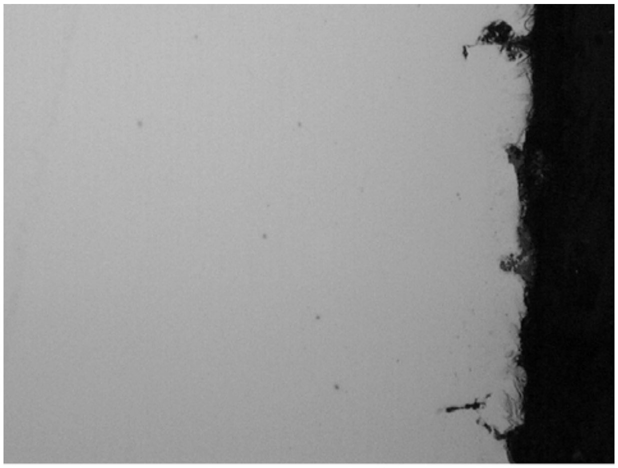
06-1552-07 A#2RBSh-8 90° 500X 10μm As polished


06-1552-12 A#2RBSh-8 180° 500X 10μm As polished

Sanicro 28 – sample #9

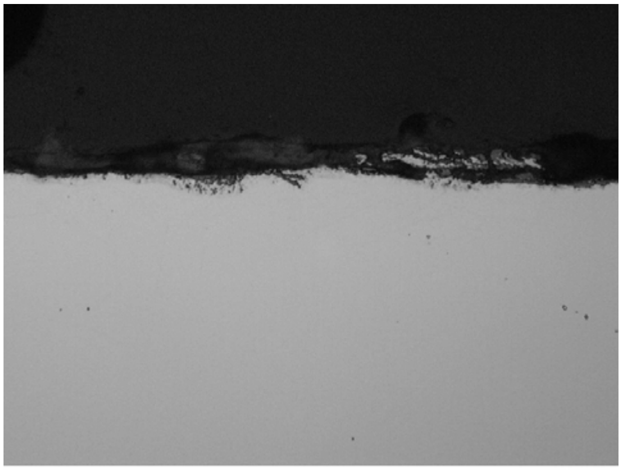
06-1553-04 A#2RBSh-9 O.D. 0° 500X 10μm As polished

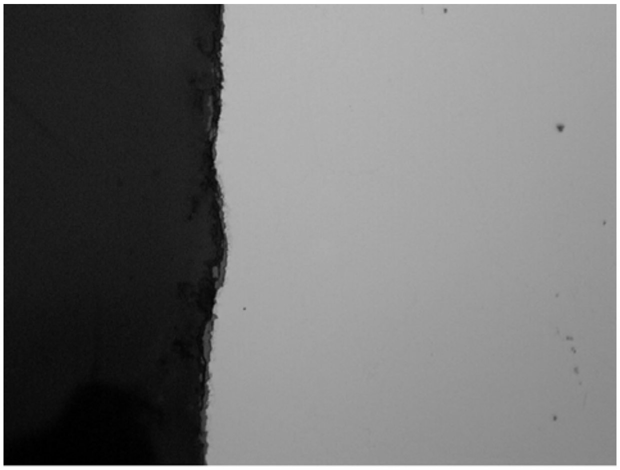
06-1553-16 A#2RBSh-9 O.D. 270° 500X 10μm As polished

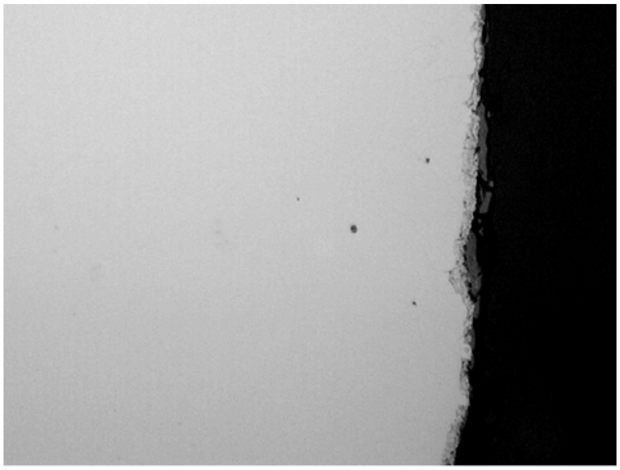
06-1553-08 A#2RBSh-9 O.D. 90° 500X 10μm As polished


06-1553-12 A#2RBSh-9 O.D. 180° 500X 10μm As polished

Inconel 693 – sample #10

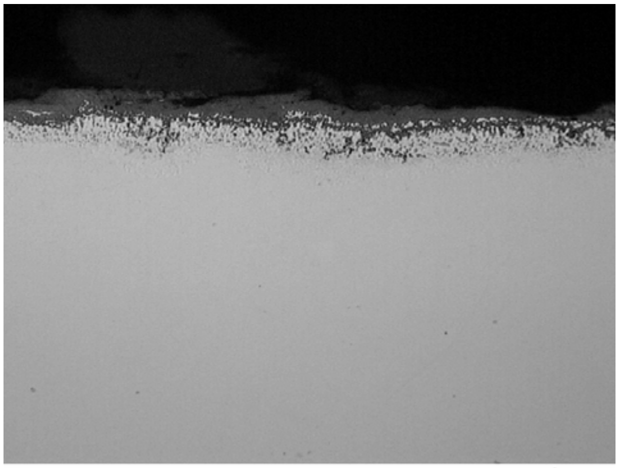

06-1554-03 A#2RBSh-10 0° 500X 10μm
O.D. As polished

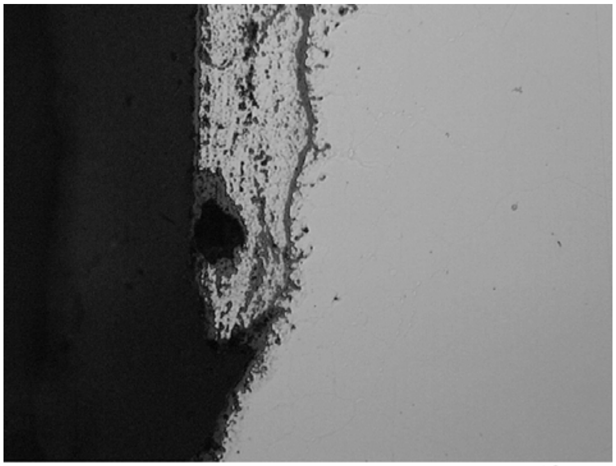

06-1554-15 A#2RBSh-10 270° 500X 10μm
O.D. As polished

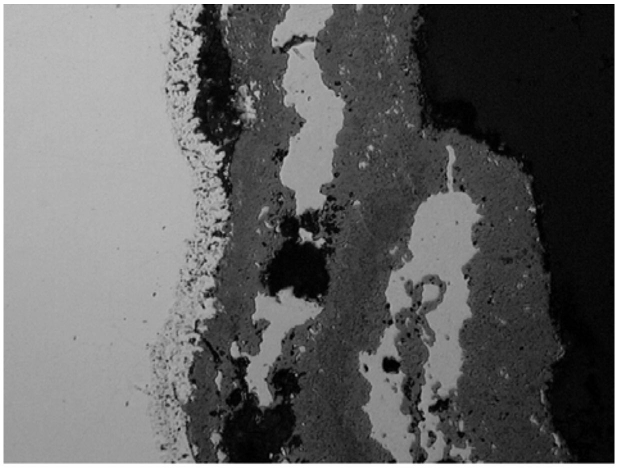

06-1554-07 A#2RBSh-10 90° 500X 10μm
O.D. As polished

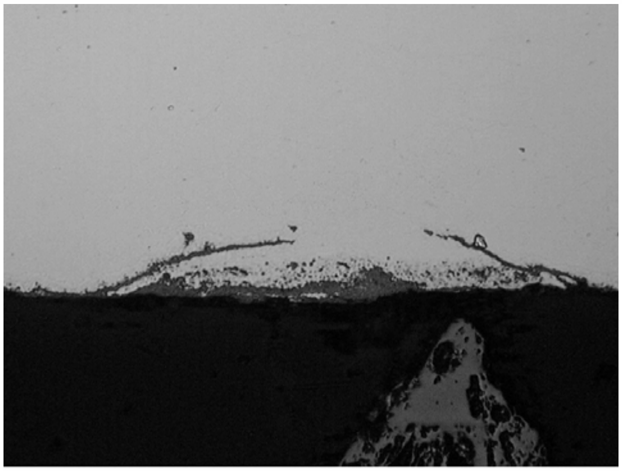

06-1554-11 A#2RBSh-10 180° 500X 10μm
O.D. As polished

347H stainless steel – sample #11

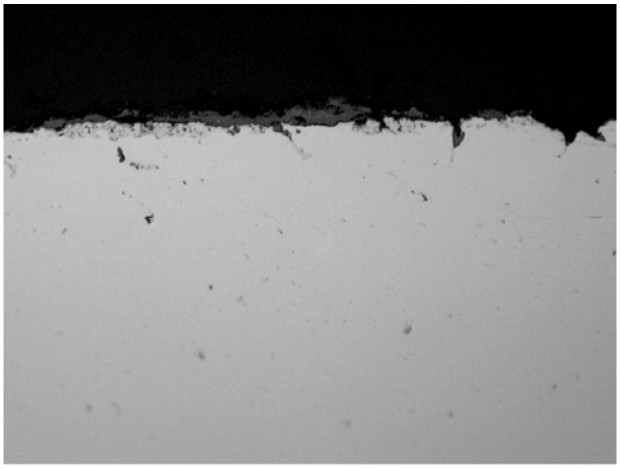

06-1555-03 A#2RBSh-11 O.D. 0° 500X 10μm As polished

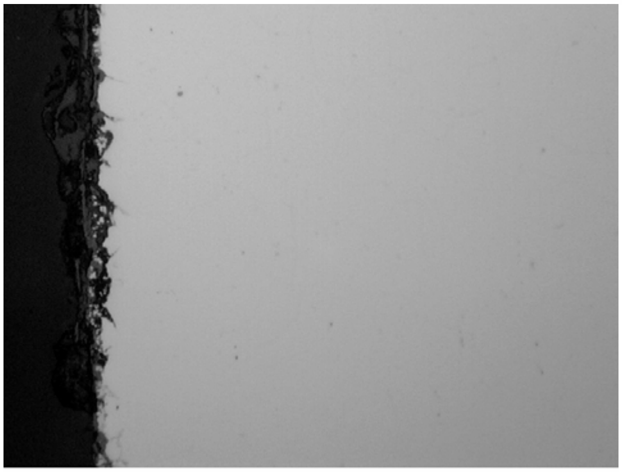

06-1555-16 A#2RBSh-11 O.D. 270° 500X 10μm As polished

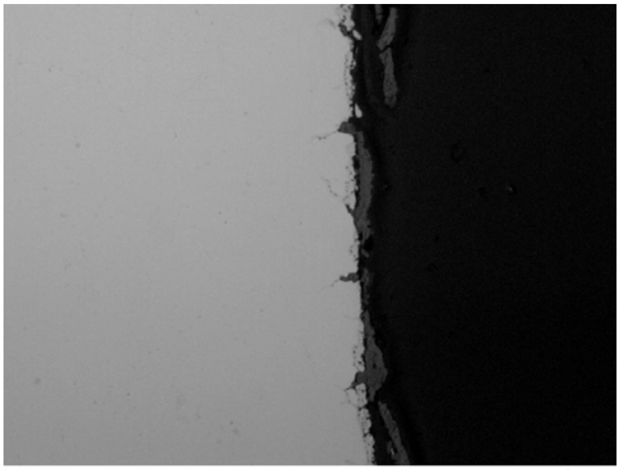

06-1555-08 A#2RBSh-11 O.D. 90° 500X 10μm As polished

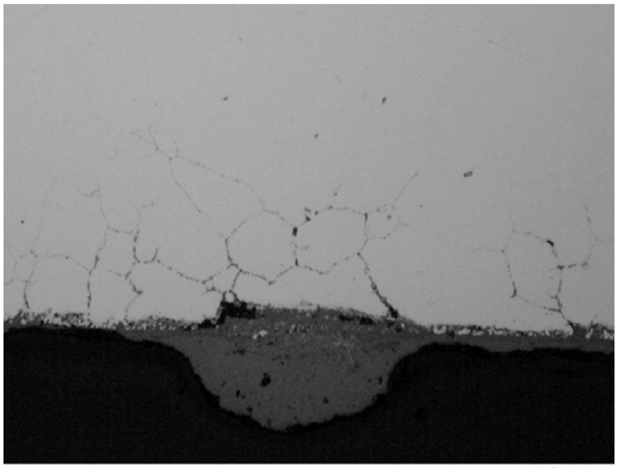

06-1555-11 A#2RBSh-11 O.D. 180° 500X 10μm As polished

310H stainless steel – sample #12

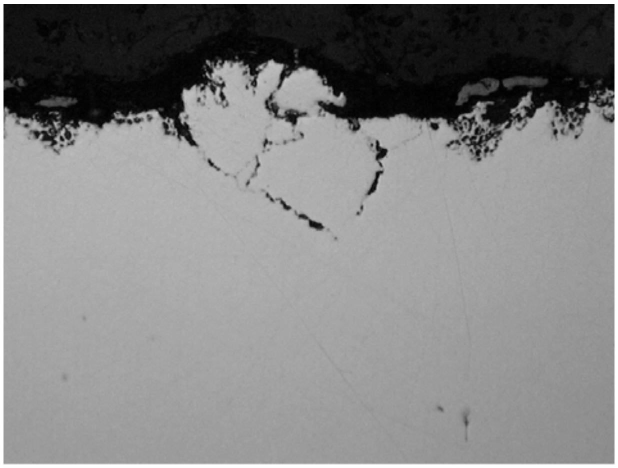

06-1556-03 A#2RBSh-12 0° 500X 10μm As polished

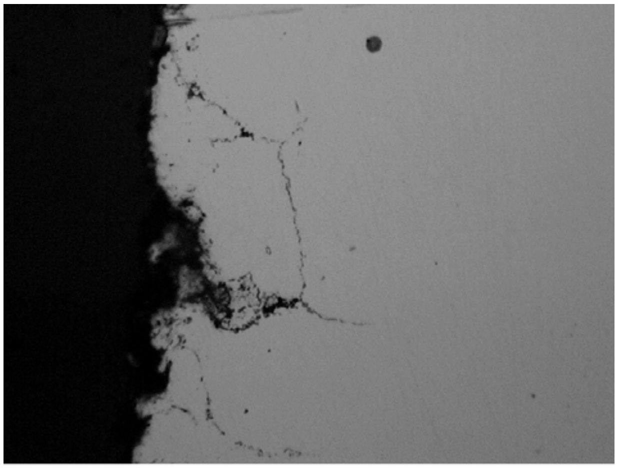

06-1556-16 A#2RBSh-12 270° 500X 10μm As polished

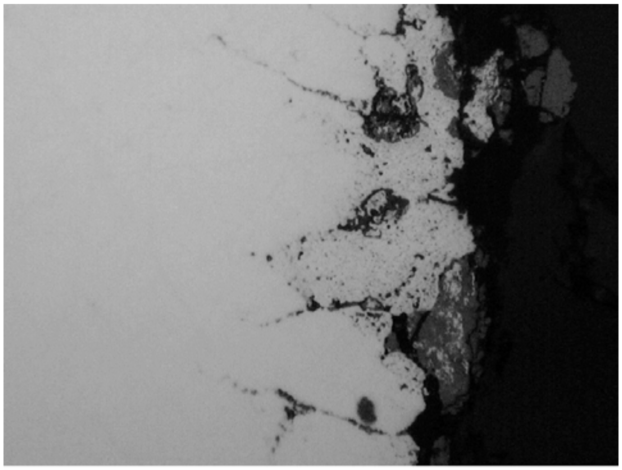

06-1556-07 A#2RBSh-12 90° 500X 10μm As polished

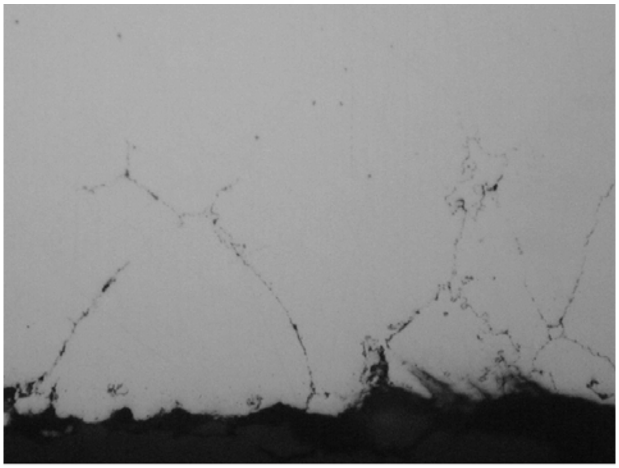

06-1556-12 A#2RBSh-12 180° 500X 10μm As polished

Sanicro 28 – sample #13

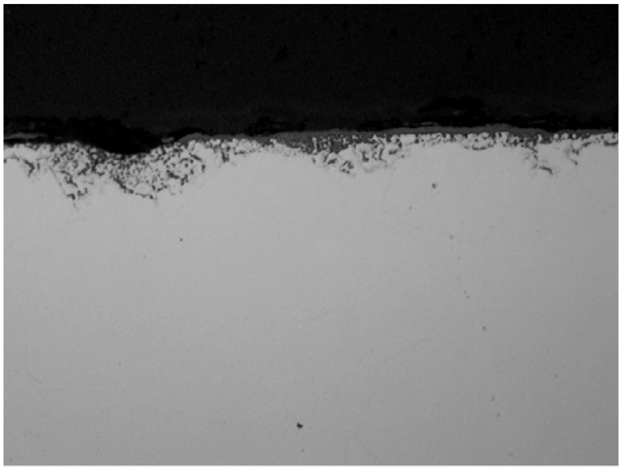
06-1557-03 A#2RBSh-13 0° 500X 10μm
O.D. As polished


06-1557-15 A#2RBSh-13 270° 500X 10μm
O.D. As polished

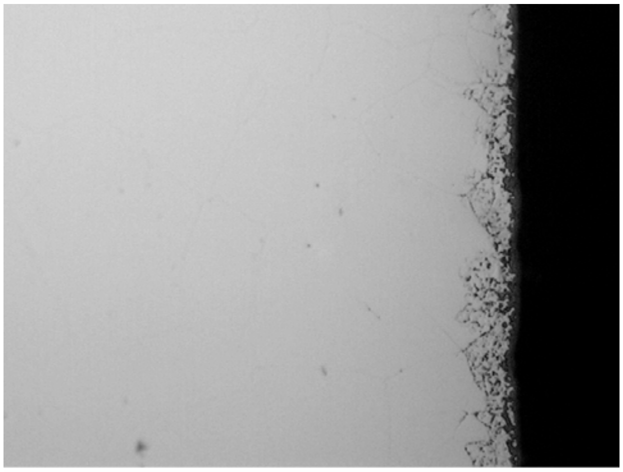
06-1557-07 A#2RBSh-13 90° 500X 10μm
O.D. As polished

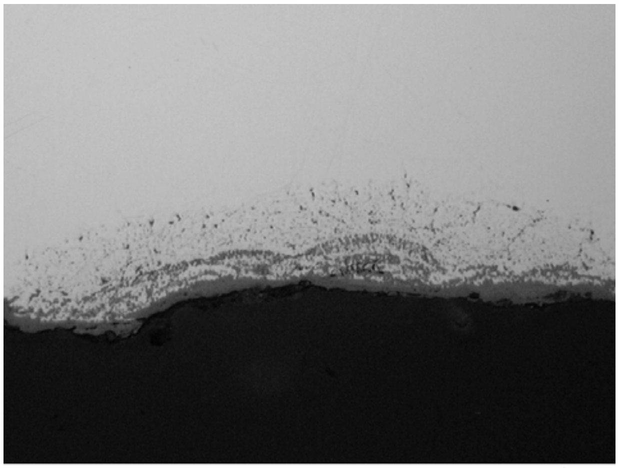
06-1557-12 A#2RBSh-13 180° 500X 10μm
O.D. As polished

Alloy 33 weld overlay – sample #14

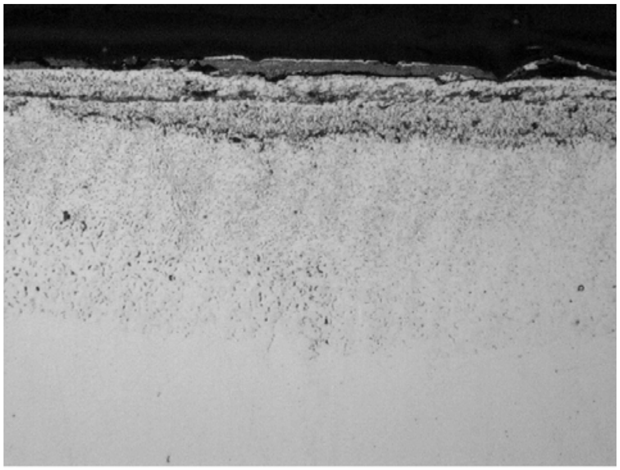

06-1558-03 A#2RBSh-14 0° 500X **10μm** As polished
O.D.

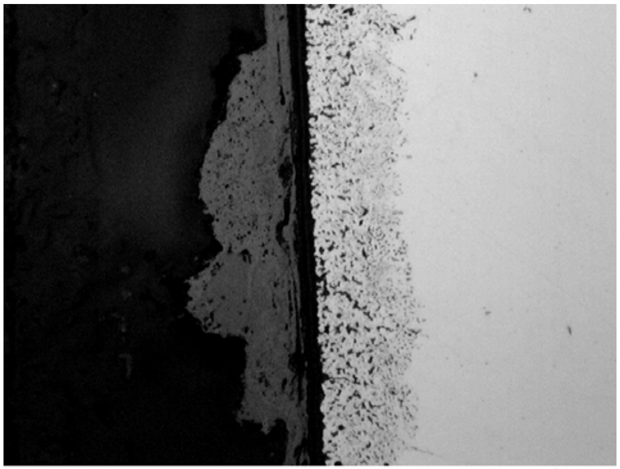

06-1558-15 A#2RBSh-14 270° 500X **10μm** As polished
O.D.

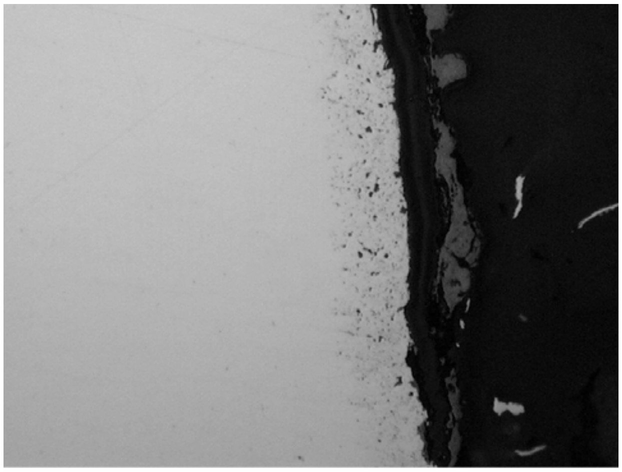

06-1558-07 A#2RBSh-14 90° 500X **10μm** As polished
O.D.

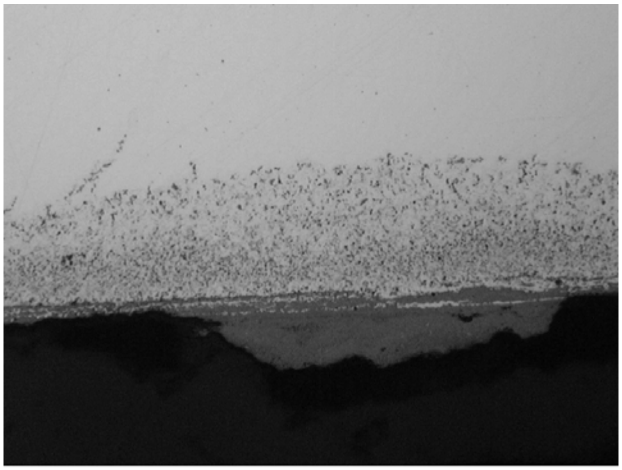

06-1558-11 A#2RBSh-14 180° 500X **10μm** As polished
O.D.

Inconel 693 – sample #15

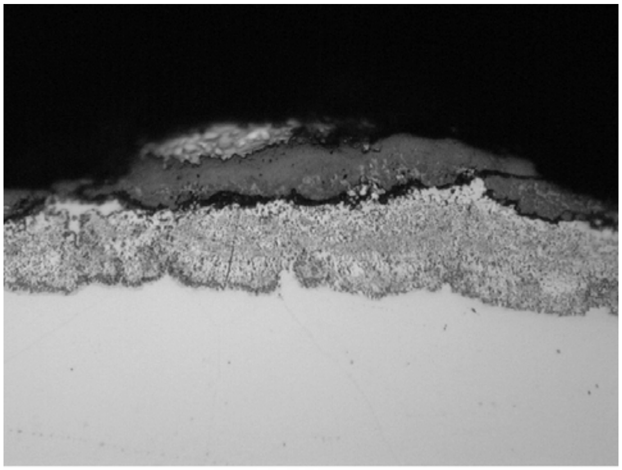

06-1559-03 A#2RBSh-15 0° 500X 10μm As polished

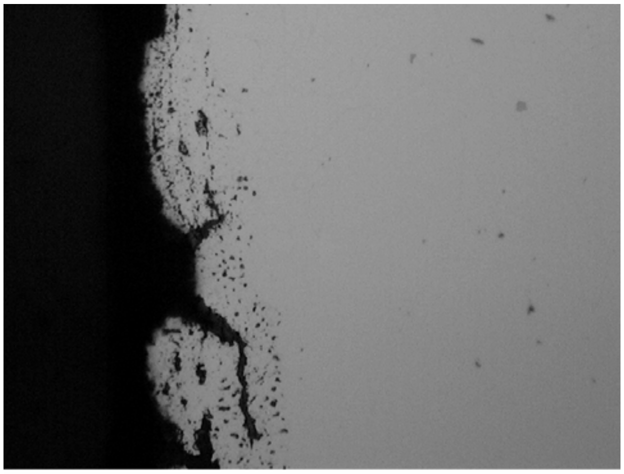

06-1559-16 A#2RBSh-15 270° 500X 10μm As polished

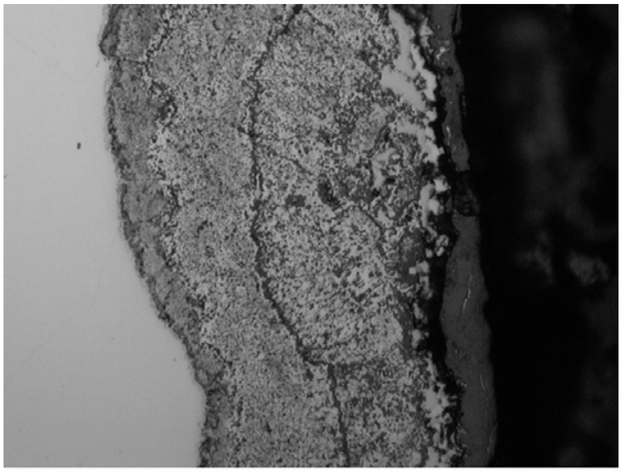

06-1559-07 A#2RBSh-15 90° 500X 10μm As polished

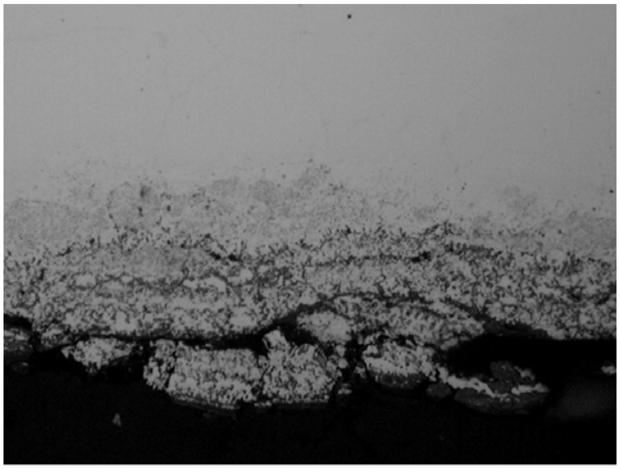

06-1559-11 A#2RBSh-15 180° 500X 10μm As polished